IGM86-401-393
CNRC 26502

FINAL REPORT

(July'84 - July'86)

CONTINUATION OF INVESTIGATION OF THE EFFECTS OF MECHANICAL STRESS ON THE MAGNETIC PROPERTIES OF PIPELINE STEELS FOR APPLICATION IN PIPELINE STRESS MONITORING

Prepared under contract: OSD84-00085
National Research Council (Industrial Materials Institute) and
Department of Energy, Mines and Resources (CANMET)

Crown Copyright of this report is reserved

D. L. Atherton
and J.A. Szpunar

Applied Magnetics Group,
Department of Physics,
Queen's University,
Kingston,
Ont. K7L 3N6

Note au lecteur:

Les idées exprimées dans ce document sont celles de l'auteur (ou du contractant) et ne sont pas nécessairement partagées par l'Institut de génie des matériaux ou par le Conseil national de recherches du Canada. L'auteur (ou le contractant) en assume l'entière responsabilité.

Si la demande est suffisante, des exemplaires supplémentaires de cet ouvrage pourront être disponibles dans la seconde langue officielle (français ou anglais).

Note to the reader:

The views expressed in this document are those of the author (or contractor) who assumes their full responsibility. They are not necessarily shared by the Industrial Materials Research Institute of the National Research Council of Canada.

If sufficient requests are received, a copy of this document will be made available in the other official language (French or English).

LIST OF CONTENTS

Part I	page no.
Executive summary	3
Part II	
Acknowledgment	7
1. Abstract	8
Résumé	9
2. Effect of stress on magnetization and magnetostriction	
2.1 Introduction	10
2.2 Experimental apparatus	11
2.3 Magnetomechanical effect and magnetostriction	12
2.4 Conclusions	12
3. Analysis of reversible and irreversible processes of magnetization	13
3.1 Definition of reversible and irreversible processes	13
3.2 Preisach diagrams for the irrreversible magnetization fraction	14
3.3 New concepts for anhysteretic curves	14
3.4 The extended Preisach model and description of complex magnetization processes	15
3.5 Conclusions and recommendations	15
4. Investigations of the effect of stress due to gas line pressure on magnetic leakage flux signals.	17
4.1 Introduction	17
4.2 The rotating drum test rig	18
4.3 Demagnetization	19
4.4 The efffect of line pressure on the amplitude of a defect signal	20
4.5 The effect of defect depth on signal amplitude variation	21
4.6 The effect of line pressure on noise	22
4.7 The effect of line pressure on signal/ noise ratio	22
4.8 Interpretation of results	22
4.9 Conclusions and recommendations	23
5. Design for a test rig for pipeline bending stress monitoring using internal magnetometer surveys	25
5.1 Introduction and objectives	25
5.2 Design concepts	27
5.3 Instrumentation and data acquisition	30
5.4 Apparatus and method	32
5.5 Pipe demagnetization	32
5.6 Recomendations	35
5.7 Conclusions	35
Appendices	
A. Effect of stress on magnetization and magnetostriction in pipeline steel	
B. Analysis of the irreversible processes of magnetization in steel	
C. A new approach to Preisach diagrams.	

1. EXECUTIVE SUMMARY

Magnetic inspection techniques are the principal methods used for in service monitoring of pipelines. Magnetic flux leakage tools are used to detect and measure defects which may lead to potentially hazardous regions of high stresses. Stress itself is a major parameter determining magnetic characteristics and magnetic measurements have potential for monitoring bending stresses directly. In order to exploit these techniques fully a detailed understanding of the interrelationships between magnetic and mechanical effects is essential. We are rapidly expanding our understanding of these interactions which are surprisingly complex. Our parallel approaches of basic studies of the magnetic behaviour of pipeline steels and detailed developments of magnetic inspection techniques continue to reinforce each other strongly.

In order to achieve a breakthrough in these studies research efforts are urgently needed. We have concentrated our research in three areas: studies of basic effects, studies of stress due to gas line pressure on magnetic flux leakage signals and the design of a pipeline bending stress monitoring test rig.

A major achievement in our basic studies is the first examination of the effect of stress on magnetostriction and magnetization for the same specimen. In order to analyse the data we introduced a method for separating reversible and irreversible processes. We also developed a new method for analysing irreversible processes using the Preisach diagram approach. The reversible component of magnetization is described by a Langevin function.

In our studies of the effect of stress on magnetic flux leakage signals we obtained very interesting results due to stress induced permeability changes. We summarize below the progress in studies of these three topics.

a) BASIC EFFECTS

Extensive measurement of magnetization and magnetostriction have been made. 1% Manganese line pipe steel has been subjected to tensile and compressive strains and magnetization and magnetostriction changes have been measured. Tensile and compressive strains have been applied in three steps, namely 200, 400 and 600 MPa. Significantly different results were obtained at different field strengths. Tension causes an increase in magnetization only at low field, where compression causes the magnetization to be slightly decreased. At 11 kA/m tension will cause an increase in magnetization only at low strain, but high tension causes a decrease in magnetization of the specimen. At field strengths higher

than 11 kA/m we observe a decrease in magnetization with compression at all levels of the observed strain. At present we cannot suggest a quantitative explanation of these phenomena but various studies of the structure are in progress.

Magnetostriction for tensile and compressive stress has been measured both along the anhysteretic and along the initial curves. The results obtained along the anhysteretic curve show more pronounced changes in magnetostriction than those along the initial curves. Tensile strain shifts the magnetostriction towards the negative direction and a stress of about 400 MPa is enough to supress the initial positive value of the magnetostriction. Changes observed in magnetostriction under compression are smaller.

The changes which were observed in magnetization and in magnetostriction are due to both reversible and irreversible processes and we are now analysing these changes in more detail. We have introduced a method which has been used to separate the reversible and irreversible changes in magnetization. We hope to learn more about the magnetoelastic interactions by using such experimental data. Preisach theory has been used to represent the irreversible changes in magnetization and we have determined ,the Preisach diagram from the irreversible magnetization changes. Such Preisach diagrams have been used to calculate minor and major hysteresis loops which compare favorably with experiments. We introduced as well an extended Preisach model including a reversible magnetization component given by a Langevin function. We are interested in applying these techniques in studying the interaction between domains as a function of the internal stresses.

We observe that the reversible fraction constitutes a high percentage of the total magnetization at very low fields and that the contribution of this fraction decreases rapidly to a few percent with increasing field strength. A gradual increase of the reversible part is observed at high field strengths, above the knee of the magnetization curve. This increase is attributed to the increasing role of rotational magnetization processes, which may have a significant reversible component.

The large contribution of the reversible processes at low field strength is due to a number of factors. We believe that the initial increase in magnetization with an incremental increase in the field strength occurs because certain domain walls are shifted from their thermodynamic equilibrium position in the grain and these shifts may

occur without pinning. Further increase in magnetization at low field strength occurs by displacement of domain walls which are already pinned. Being pinned they now contribute to an increase in magnetization by elastic deformation of the domain wall.

b) MAGNETIC FLUX LEAKAGE INSPECTION AND STRAIN

Extensive studies have been performed on the effect of stress on magnetic flux leakage inspection. Dynamic testing and calibration of new detectors and inspection pigs is often undertaken by towing them through short sections of open pipeline. These short sections may include simulated defects and anomalies.

We used here a new dynamic detector test rig which is designed to complement such test facilities. It used a rotating cylindrical drum, specifically a short section of line pipe, with stationary detectors pressed against the outside.

We have shown that gas line pressure typically has a significant effect on the performance of magnetic leakage flux detectors used for in service inspection of pipelines. In general increasing pressure and hence tensile stress in the wall tends ihitially to lower the amplitude of defect induced signals. As the pressure is further increased the effect is reduced and then reversed until, at high pressure, there is a substantial increase in signal amplitude. The effects are reversible with pressure and independent of defect penetration. Noise is reduced with increasing pressure so that the best signal to noise ratios are obtained at the highest pressures.

The effects are considered to be due to overall stress induced changes in permeability of the pipe wall steel in the general vicinity of the detector but not directly localized to the defect. A modest tensile stress causes a slight increase in the general slopes (increased permeabilities). The effect is diminished at greater stress and reversed at high stress (permeability reduced).
High flux densities in the pipe wall and therefore low permeabilities tend to give greater leakage flux signals so that it appears that stress induced changes in the overall pipe wall permeability could account qualatatively for the stress induced changes in signal amplitude. There remains however a rather surprising feature that has not yet been explained. Stress induced permeability changes are rather slight whereas the stress induced changes in signal amplitude are relativlely large. It is not yet clear whether overall permeability changes are significant enough to provide a possible quantative explanation of the stress induced changes in signal amplitude and this matter

is under further study.

It should be noted that, particularly for the pipeline steels under investigation, the effects of stress on magnetization are very complex and that this explanation of the effects of gas line pressure on stress can only be considered to be a first simple identification of the likely dominant mechanisms responsible for our experimental findings.

The first recommendation arising from this work is concerned with defect detection and is that, the highest possible pressure is preferrable in order to give the maximum signal to noise ratio and therefore maximum sensitivity.

The second recommendation is probably more important and also less obvious and is concerned with the assessment of the potentially injurious effects of defects which have been detected. It is now clear that, the pressure in the test line used for tool calibration must be similar to the pressure in the line inspected or that corrections to signal amplitude must be made before determining their depth and assessing their severity.

c) STUDIES OF A NEW DESIGN FOR A TEST RIG FOR BENDING STRESS MONITORING

We have studied the design for a bending stress monitoring test rig using internal magnetometer surveys. Such a potential technique for detecting and monitoring high bending stress regions would be most useful for pipelines traversing unstable terrain. Field measurements have shown that bending stress produces detectable changes in the magnetic fields which can be measured at typical burial depths above large pipelines.

The study shows that a pipeline bending stress monitoring test rig is a feasible proposition. Various design concepts were evaluated. We feel that the technique is potentially useful, but there was little immediate interest in applying it, it was therefore agreed to defer this application until a more immediate need was apparent.

ACKNOWLEDGMENTS

The members of the Applied Magnetics Group contributing to this work were:

D.L. Atherton (project leader)

J.A. Szpunar and B. Szpunar (research associates) M. Schonbachler, D. Anderson, T. Lorentzen, C. Welbourn (research engineers), W. Czura (technologist) D. Wilson, D. Hope Simpson, S. Brauer, S. LaRochelle (summer research assistants)

We would like to thank V. Carron, D. Mak and M. Godden (Department of Energy Mines and Resources, CANMET, Physical Metallurgy Research Laboratory) and J. Bussiere of National Research Council (Industrial Material Research Institute) for their continuing encouragement and guidance and also R. M. Jamieson of TransCanada Pipelines Ltd. for generous support both with ideas and substantial test pieces.

1. ABSTRACT

Three topics are reported here: the effect of stress on magnetostriction and magnetization, an investigation of the effect of gas pressure on magnetic flux leakage signals and a new design for a bending stress monitoring test rig using internal magnetometer surveys. In our study of basic effects we have analysed and measured the effects of tensile and compressive stresses on magnetization and magnetostriction. We have demonstrated that the stresses can increase or decrease magnetization depending on the applied magnetic field and the previous magnetic history of the specimen. We introduced a new method for separating the reversible and irreversible processes of magnetization and applied this method to predict any arbitrary changes in magnetization. We have derived a theoretical model based on Preisach diagrams to describe the irreversible processes and described the reversible processes using a Langevin function.

Extensive studies have been performed on the effect of stress on magnetic flux leakage signals using a rotating drum test rig. We consider that the changes in magnetic leakage flux signals and noise are due to overall stress induced changes in permeability of the pipewall steel in the general vicinity of the detector. As pressure is increased the amplitude of defect induced signals initially decreases and then increases again until, at high pressure, the amplitude is significantly greater than the zero stress amplitude. Noise amplitude, on the other hand, decreases with increasing pressure.

We have shown that gas line pressure has a significant effect on the performance of magnetic leakage flux detectors used for in service inspection of pipelines and have made recommendations based on our findings.

Various design concepts for a test rig for monitoring bending stresses were analysed and evaluated. It was concluded that such a test rig was a feasible and relatively economical proposition.

Résumé

Trois sujets seront présentés dans cet article. Le premier traite de l'effet des constraintes sur la magnétostriction et la magnétisation. Le deuxieme sujet sera l'étude de l'influence de la pression du gaz sur le signal produit par les fuites en flux magnétique et finalement le dessein d'un nouveau banc d'essai pour mesurer les contraintes en flexion utilisant le magnétomètre a l'intérieure du count pipe line. Dans notre étude fundamentale, nous avons analysé et measuré les effets des constraintes en tension et compression sur la magnétisation et la magnétostriction. Nous avons démontré que les constraintes peuvent augmanter ou diminuer la magnétisation tout dépendant du champs magnétique appliqué et de la mémoire magnétique précédente de l'echantillon. Nous avons introduit une nouvelle méthode afin de separer les procédés réversible et irréversible de la magnétisation et cette méthode a été appliqué dans le but de prédire les changements arbitraires de la magnétisation. Nous avons établi un method théorique basé sur les diagrammes de Preisach pour décrire les procedes irréversibles et les procedes réversibles utilisant une fonction de Langevin.

Nous avons aussi fait des études sur les effets des contraintes des signaux provenant des fuites en flux magnétique en utilisant la rotation d'un tambour éxperimental. Nous avons démontré que la contrainte introduite de la densite de flux sont due à l'encrement de la permeabilité mais non des champs locaux a la proximité de la faille. Quand la pression est augmentée, l'amplitude du signal produit par les failles diminues, et par la suite augmente encore. Quand la pression est tres élevée, l'amplitude est beaucoup plus grande par rapport a l'amplitude lorsque la pression est zéro. D'un autre côté, la bruit diminue avec une augmentation de la pression.

Nous avons montré que la pression du gaz a un effet significatif sur le rendement des détécteurs de fuite en flux magnétique qui sont utilise pour la maintenance des pipes-lines. Nous avons aussi fait des recommendations basées sur nos expériences.

Plusieurs desseins de banc d'essais pour mesurer les constraintes en flexions ont été analysés et evalués. Nous en concluons qu'en til banc d'essais est réalisable et que cette proposition est relativement économique.

2. EFFECT OF STRESS ON MAGNETIZATION AND MAGNETOSTRICTION

2.1 INTRODUCTION

In this report we performed a continuation of previous studies made between September 1981 and August 1983 on the effect of mechanical stress on the magnetic properties of pipeline steels [1-6]. The studies described in our previous report included building an experimental apparatus for magnetization measurements under stress, the development of a hysteresis theory which was used sucessfully to describe the main aspects of magnetization characteristics of materials. A major development of the project was a discovery of a shift of the magnetization under stress towards the anhysteretic magnetization (which is also stress dependant). Also several laboratory tests were made in order to illustrate not only detection of anomalous stresses in gas pipelines by magnetometer survey but also the behaviour of the magnetization curves under stress.

We have continued these fundamental studies progressing in two directions; examining simultaneously the effect of stress on magnetization and magnetostriction and making a clear distinction between reversible and irreversible processes.

An understanding of the effect of strain on the magnetic properties of pipeline steel is interesting because the complex structure of this material can contribute to a variety of interactions between the domain wall and the grain boundary, pearlite grains and cementite inclusions. Such observations of the domain wall pinning were made recently by Tanner et al. [7] and demonstrated that the interaction between the domain wall and grain boundary or inclusion is a very interesting process. Also Szpunar and Szpunar [8] have demonstrated that there are four main types of domain patterns observed in constructional steel and that the relative proportions of these different domain patterns depends on the grain size. Such dependence has been justified by a theoretical model [9].

The magnetization stress curves obtained by applying stress to a ferromagnetic material have been a subject of considerable interest for some time. Brown [10] sought to explain such a process for stresses which are sufficiently small for the rotational processes to be neglected. His theory is however difficult to extent to high stresses and

the validity of this theory under compression remains an open question. Brugel and Rimet [11] calculated the effect of tension and compression on magnetization. Calculations were based on an analysis of the variation of the different components of magnetic energy and the application of this theory to constructional steel would be extremely difficult.

There is still a long way to go until magnetoelastic interaction in such a complex system can be fully understood. In this work we progress towards an understanding of the magnetic properties initially by experiments which give us information about changes in magnetization and magnetostriction in the same steel specimens. Such studies have not been attempted previously. Also we believe that changes in magnetostriction and in magnetization have to be separated into reversible and irreversible parts because the physical processes which contribute to such changes are different.

2.2 EXPERIMENTAL APPARATUS

The turnbuckle mechanism used has been described in the previous report but several changes have been introduced as described below. For a description of the stress mechanism, ,the turnbuckle and the integrating voltmeter/ fluxmeter the reader is refered to the previous report. The principles of measurement of magnetization, field and stress remain the same. The same Varian electromagnet is used.

The AMG regulator box was removed from the current control circuit and a new Hall amplifier, see diagram (Fig.1) was inserted to measure the Hall voltage. The new amplifier consists of a variable gain instrumental amplifier and a 4th order Butterworth low pass network with a cutoff frequency of 30 Hz which can be bypassed through a unity gain buffer, if desired. The existing strain gauge amplifiers were replaced by new models (see Fig.1) using the same general layout as the Hall amplifier mentioned above, but with additional elements to balance the strain gauge bridges. The actual strain gauge bridges were moved closer to the electromagnet to minimize lead length and a feedback system (using the new amplifiers) was used to control the voltage across the bridges.

2.3 MAGNETOMECHANICAL EFFECT AND MAGNETOSTRICTION

Extensive measurements of magnetization and magnetostriction have been made on the same sample. 1% Manganese line pipe steel has been subjected to tensile and compressive strains and the magnetization and magnetostriction changes have been measured. Results of measurements and analysis are presented in Appendix A, where examples illustrating strain induced magnetization changes at various points on the anhysteretic magnetization curve and initial magnetization curve are given. Tensile and then compressive strains were applied in three steps, namely 200, 400 and 600 MPa. Significantly different results were obtained at different field strengths. Tension causes an increase in magnetization only at low field, where compression causes the magnetization to decrease. At 11 kA/m tension will cause only an increase in magnetization, but high tensile strain causes a decrease in magnetization of the specimen. At field strengths higher than 11 kA/m we observe a decrease in magnetization with compression at all levels of the observed strain. At present we can suggest only a qualitative explanation of these phenomena but various studies are in progress.

Magnetostriction curves for tensile and compressive stress have been measured both along the initial and along anhysteretic curves. Examples are given in Appendix A . The results obtained along the anhysteretic curves show much more pronounced changes in magnetostriction than those along the initial curve. Tensile strain shifts the magnetostriction towards the negative direction and a stress of about 400 MPa is enough to supress the initial positive value of the magnetostriction. Changes in magnetostriction under compression are smaller. This is thought to be due to residual compressive stresses in the material.

2.4 CONCLUSIONS

The observed changes in magnetostriction and magnetization illustrate that pipeline steel is a very complex system and we intend next to measure specimens which differ in microstructure from the specimens investigated. We would also like to investigate experimentally the role of internal stresses and the role of the grain size. The results of our experiments are included in Appendix A, however at this stage of investigation, we are unable to generalize this observation for pipeline steel and further studies are in

progress.

3. ANALYSIS OF REVERSIBLE AND IRREVERSIBLE PROCESSES OF MAGNETIZATION

3.1 DEFINITION OF REVERSIBLE AND IRREVERSIBLE PROCESSES OF MAGNETIZATION.

It is well known that processes which contribute to magnetization changes are both reversible and irreversible. The Physics of these processes is complex, but simplifying we may say that a ferromagnetic domain wall which is under the influence of an external field moves from its equilibrium position. Initially the wall is deformed elastically and if the field is removed the wall returns to its equilibrium position. However, when the field is increased still further the energy supplied to the system is lost as dissipation against pinning and cannot be recovered. Such processes are irreversible. Rotational processes take place at higher field strength when domain wall movement is limited and most grains form macrodomains. The rotational processes are largely reversible.

The same distinction between reversible and irreversible processes can be made when magnetization is measured as a function of stress. In steel the magnetocrystalline energy is much higher than the stress energy and therefore stress only inflences the distribution of magnetization directions between the various easy directions. Such a process of redistribution of magnetization directions between various easy directions of magnetization is reversible also when low stresses are involved. High stress modifies and changes the structure of the material, the density of dislocations and of structure defects increase and the increased number of pinning centres contributes to an increase in the fraction of irreversible processes.

We have shown that the reversible and irreversible changes can be separated experimentally. The following assumption is made; the reversible magnetization changes generated by the fields dH and -dH are the same therefore we assume that the total change in the magnetization dM consists of two parts reversible (dMr) and irreversible (dMi). This principle is used in experiments to separate the reversible and irreversible parts of magnetization as functions of the field and of stress. A detailed description of this procedure can be found in Appendix B.

3.2 PREISACH DIAGRAMS FOR THE IRREVERSIBLE MAGNETIZATION COMPONENT

In order to analyse the irreversible processes of magnetization we have applied the established method of Preisach diagrams. The assumption is made that the polycrystalline solid consists of elementary magnets or domains which have characteristic switching fields at which the magnetization changes from state I to state II and vice versa. Preisach diagrams have been obtained from the irreversible part of the magnetization curves. This is contrary to all previous studies where Preisach diagrams have been calculated from the total magnetization changes. The methods and the results of calculation are described in detail in Appendix B. We intend to use this method for investigating the changes in distribution of switching fields under stress. Such studies should inform us of the statistical changes in the magnetic loops characterizing the domains constituting the steel specimen. Such changes will be registered under stress and should help us to understand the effect of tensile and compressive stresses on magnetization.

3.3 NEW CONCEPTS FOR ANHYSTERETIC CURVES

In order to obtain the magnetization curves which represent the global minimum energy configurations of the magnetic domains we have used the anhysteretic curves. These curves are obtained by superimpositing, at every point of the initial curve, an AC field whose amplitude decays to zero. In Appendix C we have re-examined this concept. The discussion of the Preisach diagram shows that the anhysteretic curve depends greatly on the type of the AC pattern which is used i.e on its maximum amplitude, on the way it changes with time and on the previous magnetic history of the specimen. Therefore we believe that the concept of a unique anhysteretic curve has to be re-examined and there is no unique definition of the form of oscillation needed to drive the magnetization to its equilibrium state. The previous history of the specimen may influence the shape of the anhysteretic curve in the same field interval.

3.4 THE EXTENDED PREISACH MODEL AND DESCRIPTION OF COMPLEX MAGNETIZATION PROCESSES

In order to describe any magnetization changes we have considered separately the contribution of reversible and irreversible magnetization parts. The extended Preisach model has been used to describe the irreversible components and the reversible part is described by a modified Langevin function. We have assumed initially a constant distribution function and this makes it possible to derive analytic equations describing the complex magnetization processes and as a result to define the equations for the initial curve, the anhysteretic curve, the major loops, the anhysteretic curve for minor loops and the anhysteretic curves for lower branch minor loops. The results of this research are described in Appendix C.

3.5 CONCLUSIONS AND RECOMMENDATIONS

An experimental method which can be used to separate the reversible and irreversible components of magnetization has been demonstrated. This has been done for steel, in tension and in compression. We have demonstrated that tensile stress increases the magnetization at low fields and decreases the magnetization at high fields. Compressive strain increases the magnetization slightly at low field but at high field we observe an increase in magnetization. We know at present that these changes result from reversible and irreversible parts and that the reversible part is mainly responsible for the different behaviour of steel at low and hign field. We have shown that reversible processes can be described by a modified Langevin function and have applied Preisach diagrams to analyse the irreversible magnetization component. Preisach diagrams were obtained from the irreversible magnetization component. We demonstrated that the Preisach diagrams are symmetric and that the probability of change of state from I to II and vice versa is greatest at a field strength of 3 kA/m. This is interesting information, because we have also shown that a field of 3kA/m can significantly change the magnetization of the specimen and we can determine the fraction of the total number of elements which have changed their state of magnetization.

Advancing from descriptions of magnetization processes and using the Preisach diagram we derived analytic formulae which can be used to predict the magnetization

for any arbitrary change in field strength. We intend to study further the influence of strain on the Preisach distribution function in our attempt to determine how the switching fields are affected by tensile and compressive stresses. A better understanding of the influence of stress on reversible and irreversible processes is needed. We believe that all these fundamental studies can contribute to a better understanding of the magnetic flux leakage signals at corrosion pits and other defects.

4. INVESTIGATION OF THE EFFECT OF STRESS DUE TO GAS LINE PRESSURE ON MAGNETIC LEAKAGE FLUX SIGNALS

4.1 INTRODUCTION

Our previous work[1] on the effects of mechanical stress on the magnetic properties of pipeline steels led to a significant improvement in the basic understanding of magnetomechanical effects and showed that the first result of the application of stress was to cause an irreversible shift in magnetization toward the anhysteretic[2]. In addition to this irreversible shift there are also reversible effects, but in most cases these are less, during the initial application of stress, than the irreversible change.

These basic concepts proved to be very helpful in interpreting the results of magnetometer measurements made over pipelines[3] and near pipes stressed by bending[4,5]. We have proposed that these stress induced changes, which are primarily due to irreversible effects, could be used to monitor or detect abnormal bending stresses occuring in pipelines constructed over unstable terrain.

Since the primary use of magnetic techniques for monitoring pipelines is the use of magnetic leakage flux anomaly detectors in electronic inspection tools it was agreed that we should extend our investigations to the dynamic testing of the effects of gas line pressure stress on the performance of magnetic leakage flux inspection tools, using the rotating drum test facility[6] described subsequently.

Before testing we had anticipated that line pressure stress would have significant effects which it would be desireable to know of and understand in order to assist in interpreting magnetic flux leakage inspection logs. Our first expectation, influenced greatly by our investigations of bending stress induced magnetization changes, was that any effects would tend to be dominated by irreversible changes. This proved wrong and probably hindered initial interpretation of our experimental results. Our second expectation was that the typical background noise on which leakage flux signals are superimposed, which is due primarlily to magnetic irregularities in the steel pipe wall, would be reduced. This second expectation proved to be correct.

4.2 THE ROTATING DRUM TEST RIG

The rotating drum test rig, which is shown in Fig. 2, uses a variety of test pieces. These consist of short sections of line pipe which are supported with axes horizontal on a modified set of truck wheels. Detectors under test are pressed against the outside of the rotating drum. It will be noted that, in this system, far side defects are those on the inside of the pipe. The drum is turned by the drive wheels from a hydraulic motor system or a variable speed DC motor through a differential and chain and sprocket sets. For these experiments gas line pressure is simulated hydraulically using a drum sealed with end caps and pressurized internally. The responses to natural and simulated defects are analysed.

The test rig was conceived partly as a convenient and economical method of performing laboratory dynamic testing of anomaly detectors and partly to meet some special objectives not readily obtainable using other test facilities.

The first of the special objectives was to examine the effects of pipewall stress due to line pressure on the performance of magnetic inspection pigs. Testing magnetic inspection pigs by drawing them through open lines omits any consideration of line pressure stress effects, furthermore, most proposals for providing or simulating varying line pressure stress for pig testing lead to very expensive test facilities and serious safety engineering considerations. Our test rig permits the use of a line pipe section sealed with end caps. This can be hydraulically pressurized to simulate line pressure effects safely and conveniently. It will be noted that filling the pipe with water does not impede the relative motion of the detector since the detectors are mounted against the outside of the drum.

A second special objective was to provide easily monitored and highly repeatable dynamic testing. A stationary detector, with the relative motion provided by drum rotation, is particularly easy to instrument. Since the detector scans the same circumferential path for each drum rotation, signals are highly reproducable.

We have several test sections of line pipe available and planned. These are nominally 914mm (36") in diameter and about 1.8m long. The first set are open cylindrical drums with wall thicknesses in the 10mm to 30mm range which have been used first to investigate demagnetization techniques and then to examine the effects of pipewall flux density and sensor mountings on detector performance. All drums have a number of circumferential tracks with a series of natural anomalies and a variety of blind milled

holes simulating further defects. For the tests described here we have another section which is sealed with end caps and which can be pressurized hydraulically to simulate line pressure stress.

The test drum is supported, with its axis horizontal, on a set of light truck wheels, tires and rear axles mounted in an aluminum frame. The axles have been shortened to a span of 1.3m and the differential left intact on one of them. The drive shaft stub of this differential is driven by either a 3.7kW variable speed DC motor or a hydraulic pump and motor through sets of chains and sprockets. There is sufficient friction between the drum and the rubber tires to maintain traction even under full load. The motors provide adequate braking. The drum may be "steered" to eliminate axial runout by small torsional deformations of the frame. Safety is provided by the heavy frame and by hoops of high tensile cable which enclose the pipe. Runout limit switches and panic switches are included in the drive motor controls.

Detectors under test are mounted to the main frame and held against the drum with controlled and measured loads. The active leakage flux detectors use both electromagnet and permanent magnet excitations. We can measure magnetic hysteresis characteristics for complete detector/pipe magnetic circuits when open cylindrical drums are used and we map both fringing fields and pipewall flux density. The latter is measured using integrating flux coils threaded through the pipe wall.

The instrumentation, in addition to the drive control system, includes an angular position to voltage converter and a PC based data acquisition and control system. This records the detector output from a circumferential track and subsequently outputts it on digital or analogue plotters. It is also used to monitor and control demagnetization routines. It can also be used for signal processing. A block diagram of this system is shown in Fig. 3.

4.3 DEMAGNETIZATION

In order to obtain reproducible results it is, of course, necessary to control the magnetic history of the drum under test. This often implies demagnetization. In this case demagnetization techniques were developed initially using an open drum with a large coil wound through it and later by using an external electromagnetically energized detector, as shown in Fig. 4. Very low frequency (0.1 Hz) AC of steadily diminishing amplitude combined with drum rotation is used. The AC is

generated by a computer controlled bipolar power supply in order to avoid switching transients during current reversals and to ensure reproducible preset current waveforms thus enabling successful demagnetizations to be repeated. We have invariably found the development of satisfactory demagnetizing procedures to be a tedious and time consuming process.

4.4 THE EFFECT OF LINE PRESSURE ON THE AMPLITUDE OF A DEFECT SIGNAL

All measurements were made using Hall probes in order to measure the leakage flux densities directly. These can then be differentiated subsequently to give the signals that would be obtained using an inductive sense coil (of the same width) and a second differentiation can be performed to give the results which would be obtained from a pair of differentially connected sense coils which are used to buck microphonic pickup from vibration in the detector leakage fluxes. We normally prefer to analyse the field signals themselves, being the primary data, although, in this case results from analysing the differential signals are of the same form since the defect signals are from pits which are all of the same diameter.

Our data acquisition system samples and records the leakage field at fixed intervals of 0.8mm around the full circumference of the drum. These records can then be outputted on a digital plotter. Examples of such records made at internal gage pressures of 0, 2.8 and 6.3 MPa are given in Figs. 5, 6 and 7 showing typical defect induced signals, background noise and weld responses. The background noise is absolutely repeatible and is due to magnetic irregularities in the pipe and not due to any electrical or mechanical disturbances since these records have been made at rather slow speeds; it is therefore information rather than noise.

The internal pressure in the pipe generates a circumferential hoop stress in the pipewall. In calculating this an allowance for the support provided by the end caps sealing the ends must be included. There is also an axial stress due to the pressure acting on the end caps. The combined effect of these stresses indicates that an internal pressure of about 8.3 MPa should cause yielding of the pipewall in even uniform defect free regions.

Figs. 8, 9 and 10 show the records made at 0, 2.8 and 6.9 MPa differentiated to give the outputs which would be obtained with an inductive sense coil and Figs. 11, 12 and 13 show doubly differentiated records simulating the

ouputs from paired sense coils.

Fig. 14 shows the variation with internal pressure of the amplitude of a far side defect with 60% penetration, made with increasing internal pressure. The signal amplitude decreases with pressure up to about 3 MPa above which it increases until by 6.9 MPa it is 50% greater than at zero gage pressure. Our initial interpretation was that this might be due to local stress effects concentrated in the region of the defect. The inversion pressure appeared to coincide with the pressure at which local yielding in the remaining thickness of the wall at the defect would be expected.

Fig. 15 is a continuation of the same analysis and includes data from records made as the internal pressure was reduced. It shows that the effects appear to be essentially reversible with pressure. The reversibility of the effects suggests that they must be due to some cause other than local yielding.

There is no resolveable change in the width of the signal with pressure although a variation might be expected if pressure effects were due to local yielding.

Multiple data points at some pressures indicate records made at different times and include tests of the effects of demagnetizing and of reducing the gage pressure to zero and repressurizing. Scatter in the data is due to small variations in the position of the circumferential track scanned in relation to the center line of the defects and to slight variations in the current in the electromagnetically energized detector. Within experimental errors data points appear to be both repeatable and reversible.

4.5 THE EFFECT OF DEFECT DEPTH ON SIGNAL AMPLITUDE VARIATION

Similar analysis of the amplitude of the signals from other defects showed similar variations with pressure. In particular the inversion pressure for far side defects with 20%, 40% and 60% pipewall penetration and 40% near side defect signals was identical. Fig. 16 shows the variation with internal pressure of the average of the normalized signal amplitude for all such signals. Similiar behaviour is found for differentiated and doubly differentiated records as shown in Figs 17 and 18.

These results are interpreted to preclude the possibility of their being due to local yielding in the

vicinity of the defects since the inversion presure would then be expected to depend on the depth of the defect.

4.6 THE EFFECT OF LINE PRESSURE ON NOISE

The effect of internal presure on noise (due to the magnetic irregularities of the pipe) was examined by removing the known defect signals from the records and determining the standard deviations of the remaining lengths of records. These are shown as funcions of pressure in Figs 19, 20 and 21 for the leakage fields, the differentiated records and the doubly differentiated records respectively. In all cases the noise levels fall monotonically with increasing pressure and again the effects are both reversible with pressure and repeatable after demagnetization and after depressurizing and repressurizing. In this case the results were as anticipated and are thought to be due a tendency for stress to average local magnetic irregularities over larger areas at higher stress.

4.7 THE EFFECT OF LINE PRESSURE ON SIGNAL/NOISE RATIO

A parameter of great significance in assessing record quality is, of course, signal to noise ratio. This varies with pressure due to both the variation of the signal and of the noise. The resultant variation in signal to noise ratio with pressure for leakage field records, differentiated and doubly differentiated records are shown in Figs 22, 23 and 24. The most favourable signal to noise ratios are obtained at the highest pressures and are also rising most rapidly then.

4.8 INTERPRETATION OF RESULTS

Fig. 25 shows a greatly simplified leakage flux detector together with some resulting field lines. For still greater simplicity we will consider only the axial component of the field in the pipe wall, whose variation with axial displacement is also shown. As the detector is moved along the pipe, a fixed part of the wall will first of all experience a small reverse field as the detector approaches, then a strong forward field as the flux connectors (often steel brushes) pass, then a slightly reduced field towards the center of the detector (due to slight circumferential flux spreading and leakage), then a

further strong forward field as the trailing flux connectors pass and then a slight reverse field which decays to zero. The corresponding B-H hysteresis sequence is shown in Fig. 26. It is dominated by a large assymetric loop predominantly in the first quadrant with its maximum value tending toward saturation.

4.9 CONCLUSIONS AND RECOMMENDATIONS

We have shown that gas line pressure typically has a significant effect on the performance of magnetic leakage flux detectors used for in service inspection of pipelines. In general increasing pressure and hence tensile stress in the wall tends initially to lower the amplitude of defect induced signals. As the pressure is further increased the effect is reduced and then reversed until, at high pressure, there is a substantial increase in signal amplitude. The effects are reversible with pressure and independent of defect penetration. Noise is reduced with increasing pressure so that the best signal to noise ratios are obtained at the highest pressures.

The effects are considered to be due to overall stress induced changes in permeability of the pipe wall steel in the general vicinity of the detector but not directly localized to the defect. A modest tensile stress causes a slight increase in the general slopes (increased permeabilities). The effect is diminished at greater stress and reversed at high stress (permeability reduced).

It should be noted that, particularly for the pipeline steels under investigation, the effects of stress on magnetization are very complex and that this explanation of the effects of gas line pressure on stress can only be considered to be a first simple identification of the likely dominant mechanisms responsible for our experimental findings.

The first recommendation arising from this work is concerned with defect detection and is that, the highest possible pressure is preferrable in order to give the maximum signal to noise ratio and therefore maximum sensitivity.

The second recommendation is probably more important and also less obvious and is concerned with the assessment of the potentially injurious effects of defects which have been detected. The most important factor to be considered is shown by fracture mechanics analysis to be defect penetration. This is generally assessed from signal amplitude by comparing the amplitude of the signal from the defect under consideration with a set of calibration signals obtained from known, probably artificial, defects

of measured penetration in a test pipe through which the tool is run for calibration. It is now clear tnat, for these calibration signals to be meaningful, the pressure in the test line used for tool calibration must be similar to the pressure in the line inspected or that corrections to signal amplitude must be made before determining their depth and assessing their severity.

5. DESIGN FOR A TEST RIG FOR PIPELINE BENDING STRESS MONITORING USING INTERNAL MAGNETOMETER SURVEYS

5.1 INTRODUCTION AND OBJECTIVES.

Previous field measurements (3) during pipeline construction and laboratory scale testing (4,5) of bending pipes have shown that bending stress produces readily detectable changes in the magnetic fields measured at typical burial depths above large pipelines. This raises the possibility of monitoring lines laid on unstable terrain, such as permafrost or river crossings. Anomalous stresses or changes in stress would be detectable from changes in the magnetic fringing fields. For lines which are capable of being pigged (inspected internally using tools which are blown through the pipe by gas pressure), monitoring could be performed internally using pig-born magnetometers and this would have the advantage of better control of the path followed in making the magnetometer surveys. Testing of interior surveys under well controlled conditions is needed. Previous laboratory tests were made using 110mm diameter pipe and only external field measurements could be made. A larger scale test system would be needed in order to allow the magnetometer surveys to be made inside the pipe. This section report considers how this might best be done.

The objectives and findings of previous laboratory scale testing are first reviewed, then the objectives of larger scale bending stress monitoring tests and demonstration are detailed and discussed.

Previous laboratory scale tests used two steel pipes 3.8 m long x 110 mm diameter. These could be oriented at any angle to the earth's field. The pipes were separated in the middle by a saddle and could be stressed in bending by holding them together with a cable at one end and using a jack to spring the other ends together. The effects of internal line pressure were tested using hydraulic pressure. The objectives and findings are summarized below. Further details are contained in references 4 and 5. Concurrent studies of the effect of stress on the magnetization of small samples of pipeline steels (2) proved crucial to the interpretation of these results.

The initial objectives of the previous tests were to investigate the effects of varying bending stresses within the elastic range, to determine the effects of orientation

with respect to the earth's field and to investigate the effects of internal pressure, all in a well controlled laboratory demonstration. It was not clear at first what parameters needed to be controlled but it was learnt that both magnetic and stress histories were important and consequently the effects of demagnetization and remagnetization and of multiple stress cycles were investigated.

It was found that stress induced changes in external magnetic fields due to bending and/or internal pressure were readily detectable and showed both reversible and irreversible components. The changes increased with the applied stress but were only slightly affected by the pipes' orientation in the earth's field. The changes due to stress generated by either bending or internal pressure were similar. The radial field changes were most distinct and produced a pattern resembling that of a bar magnet of approximately the length of the pipe. Most of the irreversible changes occured during the intial stressing. Subsequent stress cycles produced reversible changes smaller than the irreversible changes by factors of typically 10. The irreversible changes were an order of magnitude larger for pipes magnetized to simulate magnetic inspection pigging than for demagnetized pipes. Remagnetization after multiple stress cycling of magnetized pipes produced large changes in the fringing fields due to the large change in magnetization but the large irreversible changes of field with stress were also reinitialized and were the dominant factor in the next application of stress.

In pipeline inspection applications, differences between a recent magnetometer survey and an earlier baseline survey would be examined. Ideally the baseline would be established following a magnetic inspection and several normal pressure cycles. This would make the technique relatively insensitive to working stress fluctuations (since the associated magnetization changes would be small) but sensitive to higher stresses since the associated magnetization changes would be irreversible and large. Abnormal bending stresses would cause anomalous changes in the magnetometer survey logs. This would therefore monitor the maximum stress that the line had been subjected to since the last magnetic inspection pigging.

The major objective in considering a larger scale demonstration and test system is the need to make magnetometer scans inside the pipe, probably along the pipe axis. We expect to use a relatively compact fluxgate magnetometer for this, but the probes are nearly 10 cm long with an active length of a few cms. This implies a pipe diameter of not less than 20 cm and preferrably

somewhat larger.

The second objective is to try to minimize end effects. In previous tests field changes occured over virtually the full length of pipe under test. It would be desireable to use a relatively short stressed section in a relatively longer total length of pipe.

Our previous work has shown that there are some effects which probably do not need further examination at this stage, namely internal line pressure and the earth's field. The magnetic effects of internal pressure and bending stress appear to be similar (ref. 5) and so hydraulic simulation of gas line pressure is not needed. Investigating bending stress only will be a great help in this case because we will be working inside the pipe and sealing it would be difficult. Orientation in the earth's field has a significant effect on the magnetic fields around a pipe but it is not important so far as the stress induced magnetization changes are concerned. There is therefore no need for more than a relatively simple alignment system for the test line. It should be noted that our previous work has shown that it is absolutely essential to be able to magnetize and demagnetize the pipe under test and that magnetic east-west alignment is required for demagnetization.

5.2 DESIGN CONCEPTS

It was decided that the concept used to stress the pipe should be able to produce yield stress (500 MPa) in a pipe with a diameter not less than 20cm (8"). A number of different concepts were evaluated: such as "the nutcracker" (two pipes bent against each other over a central saddle, see fig.27) "the bow" (a single pipe used as a member of a simple truss, see fig.28a and fig.28b), a simple supported line loaded by its own weight (fig.29), a line loaded by a moment at one end (fig.30), a line with a fixed end condition (fig.31) and a supported line with deloadable weights (fig.32).

The nutcracker (Fig.27) used in previous experiments (5,12) had the advantage that the system itself was stable without any need for anchor other than simple supports. The second advantage was that the two pipes formed a closed magnetic circuit to facilitate magnetization and demagnetization. A disadvantage is that the second pipe will affect the magnetic field of the pipe under investigation.

Regarding anchor demands the bow configurations shown in fig.28a and 28b are similar to the nutcracker. Both have the advantage that the system is stable in itself and does not require the transfer of reaction forces to the ground. Changing to the double column bow (fig.28b) does not change the wire tension required, but it provides a region of constant stress between the columns which is convenient for our investigations. Wire tension could be created with a hydraulic cylinder, a turnbuckle, or other hoisting/pulling device.

A supported line loaded by its own weight (Fig.29) was then considered but the length needed made the test bed inconveniently long. For a pipe with 25cm (10") diameter a length of approximately 60 m is needed to create yield stress.

A pipe loaded by applying a moment directly at one end (Fig. 30) has the advantage of constant stress between the supports and unstressed sections beyond the supports. This configuration gives easy access to the pipe from all sides but creating the moment is a difficult problem. A similar system under consideration was a piece of pipe with one end fixed and, if needed, a load at the free end (Fig. 31). A length of 30m (95') is needed to create yield stress in a pipe with 25cm (10") diameter, and the deflection at the free end is approximately 4.6m . Again it is a difficult task to create the fixed end condition and the large deflection makes the test bed inconveniently nigh.

A supported line with deloadable weights (Fig.32) was investigated and found to be a simple way of loading the pipe. By laying the pipe on two supports and loading it with weights placed inside or outside of these, the pipe between the interior load points is under a constant moment and therefore a constant bending stress. Concrete blocks supported by jacks are an easy way of adjusting the load, and extending the pipe past the outer load points provides the desired unstressed sections.

The supported line with deloadable weights and the two bow configurations are good methods of loading the pipe. The bow configurations are easier to handle because they do not involve large concrete blocks. The "two column bow" is recommended because it provides a region of constant stress. Magnetically, two cylinders are dimensionally similar if they have the same length to diameter ratio (l/d). Real pipelines are constructed from joints of pipe typically 12m in length. Before construction each joint is naturally magnetized in the axial direction (with N and S poles near the ends) and after construction each joint retains, to a first approximation, its individual magnetic identity. This

observation has not been investigated for pipelines which have been magnetized after construction (e.g. by magnetic inspection tools) and so will require further testing but it appears that the magnetic building blocks of a pipeline correspond to the physical building blocks. It is suggested that the experiment use pipe made from joints with l/d = 15 in order to model a 1m (36") pipeline.

Measurements of radial and axial magnetic field changes inside a long pipe as a function of stress and magnetic history have been proposed. Of particular interest are radial and axial fields on the axis of the pipe as well as near the wall (see Fig. 33). To make a meaningful radial field measurement the pipe diameter must be "large" compared to the size of a magnetometer probe (0.9cm dia. x 7.6cm long, see Instrumentation and Data Acquisition). A pipe diameter of 25cm (10") represents a compromise between radial field resolution and manageable pipe size.

Schemes for applying a bending stress up to the yield point have already been discussed. The preferred method makes the pipe a member of a simple truss (see Fig. 34). To keep load handling equipment down to a manageable size and to provide an adequate region of constant stress, an outer load point span of 14m (with a 2m inner load point span) is the shortest suggested length for the pipe. A layout such as Fig.34, where at least one end (and preferably both ends) contains an unstressed joint, could be used to simulate bending stress in the middle of an infinite pipe.

The first requirement is space. Previous work (4,5) has shown that the pipe's axis must be perpendicular to the earth's field to achieve complete demagnetization. The location must therefore have enough room to mount the pipe horizontally and align it in an east-west direction. The mountings should permit about +/- 3 degrees of directional adjustment. Poured concrete, railway ties, or even exposed bedrock would make suitable platforms for the loads and supports. Some excavation and construction may be necessary but the installations need not be permanent.

A second requirement for good demagnetization and good magnetic measurements in general is ambient field homogeneity. The pipe must be located "far" from large ferromagnetic objects such as structural steel, automobiles, etc. The meaning of "far" is not well defined but a minimum of 30m from a garbage truck has proven necessary in the past and therefore a minimum distance of 50 m from other activities is recommended. A vacant lot would probably be adequate, the rooftop workspace used previously (5) would probably not be adequate because of the high field gradients encountered

(not to mention the structural difficulties).

The third requirement is shelter and power. The pipe itself need not be enclosed but the instrumentation systems will need protection. If no building is available a small garden shed or other portable structure could be erected. The estimated minimum power requirements are 20 A, 120 VAC. Most of this will be used to magnetize/demagnetize and to pull instrumentation through the pipe. If the site is not serviced a portable generator could be used.

5.3 INSTRUMENTATION AND DATA ACQUISITION

The three variables to be measured are magnetic field, probe position and stress/strain. Appropriate instrumentation and data acquisition are discussed below.

The experiment requires measurement of vector components of a magnetic field to the following specifications

resolution: +/- 10 nT
dynamic range:+/- 20,000 nT (minimum),'+/- 100,000 nT (preferred)
baseline: +/- 60,000 nT (minimum), +/- 100,000 nT (preferred)
directional resolution: +/- 1 degree
spatial resolution: sensitive volume (= 50 cm^3.

A fluxgate magnetometer is the instrument best suited to this application.

Previous measurements of magnetic field changes near stressed pipes (5,12) were made using an RFL Model 101 fluxgate magnetometer (RFL Industries Inc., Boontown, N.J.). This is a single axis device with a probe size of 1.9cm dia. by 12cm long. It meets the requirements above (+/- 100,000 nT dynamic range, +/- 60,000 nT baseline) but the construction is not particularly rugged. The major weakness is the cable connecting the probe to the electronics which would have to be lengthened from 3m to 30m with unknown effects on instrument response.

Also available is an EDA Model FM-100B fluxgate magnetometer (EDA Instruments Inc., Toronto, Ont.). This is a 3 axis device with a probe size of 0.9cm dia. by 7.6cm long. It was designed for long-term observation of geomagnetic fields and is a rugged, stable instrument. There is 30m of reinforced cable between the probes and the electronics box. The original dynamic range of +/- 1,000 nT has been extended to +/- 20,000 nT on 2 axes. One of these axes has a baseline of +/- 70,000 nT and the other of +/- 40,000 nT. The improved dynamic range was

found inadequate for previous work (5,12) and will probably have to be extended to +/- 100,000 nT. This is not a difficult modification.

The EDA is the preferred instrument. Although some modifications will be necessary its ruggedness, cabling, 2 axis capability and smaller probes make it superior to the RFL.

Positioning will be required for measurements inside and outside the pipe. This experiment will be concerned mostly with interior positioning but some exterior positioning will be necessary to confirm previous results. Reference coordinates must be chosen carefully in this instance since the pipe will undergo significant deflection between measurements. The reference coordinates for interior positioning will be defined by the axis of the pipe in conventional cylindrical form. The appropriate reference for the exterior positioning system is not as obvious. Previously, (5) used the pipe's axis as an exterior reference and (4) used a combination of the pipe and the fixed earth frame. Both gave similar results but the deflections and rotations involved were small (5-10 cm and +/- 1 degree over 12 m).

The positioning system must provide a voltage proportional to probe position for use by the data acquisition system. An odometer wheel mounted on the probe carrier and rolling on the pipe wall has been suggested. The transducer would be a multi-turn potentiometer or a shaft encoder. For interior measurements, centralizers sprung against the walls would locate the axis of the pipe. For exterior measurements a saddle sliding on fixed rails would define the desired reference frame. Simple beam theory allows accurate calculation of the strain at any point in the pipe from measurement of the deflections. These calculations will be verified by conventional strain gauges.

The minimum data acquisition system will be a notebook (to record stress/strain levels) and an X-Y recorder (to plot magnetic field against position). Since plots of magnetic field differences between stressed and unstressed pipe are required and since the magnetometer has a multi-axis output, a small computerized data acquisition system with 3 channels of analog input and some means of generating hard copy output (a digital plotter or 2 channels of analog output or a graphics printer) would be a useful tool. Our lab already supports a suitable system (Tecmar Labmaster/IBM PC). A preliminary sketch of the complete system is shown in Fig. 35.

5.4 APPARATUS AND METHOD

Both instrumentation and demagnetization piglets must be pulled through the pipe at an estimated maximum velocity of 0.5 m/s. The system shown in Fig. 37 is recommended. It has the advantage that several scans can be made without removing the piglet from the pipe. It also provices the possibility of making scans in both directions and avoids problems with spooling the tow cable. Ease of use, safety and expense are the major considerations in a load handling system of this size.

The deloadable weight scheme uses concrete weights to bend the pipe. The loads involved are approximately 42kN for the dimensions suggested (Fig. 34) but the deflections (34cm) are well within the range of large truck jacks, etc. Hydraulic or mechanical jacks could raise and lower the weights to load and unload the pipe. Hydraulic jacks can be cross-linked to create even load application and also allow load measurement with pressure gauges but they are subject to leaks and creep. Mechanical jacks are harder to operate in unison but they are cheaper and more reliable than hydraulics. Hydraulic lifting and mechanical clamping would be suitable.

The bow scheme creates a bending moment similar to the loaded beam scheme by making the pipe a member of a simple truss. The "two column bow" is the preferred design because there are no bulky weights and only a single tensioning device is required (Fig. 34).

5.5 PIPE DEMAGNETIZATION - A PRELIMINARY STUDY

The ability to demagnetize the specimen is crucial to obtaining meaningful and repeatable results in experiments of this type. A sample can be demagnetized by applying a symmetric AC field whose amplitude is slowly reduced to zero. The initial amplitude must be larger than any field applied since the last demagnetization and the frequency must be low enough to allow full flux penetration (typically 0.1 Hz for large samples). An amplitude reduction rate of 1-5% per cycle gives reliable results for pipeline steel. In this proposal the length of the pipe and the lack of a return flux path make it practically impossible to apply a field to the entire pipe simultaneously. Instead, some sort of piecewise demagnetization must be used. To this end, preliminary demagnetization experiments were completed using the same 110 mm diameter pipe and an electromagnetic piglet (shown

in figure 36).

Several strategies for pipe demagnetization were investigated:

a series of stationary demagnetizations (decreasing amplitude AC current) at short intervals along the pipe

pull-through(s) with constant amplitude AC current whereby each portion of the pipe experiences a decreasing field amplitude as the piglet is pulled away from it

repeated pull-throughs with DC current which is reversed and reduced after each pass

A mounting system was constructed to hold the pipe sample and a two component fluxgate probe. The probe could be positioned repeatably along the pipe at different radii from it. Measurements were taken of axial and radial fields. An electromagnetic piglet, equipped with steel brushes which fitted tightly to the walls of the pipe to provide good magnetic contact, was pulled through the pipe by hand cranks on either end. Data was recorded by plotting the radial field component vs. axial displacement with an X-Y plotter plotter.

During "piecewise" demagnetization runs, the alternating field produced by the piglet was slowly reduced to zero while the piglet was held fast at various positions along the pipe. It was found that this technique actually demagnetized the section near the piglet. Unfortunately, while demagnetizing adjacent sections, the remnant field in still magnetized regions of the pipe remagnetized the first section(s). This was the case when piecewise demagnetization runs were begun at either end or in the center. All such strategies yielded unsatisfactory results.

Single slow AC pull throughs also failed to demagnetize the sample reliably. Many permutations of different induced field magnitudes, frequencies and pull through speeds were examined, all with limited success, although very slow speeds were used (the lowest being approximately 1 mm/s). It is believed that the flux in such a system decays in too short a section behind the piglet to allow the pipe to experience a sufficient number of decreasing amplitude field cycles. At the low frequencies required by skin depth considerations, velocities slower than 0.1 mm/s would be necessary. At these speeds, pull through demagnetization times would be impractically long.

Exploring the usefullness of multiple DC pull throughs, more acceptable results were obtained. This method has the disadvantage that it is somewhat tedious and time consuming but fortunately it works for any magnitude of remnant field. The best technique involves a two part demagnetization as described in the subsequent section.

Although single pull throughs at each DC current level do not demagnetize to especially small fields, this technique can be used to "capture" any remnant magnetization in the pipe and bring the radial field component down to a variation of +/- 15k gamma along the pipe (at two diameters away). This is 2-3 times larger than the final remnant magnetism. The pipe sample can then be further demagnetized by increasing the induced field (current) to 20-30% of its last initial maximum, and pulling the piglet through three times after each current decrement. The necessity for this was determined experimentally and is based on a need to have the flux within the pipe travelling in different direction relative to the pull through direction for effective demagnetization. The resulting radial field profile varies +/- 6k gamma along the length of the sample, as measured two diameters away. This is excluding end effects which remain in the extreme sections; 6-7 pipe diameters from each end.

Of course, the initial piglet current must produce sufficient magnetic intensity, (H), to overcome the remnant magnetism of the sample. Current decrements throughout should be 1-3% of this initial current. Pull through speeds of 0.1 - 0.2 m/s work well for pipe of 0.5 cm wall thickness and for any magnitude of field induced therein.

However, there are precautions which must be heeded in order to obtain acceptable results. Primarily, it is important that the piglet maintains magnetic contact with the pipe throughout each part of the demagnetization process. Attempts to alleviate end effects, by holding the piglet past the steel ends of the pipe while reversing the current direction, proved unsuccessful in DC runs. Discontinuity of the field hampers the success of the demagnetization. In AC trials too, sharp end effects became more drawn out at the opposite end, when the still live piglet was pulled past one end of the pipe.

Furthermore, in the first portion of the demagnetization, best results are obtained if the field induced within the pipe is in the same direction as the direction of travel of the piglet. These effects have been carefully examined experimentally although a precise explanation is difficult due to the complexity of the

situation.

5.6 RECOMMENDATIONS

Both the "bow" (fig.28) or the supported line with deloadable weights (fig.32) appear to be viable approaches. At this stage our preferrence is for the "two column bow" because the groundwork support and the method of applying stress seem slightly simpler.

No detailed costing has yet been made yet, partly because this will almost certainly be site specific. It is clear though that this will not be a multi-million dollar proposal. It is believed that Queen's has available, or can arrange for, a suitable country site for the test system. Our first estimate of the cost is in the $50,000 - $100,000 range and will depend on the final site, the apparatus selected and what auxiliary features are needed including possibly transportation. The first conclusion though is that the system should not be prohibitively expensive.

5.7 CONCLUSIONS

This design proposal was circulated for comment during the fall of 1985. The consensus view was that such a potential technique for detecting and monitoring high bending stress regions in pipelines would be most useful for pipelines transversing unstable terrain such as permafrost regions or offshore lines but the present interest was relatively low.

The study showed that a pipeline bending stress monitoring test rig large enough to demonstrate stress monitoring using internal magnetometer surveys was a feasible proposition and should not be prohibitively expensive. Various design concepts were evaluated and a preferred design selected. Preliminary test were made to establish demagnetization techniques. The assessment suggested that, whilst the technique was felt to be potentially useful, there was little immediate interest in applying it. The proposal is therefore ahead of its time and it is recommended that, until there is more industrial interest in its application, efforts should be concentrated on further understanding the basic effect of stress on the magnetic properties of pipeline steels.

REFERENCES

[1] D. L. Atherton and D. C. Jiles "Investigation of the effects of mechanical stress on the magnetic properties of pipeline steels for pipeline stress monitoring" Final report DSS Contract No. 1 SU81-00265 (CANMET/ImRI), Aug. '83.

[2] D. C. Jiles and D. L. Atherton, "Theory of the magnetisation process in ferromagnets and its application to the magnetomechanical effect", J. Phys. D: Appl. Phys., No. 17, pp. 1265-1281, 1984.

[3] D. L. Atherton and A. Teitsma, "Detection of anomalous stresses in gas pipelines by magnetometer survey", J. Appl. Phys., Vol. 53, No. 11, pp. 8130-8135, Nov., 1982.

[4] D. L. Atherton, L. W. Coathup, D. C. Jiles, L. Longo, C. Welbourn and A. Teitsma, "Stress Induced Magnetisation Changes of Steel Pipes - Laboratory Tests", IEEE Trans. on Magnetics, Vol MAG-19, No.4 pp. 1564-1568, July 1983.

[5] D. L. Atherton, C. Welbourn, D. C. Jiles, L. Reynolds and J. Scott-Thomas, "Stress-Induced Magnetization Changes in Steel Pipes - Laboratory Tests, Part II" IEEE Trans. on Magnetics, MAG-20, Vol. 6, pp.2129-2136, Nov. 1984.

[6] D. L. Atherton and C. Welbourn "A Rotating Drum Test Rig for the Development of Pipeline Monitoring Tools", C.S.N.D.T. Journal, Vol. 6 No. 6, pp.51-56, Sept. 1985.

[7] B. K. Tanner , J. A. Szpunar, M. G. Hetherington and J. P. Jacubovics," High voltage Lorentz electron microscopy studies of domain structure in pearlitic steels", Phil. Mag. (to be published)

[8] J. A. Szpunar and B. Szpunar,"Magnetic domains in construction steel", IEEE Trans. on Magnetics, vol Mag-21, No.6, pp 2613-2619, Nov. 1985.

[9] J. A. Szpunar and B. Szpunar,"Simple model of the magnetic interaction between grains", J. Appl.

Phys. vol 58, pp 4465-4467, Dec 1985.

[10] W. F. Brown, Phys. Rev. "Irreversible magnetic effects of stress", vol 75, pp 147, 1949.

[11] L. Brugel and G. Rimet," Interpretation des effets irreversibles des contraintes au moyen d'un modele d'hysteresis dans l'espace", Journal de Physique", vol 27, pp 589-597.

FIGURE CAPTIONS

Fig. 1: Schematic diagram for magnetic measurements.

Fig. 2: The rotating drum test rig showing a magnetic leakage flux detector, with electromagnet excitation, pressed against the outer surface.

Fig. 3: A block diagram of the data acquisition system. Positional information is provided by an incremental shaft encoder driven by an odometer wheel rolling on the pipe. Each pulse from the shaft encoder triggers a sample burst on the ADC. Digital data is processed by a microcomputer. Hard copy is available from a plotter. The shaft encoder pulses can also be counted and the total converted to an analog voltage for use with direct displays such as a storage oscilloscope or analog plotter. An optical or mechanical trigger synchronizes counter resets with drum rotation. A frequency counter on the shaft encoder output measures surface speed.

Fig. 4: The electromagnetically excited magnetic leakage flux detector used both for obtaining leakage flux signals and also for demagnetizing tracks around the drum by using AC through the coil.

Fig. 5: The radial component of the magnetic leakage flux density recorded around the circumference of the sealed drum with an internal gage pressure of 0.

Fig. 6: The radial component of the magnetic leakage flux density recorded around the circumference of the sealed drum with an internal gage pressure of 2.8 MPa.

Fig. 7: The radial component of the magnetic leakage flux density recorded around the circumference of the sealed drum with an internal gage pressure of 6.9 MPa.

Fig. 8: Differentiated radial component of the magnetic leakage flux density recorded around the circumference of the sealed drum with an internal gage pressure of 0. (This gives the output which would be obtained from an inductive sense coil).

Fig. 9: Differentiated radial component of the magnetic leakage flux density recorded around the circumference of the sealed drum with an internal gage pressure of 2.8 MPa.

Fig. 10: Differentiated radial component of the magnetic leakage flux density recorded around the circumference of the sealed drum with an internal gage pressure of 6.9 MPa.

Fig. 11: Second differential of the radial component of the magnetic leakage flux density recorded around the circumference of the sealed drum with an internal gage pressure of 0. (This gives the output which would be obtained from a bucking pair of inductive sense coils).

Fig. 12: Second differential of the radial component of the magnetic leakage flux density recorded around the circumference of the sealed drum with an internal gage pressure of 2.8 MPa.

Fig. 13: Second differential of the radial component of the magnetic leakage flux density recorded around the circumference of the sealed drum with an internal gage pressure of 6.9 MPa.

Fig. 14: The variation of amplitude of the signal from a 60% penetration far side defect with internal line pressure, shown for increasing pressure.

Fig. 15: The variation of amplitude of the signal from a 60% penetration far side defect with internal line pressure, shown for increasing and decreasing pressures.

Fig. 16: The variation with pressure of the average normalized signal amplitude for the radial field component of the leakage flux from 20, 40, and 60% penetration far side defects and a 40% near side defect.

Fig. 17: The variation with pressure of the differentiated normalized signal amplitude for the radial field component of the leakage flux from 20, 40, and 60% penetration far side defects and a 40% near side defect.

Fig. 18: The variation with pressure of the average normalized doubly differentiated normalized signal amplitude for the radial field component of the leakage flux from 20, 40, and 60% penetration far side defects and a 40% near side defect.

Fig. 19: The variation with pressure of the standard deviation of the noise.

Fig. 20: The variation with pressure of the standard deviation of the differentiated noise.

Fig. 21: The variation with pressure of the standard deviation of the doubly differentiated noise.

Fig. 22: The variation with pressure of the signal to noise ratio for the leakage flux record.

Fig. 23: The variation with pressure of the signal to noise ratio for the differentiated leakage flux record.

Fig. 24: The variation with pressure of the signal to noise ratio for the doubly differentiated leakage flux record.

Fig. 25: Simplified magnetic leakage flux detector and corresponding profile of the axial component of the field in the pipe wall. As the detector passes over a given section of pipe it experiences first of all a small reverse field, [2], then a high forward field at the flux connector. [3], followed by a slightly reduced field due to spreading of the flux toward the center of the detector, [4], then another peak field at the trailing flux connector [5] which is followed by another slight reverse field, [6].

Fig. 26: B - H plot of the magnetization sequence due to the axial field variation shown in Fig. 25.

Fig. 27: "The Nutcracker" Two pipes bent against each other over a central spacer.

Fig. 28: "The Bow" A single pipe used as a member of a simple truss.

Fig. 29: A pipe loaded by its own weight.

Fig. 30: A pipe loaded by applying a moment at one end.

Fig. 31: Cantilevered pipe with fixed end.

Fig. 32: Supported pipe loaded with weights. Positions of supports and weights may be interchanged.

Fig. 33: Cross section of pipe showing suggested positions of magnetometer probe.

Fig. 34: Suggested pipe dimensions for either the "two-column bow" or the "deloadable weight" loading schemnes.

Fig. 35: Data acquisition system.

Fig. 36: Magnetizing/Demagnetizing piglet.

Fig. 37: Pull-through system for instrumentation and

demagnetization.

Fig. 38: The two column bow - detail.

Fig. 39: Diagram of loads and dimensions for the two column bow loading scheme.

Fig. 40: Diagram of loads and dimensions for the deloadable weight loading scheme.

SCHEMATIC: ELECTROMAGNET
MAY. 1986 (SYSTEM ELECTRONICS)

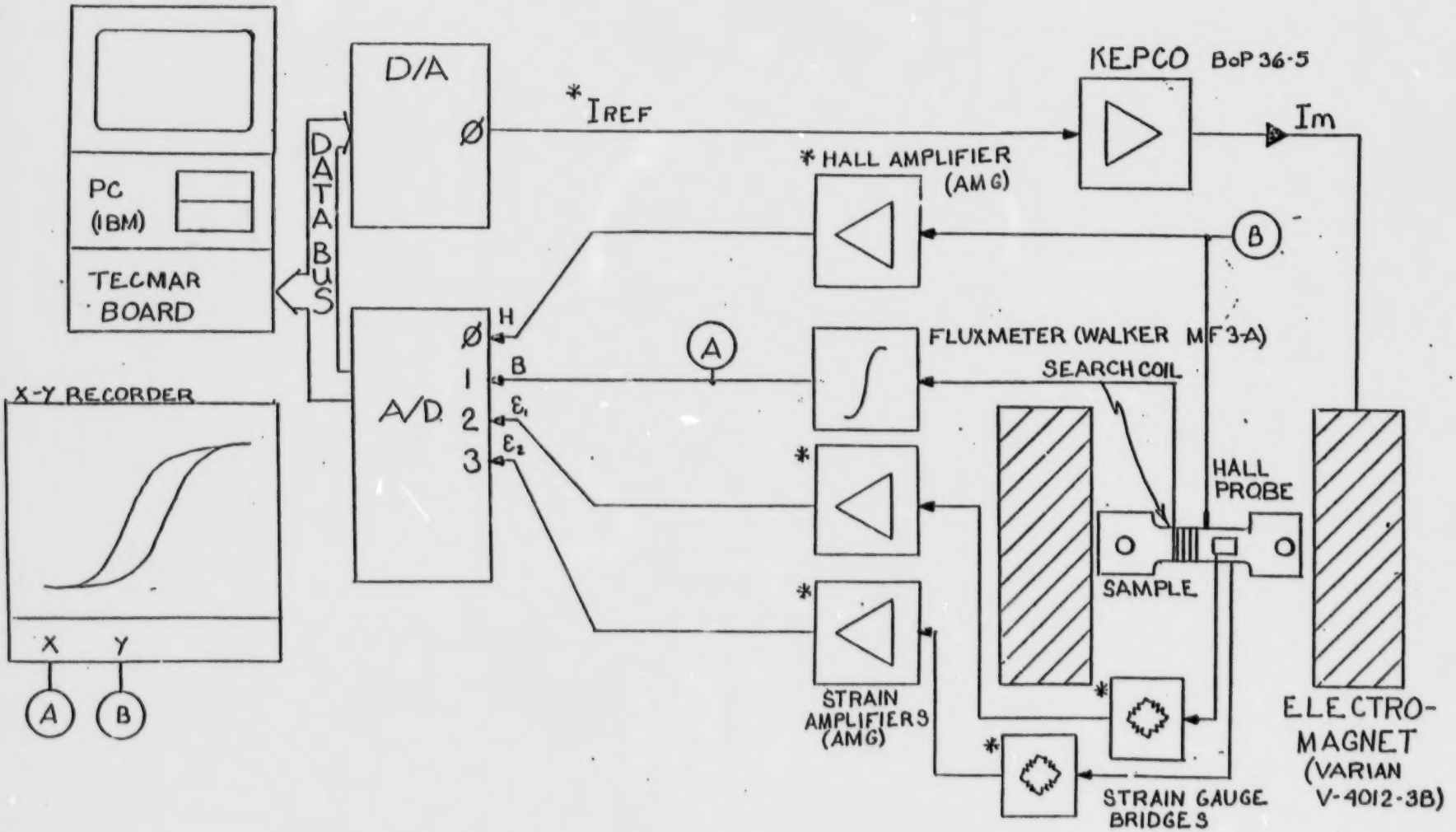

NOTE: * - INDICATES CHANGE FROM DEC. 1985 SYS

Fig.1: Schematic diagram for magnetic measurements.

Fig. 2: The rotating drum test rig showing a magnetic leakage flux detector, with electromagnet excitation, pressed against the outer surface.

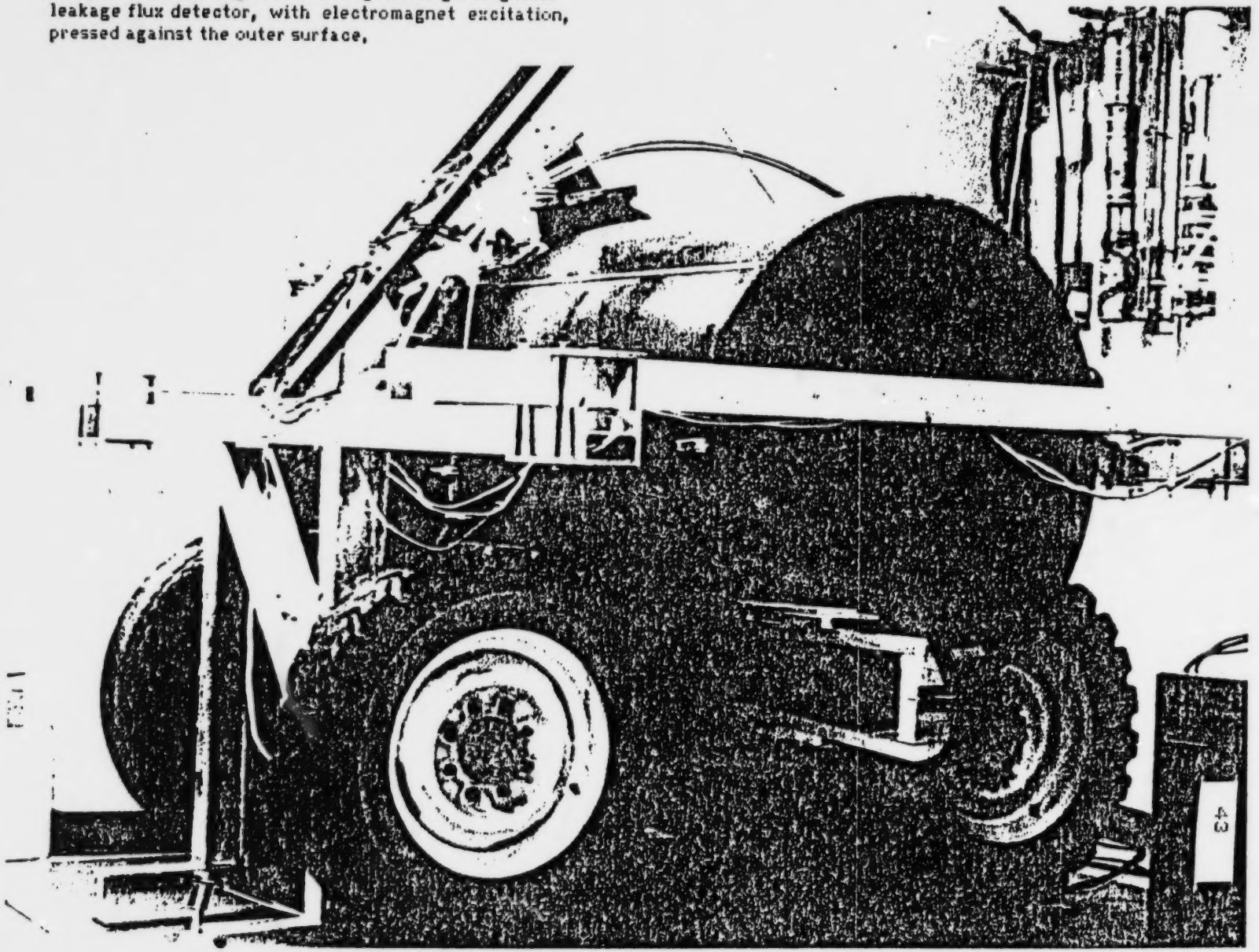

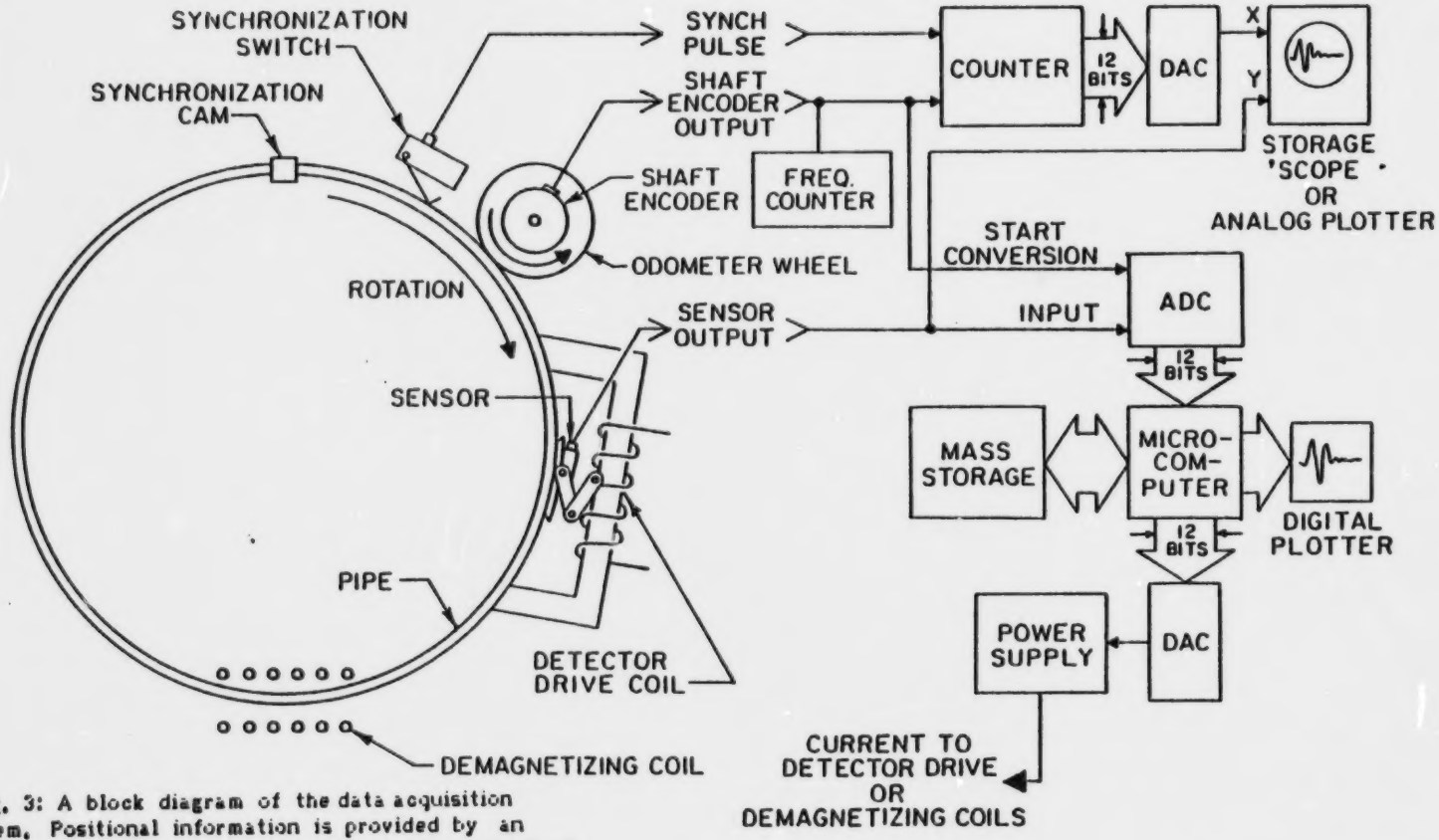

Fig. 3: A block diagram of the data acquisition system. Positional information is provided by an incremental shaft encoder driven by an odometer wheel rolling on the pipe. Each pulse from the shaft encoder triggers a sample burst on the ADC. Digital data is processed by a microcomputer. Hard copy is available from a plotter. The shaft encoder pulses can also be counted and the total converted to an analog voltage for use with direct displays such as a storage oscilloscope or analog plotter. An optical or mechanical trigger synchronizes counter resets with drum rotation. A frequency counter on the shaft encoder output measures surface speed.

Fig. 4: The electromagnetically excited magnetic leakage flux detector used both for obtaining leakage flux signals and also for demagnetizing tracks around the drum by using AC through the coil.

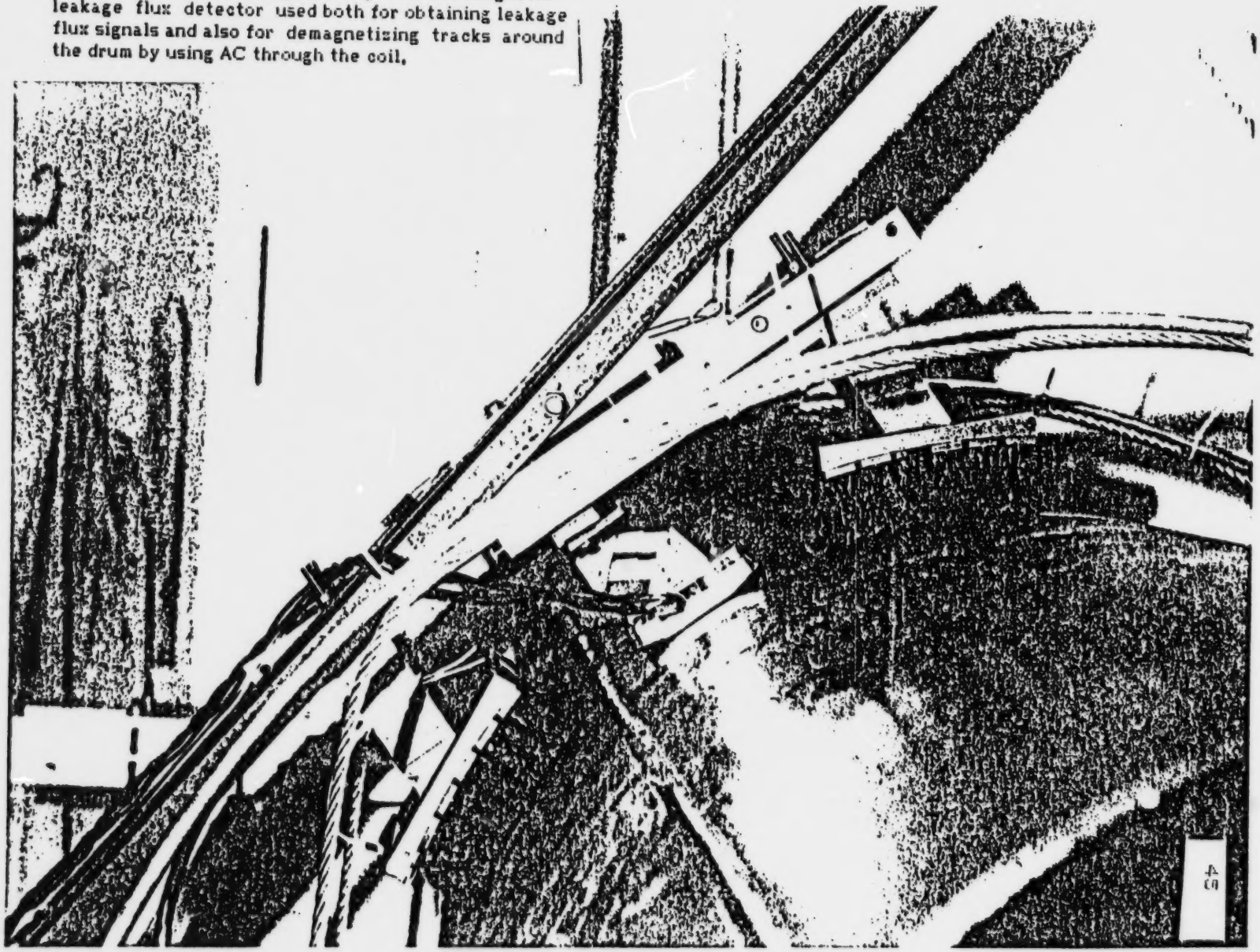

Fig. 5: The radial component of the magnetic leakage flux density recorded around the circumference of the sealed drum with an internal gage pressure of 0,

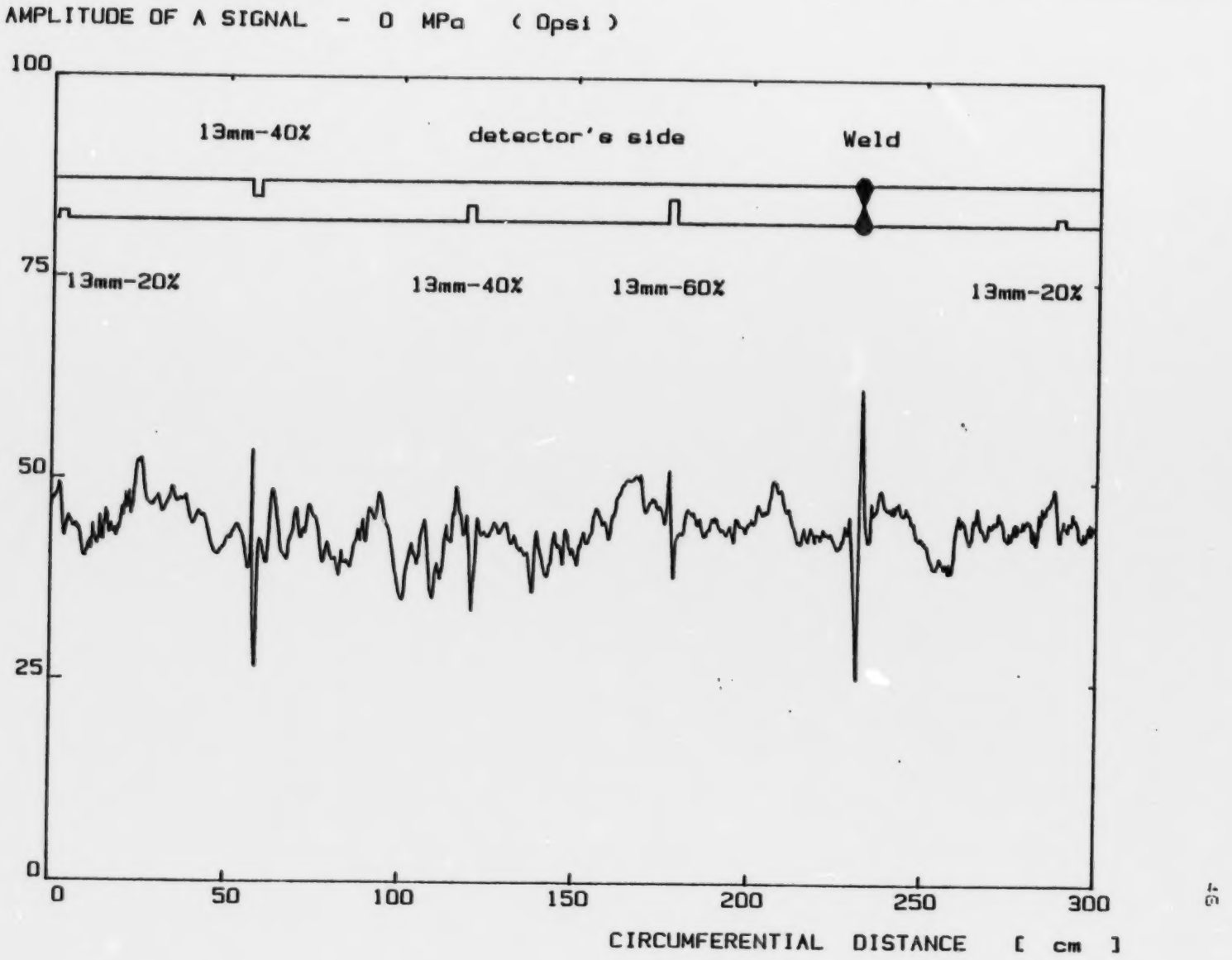

Fig. 6: The radial component of the magnetic leakage flux density recorded around the circumference of the sealed drum with an internal gage pressure of 2,8 MPa.

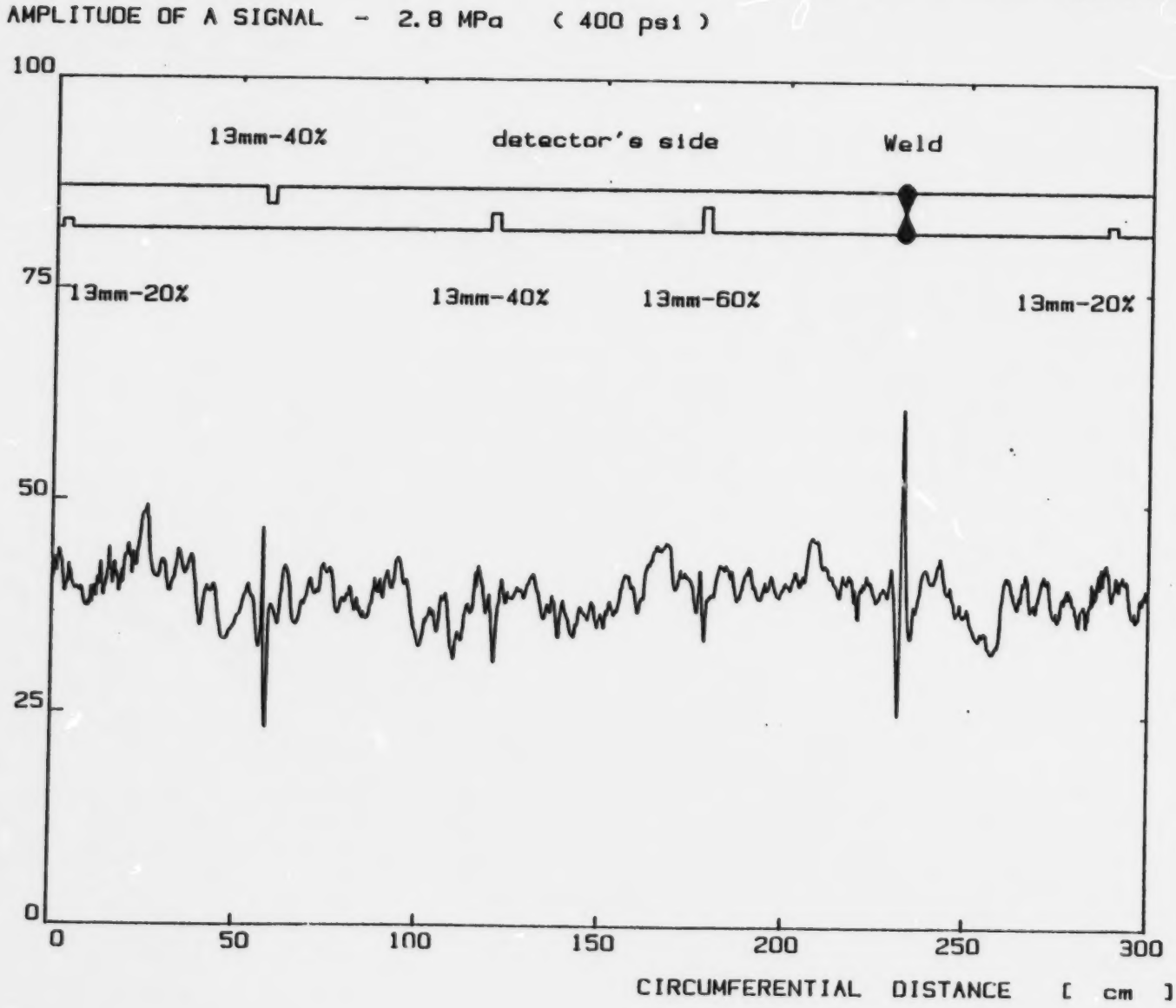

Fig. 7: The radial component of the magnetic leakage flux density recorded around the circumference of the sealed drum with an internal gage pressure of 6.9 MPa.

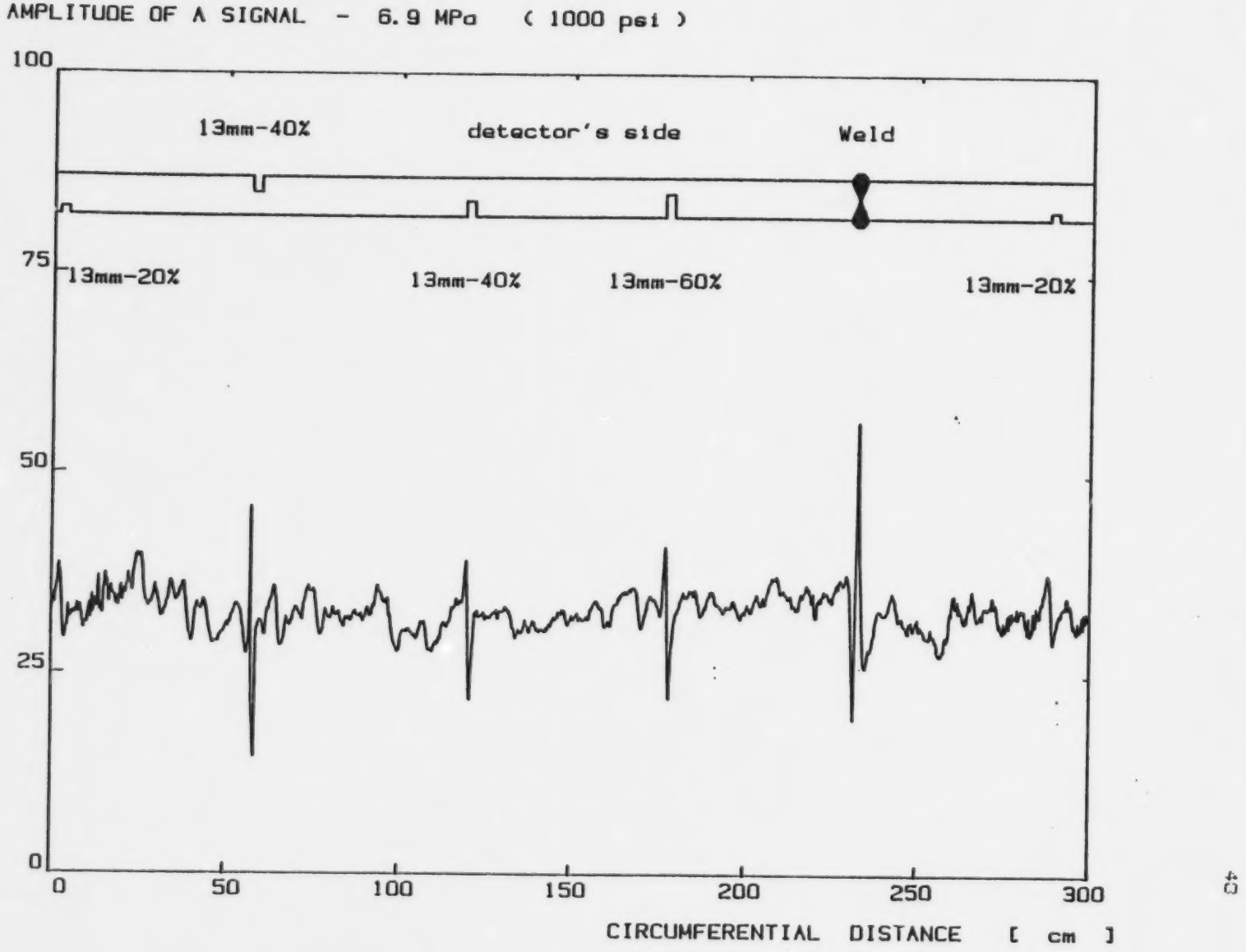

Fig. 8: Differentiated radial component of the magnetic leakage flux density recorded around the circumference of the sealed drum with an internal gage pressure of 0. (This gives the output which would be obtained from an inductive sense coil).

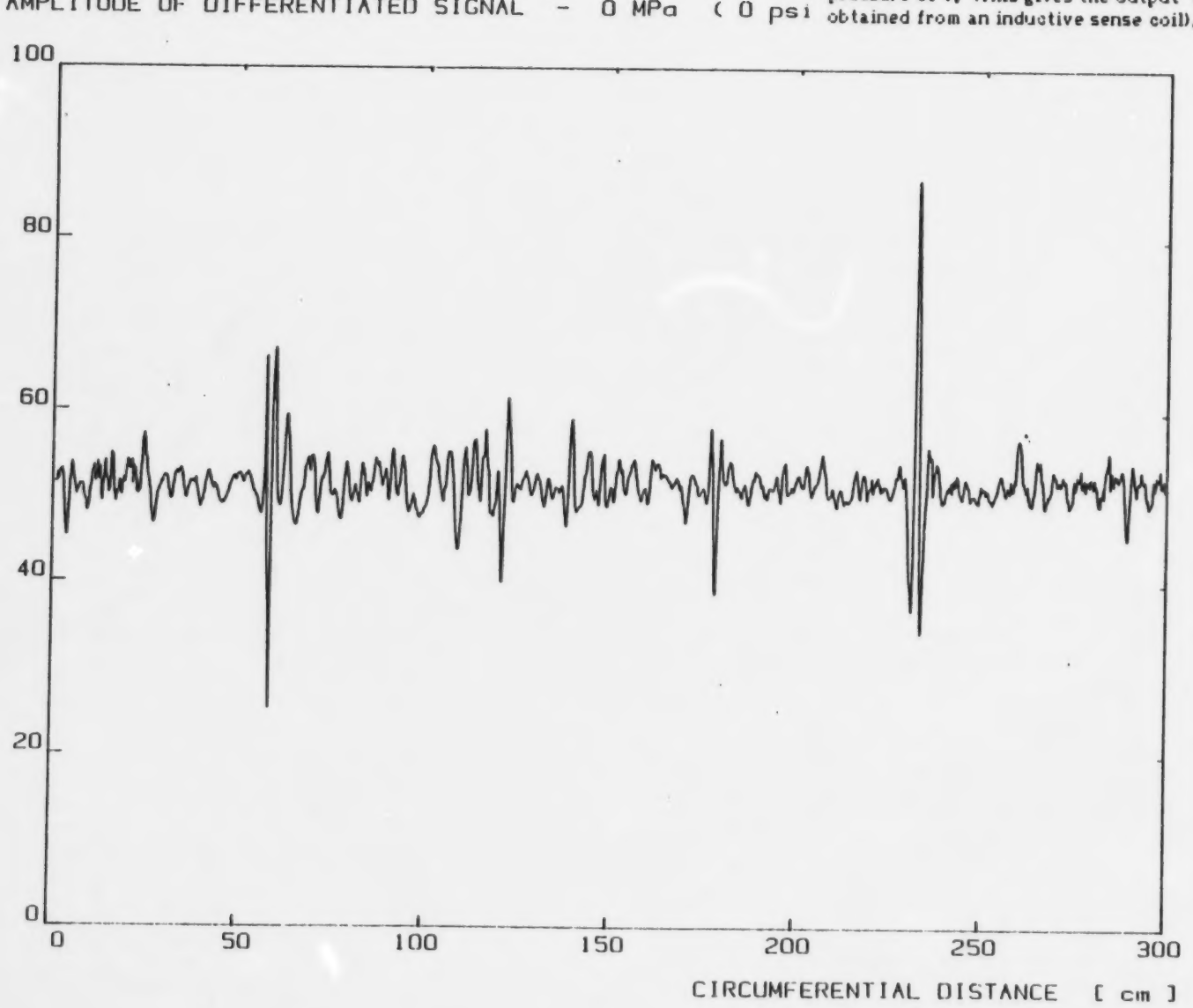

Fig. 9: Differentiated radial component of the magnetic leakage flux density recorded around the circumference of the sealed drum with an internal gage pressure of 2,8 MPa.

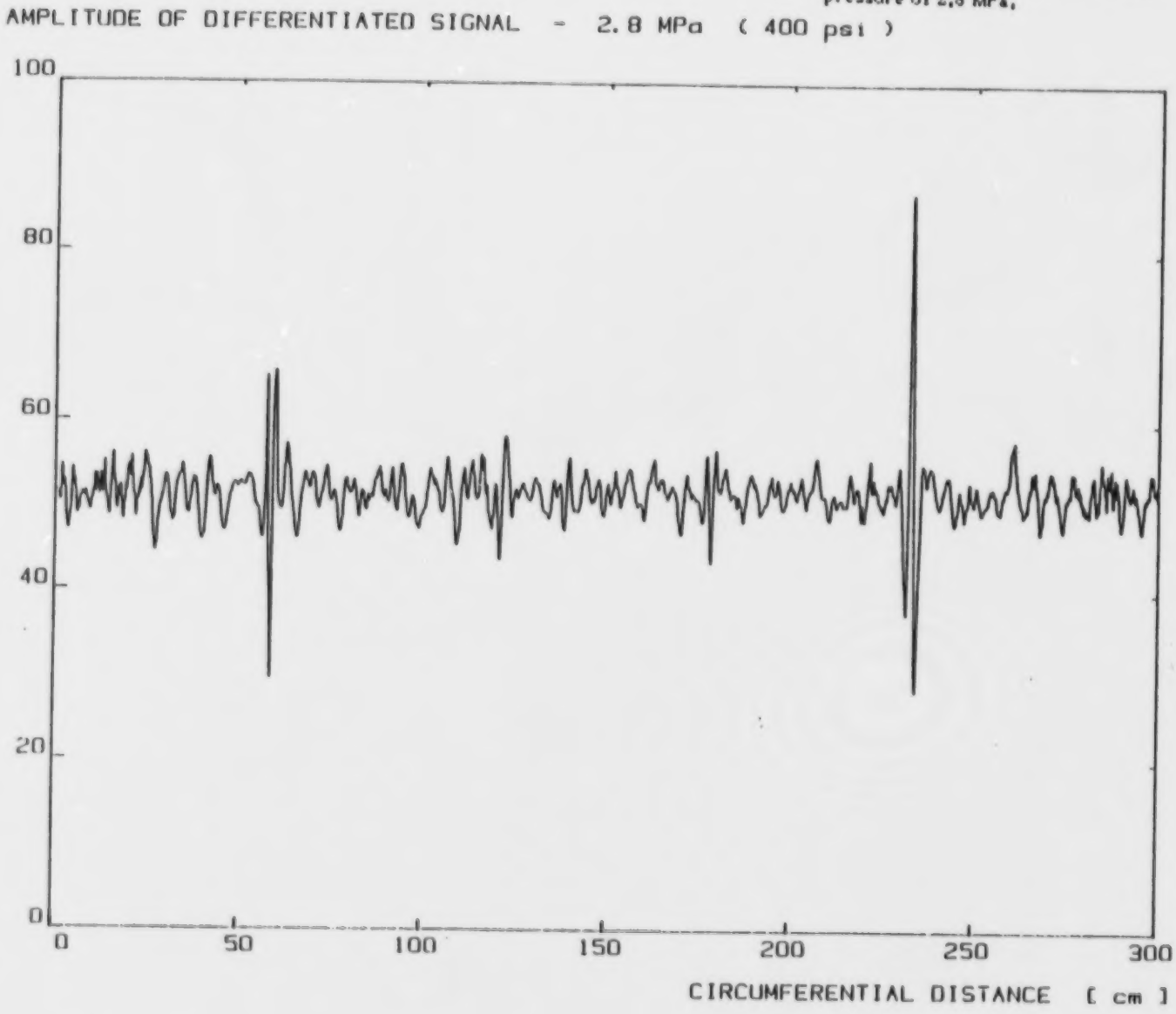

Fig. 10: Differentiated radial component of the magnetic leakage flux density recorded around the circumference of the sealed drum with an internal gage pressure of 6,9 MPa.

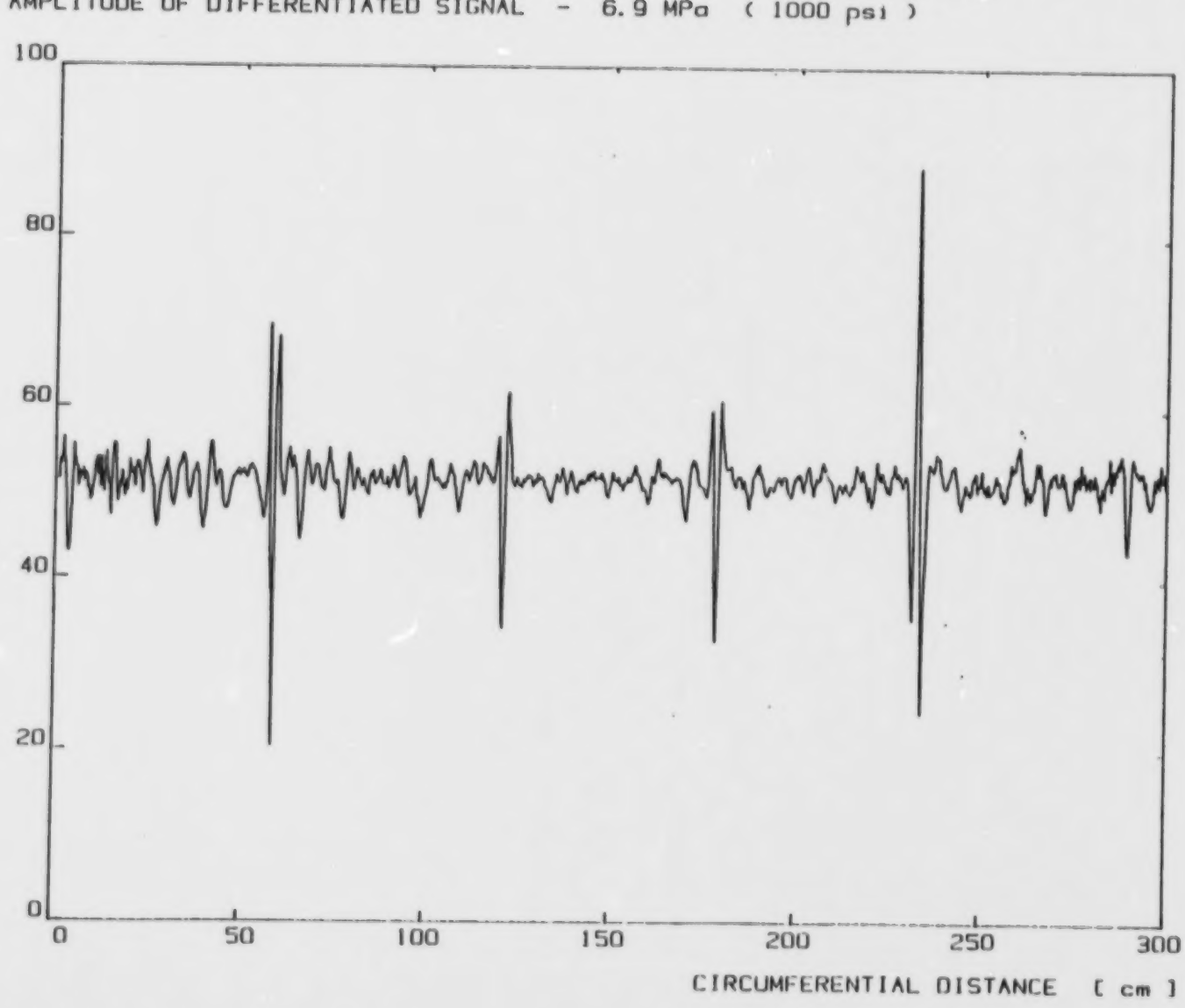

Fig. 11: Second differential of the radial component of the magnetic leakage flux density recorded around the circumference of the sealed drum with an internal gage pressure of 0, (This gives the output which would be obtained from a bucking pair of inductive sense coils).

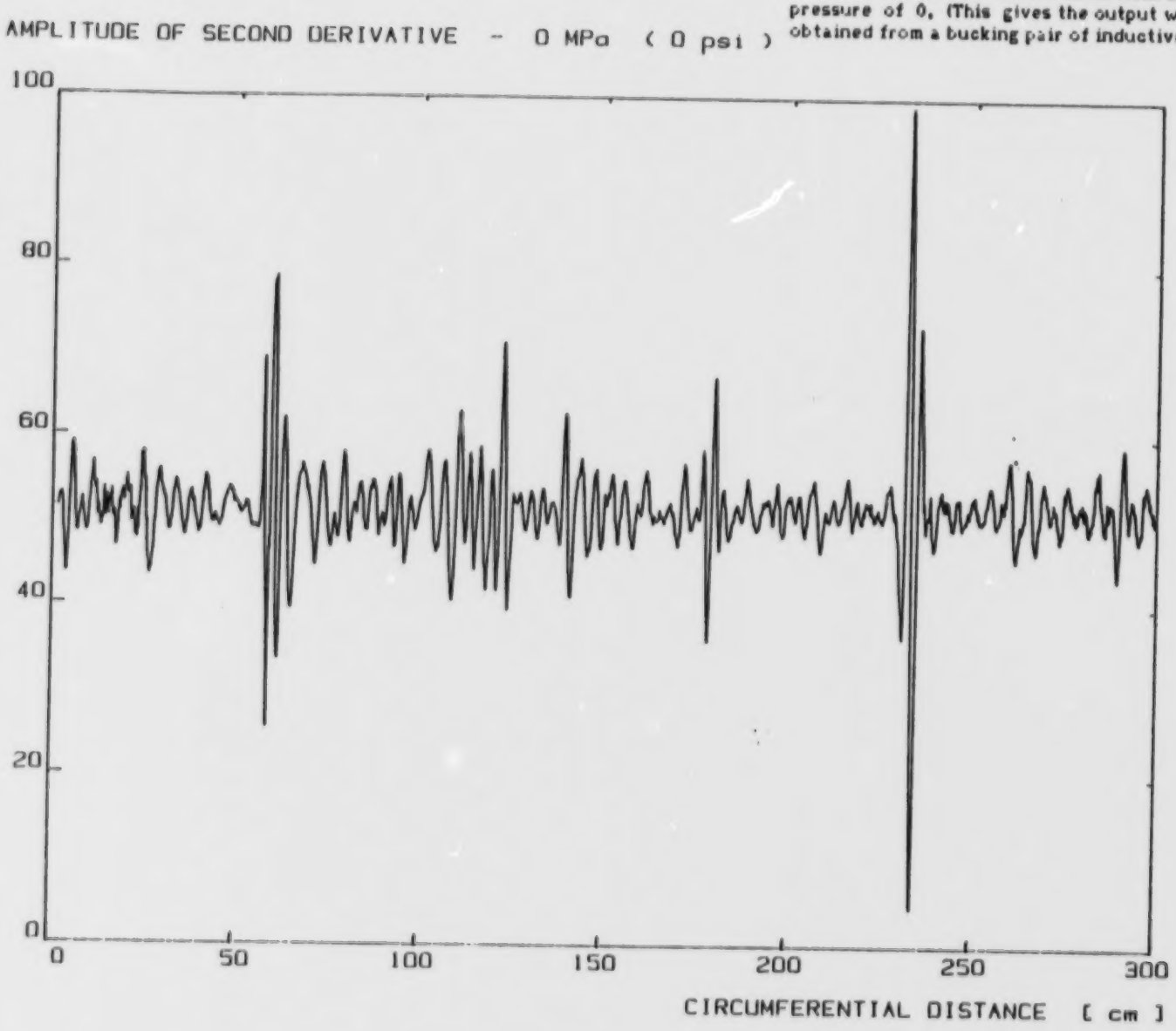

Fig. 12: Second differential of the radial component of the magnetic leakage flux density recorded around the circumference of the sealed drum with an internal gage pressure of 2,8 MPa.

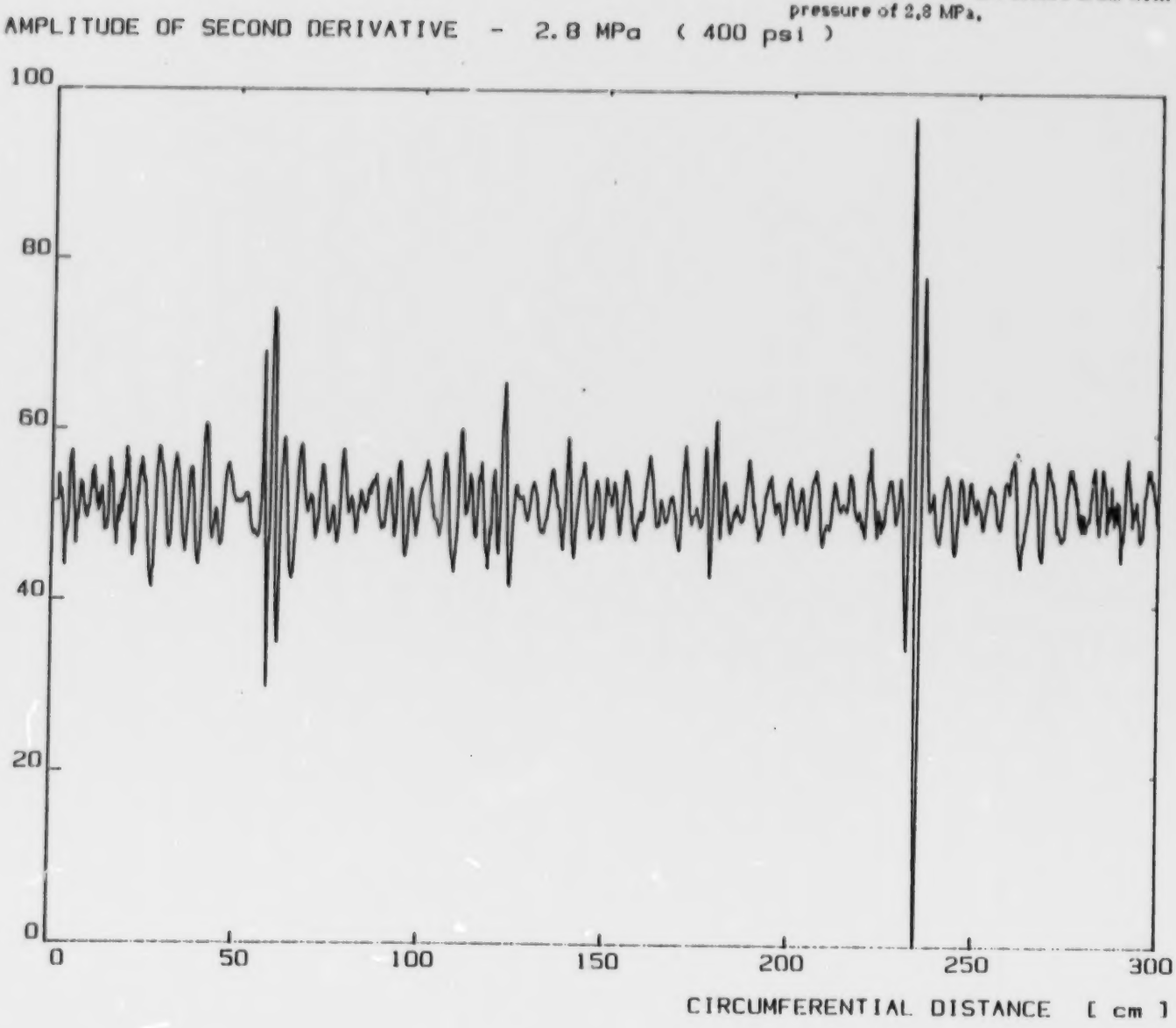

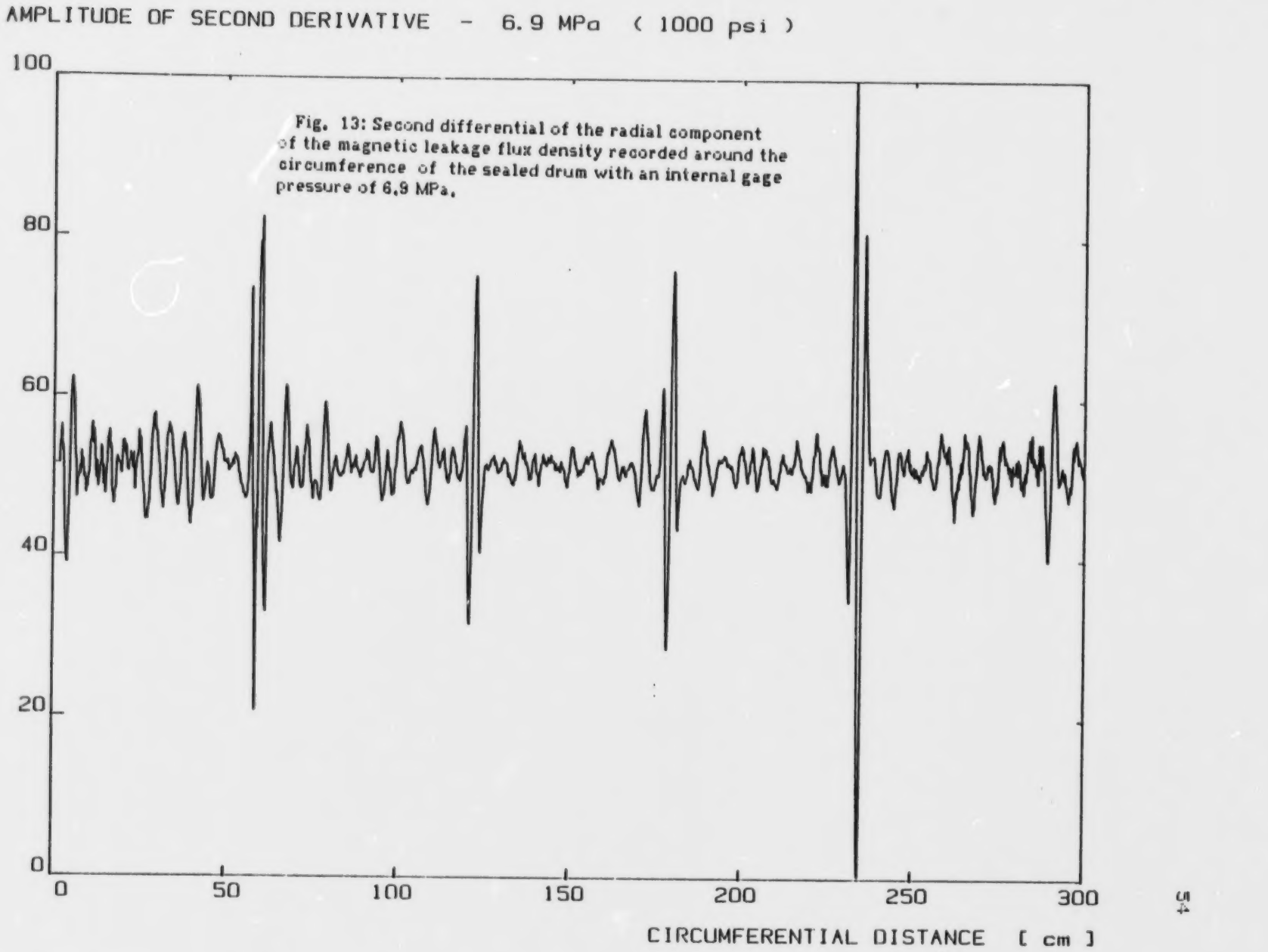

Fig. 13: Second differential of the radial component of the magnetic leakage flux density recorded around the circumference of the sealed drum with an internal gage pressure of 6.9 MPa.

Fig. 14: The variation of amplitude of the signal from a 60% penetration far side defect with internal line pressure, shown for increasing pressure.

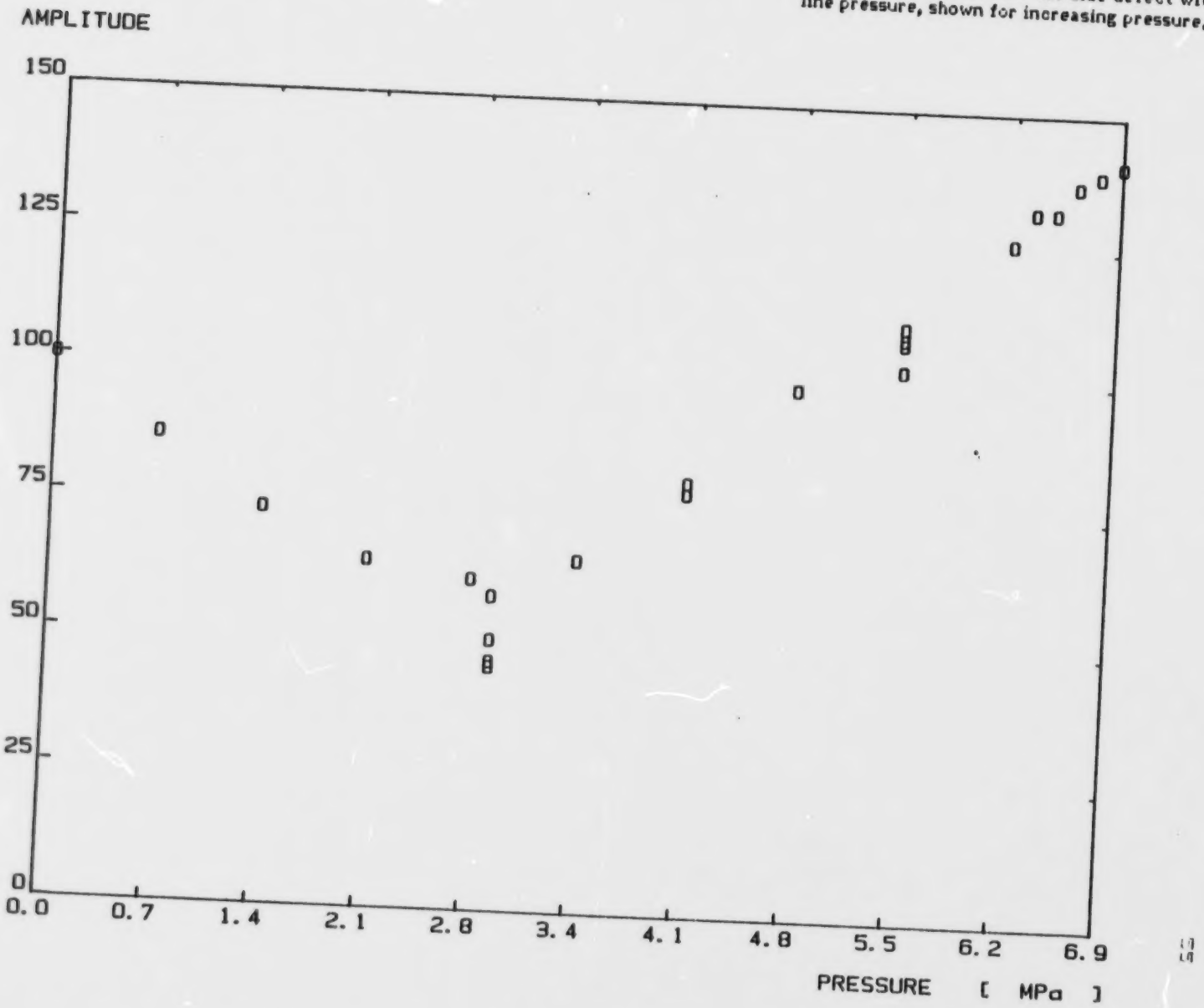

Fig. 15: The variation of amplitude of the signal from a 60% penetration far side defect with internal line pressure, shown for increasing and decreasing pressures.

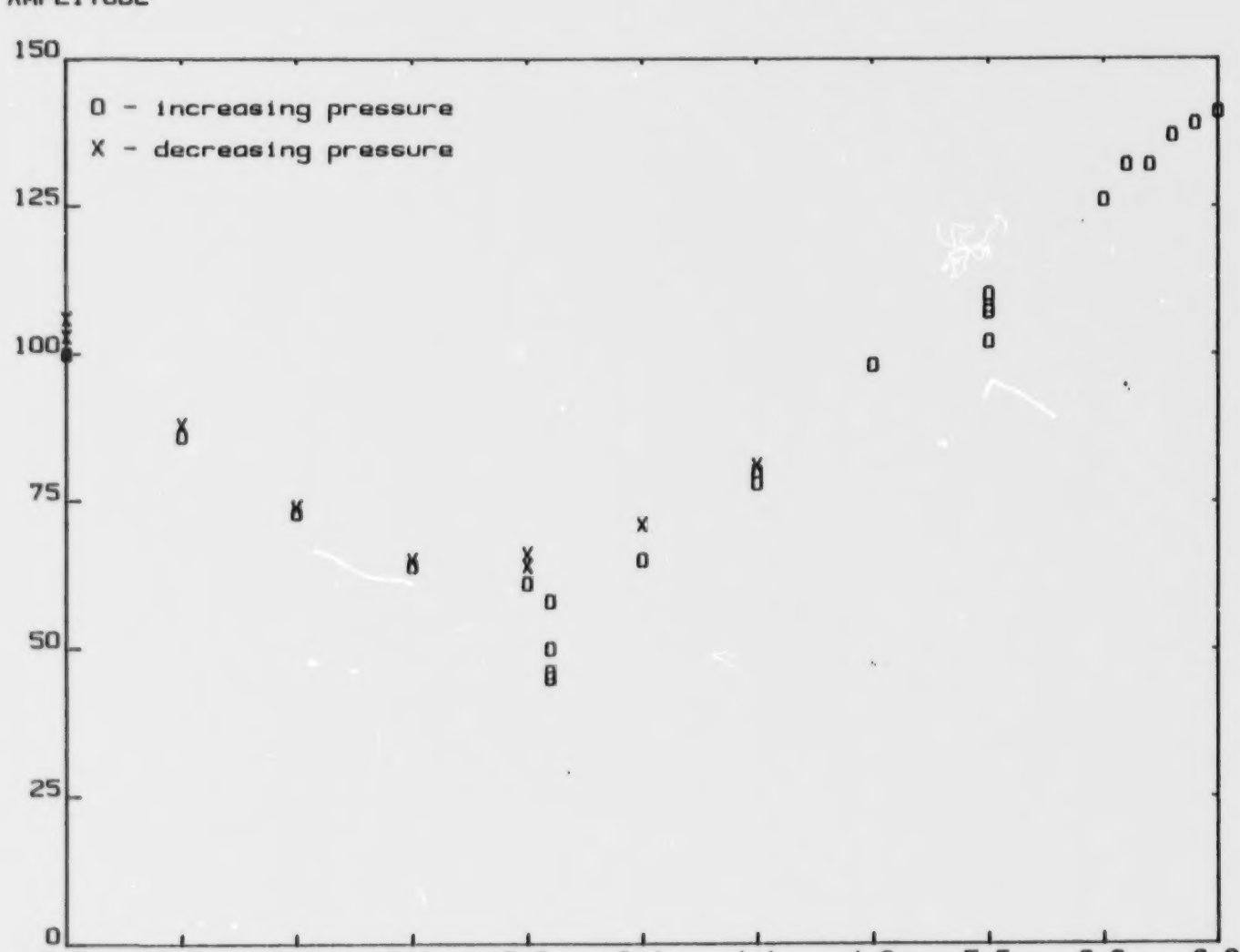

Fig. 16: The variation with pressure of the average normalized signal amplitude for the radial field component of the leakage flux from 20, 40, and 60% penetration far side defects and a 40% near side defect.

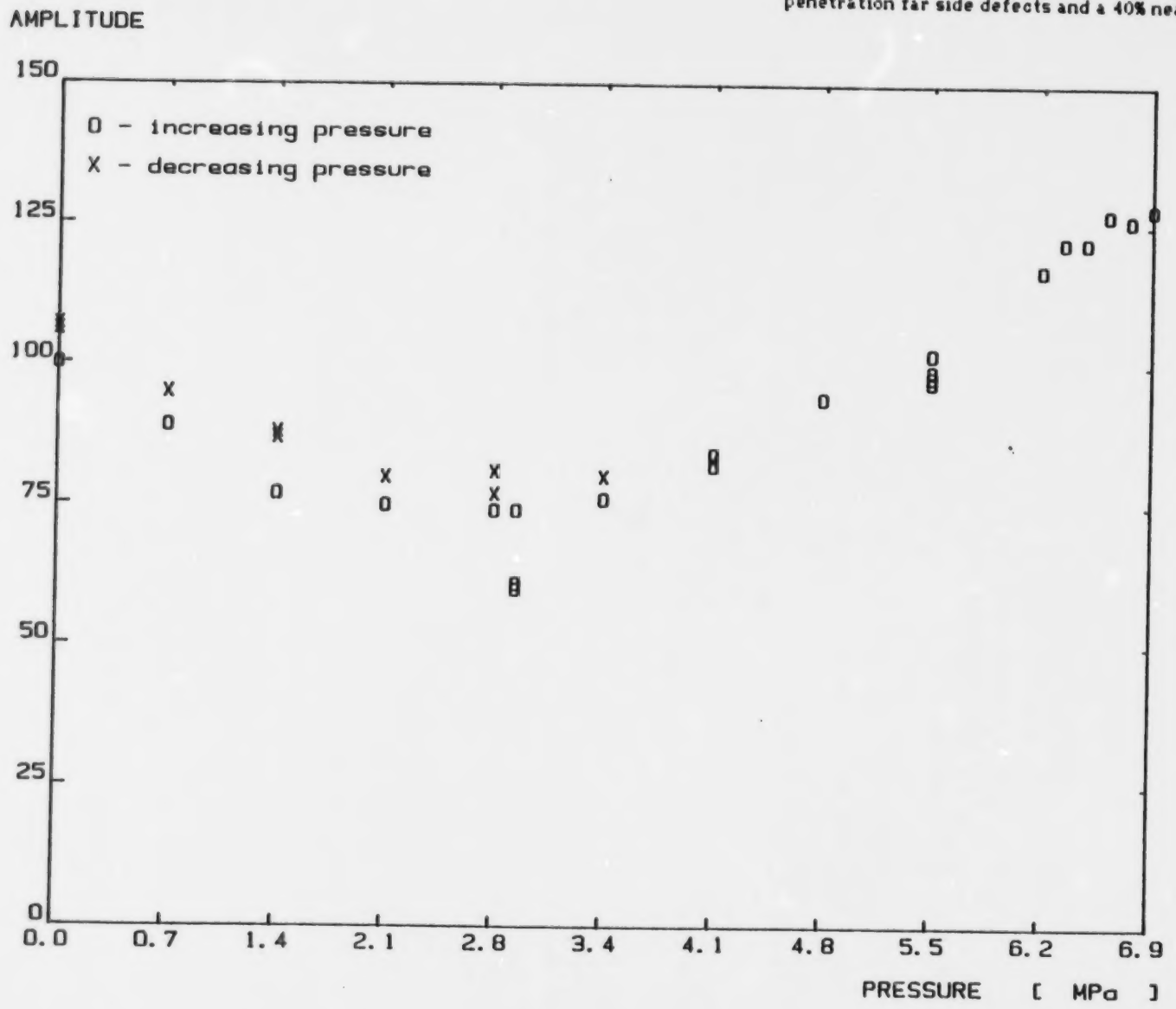

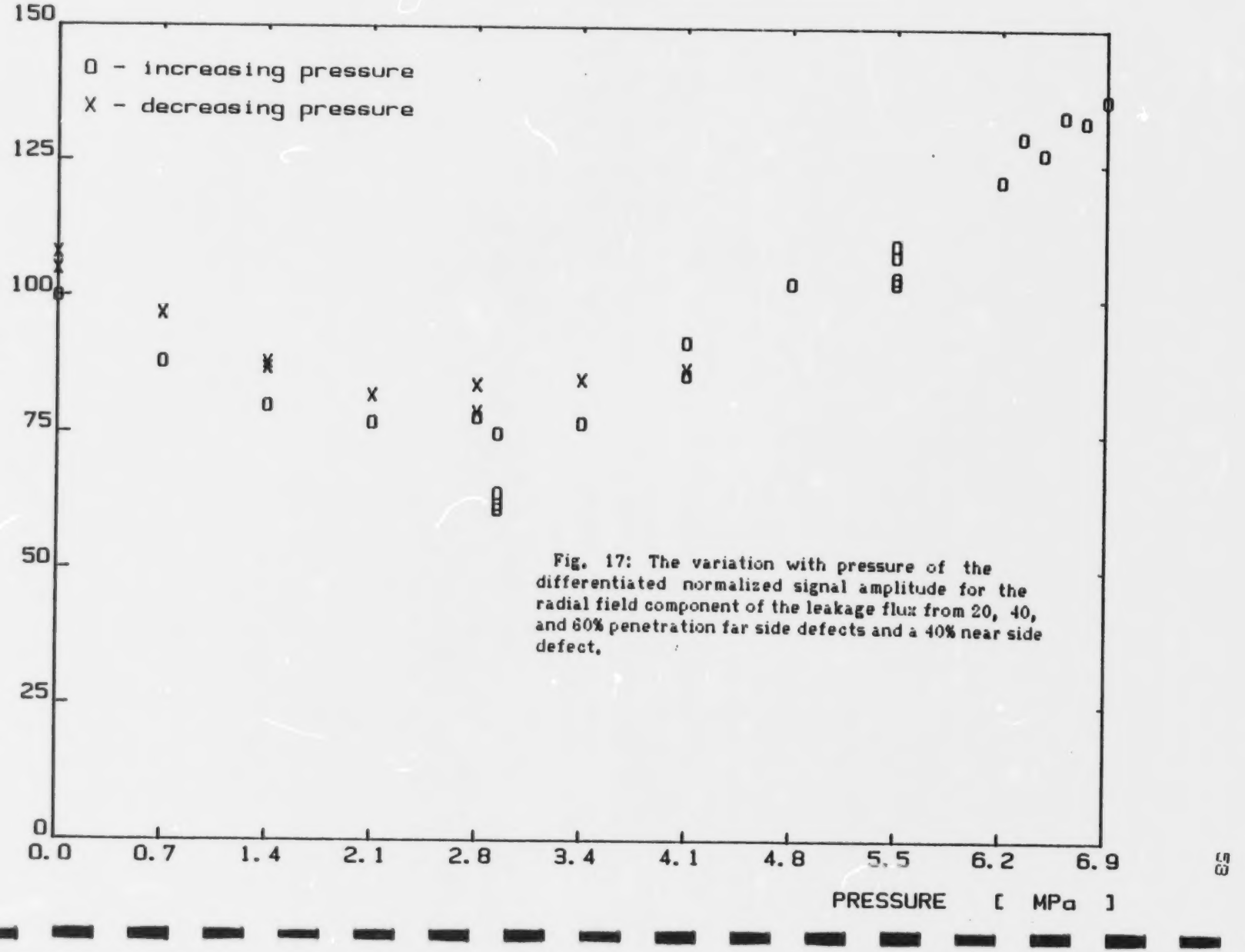

Fig. 17: The variation with pressure of the differentiated normalized signal amplitude for the radial field component of the leakage flux from 20, 40, and 60% penetration far side defects and a 40% near side defect.

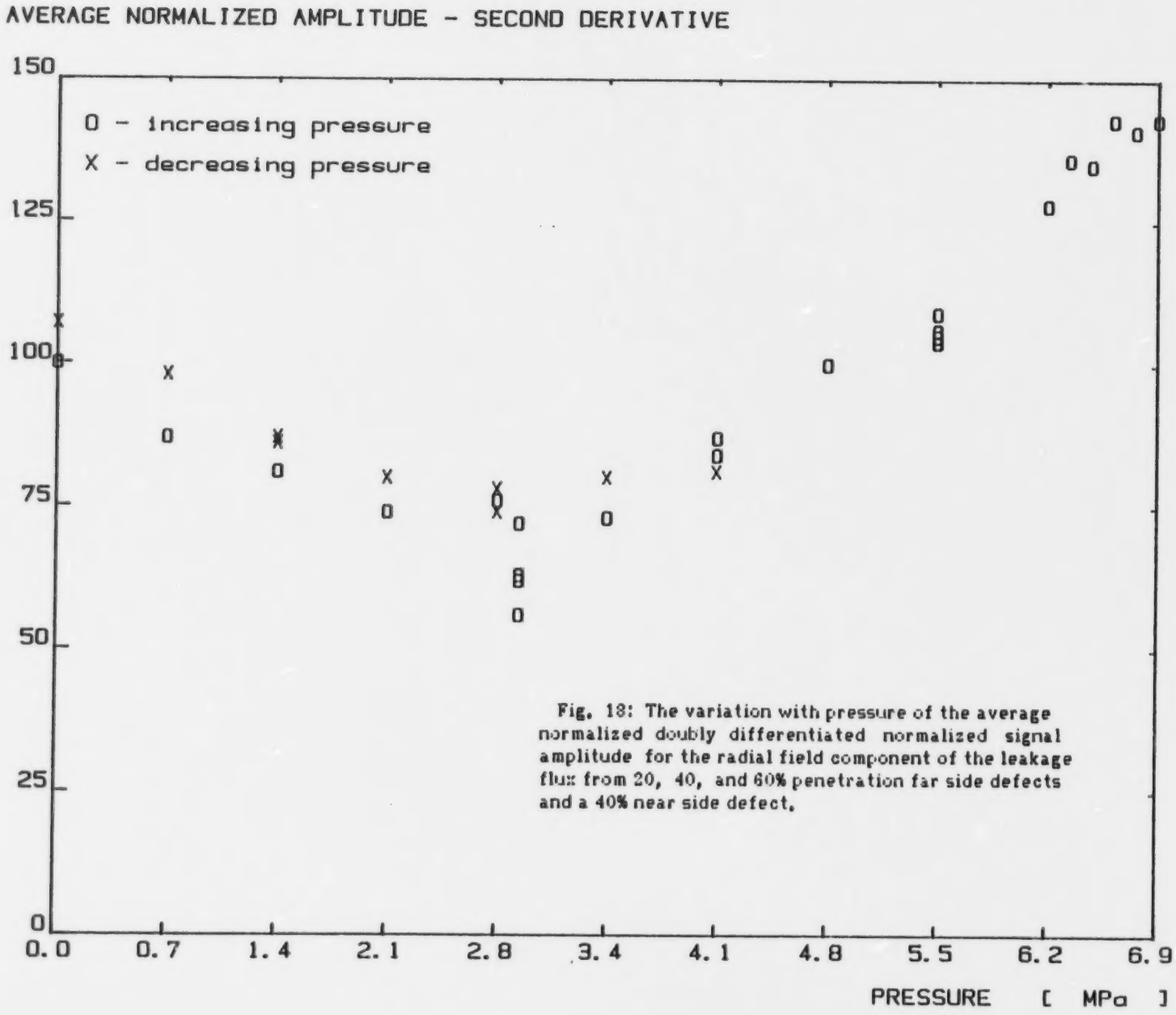

Fig. 18: The variation with pressure of the average normalized doubly differentiated normalized signal amplitude for the radial field component of the leakage flux from 20, 40, and 60% penetration far side defects and a 40% near side defect.

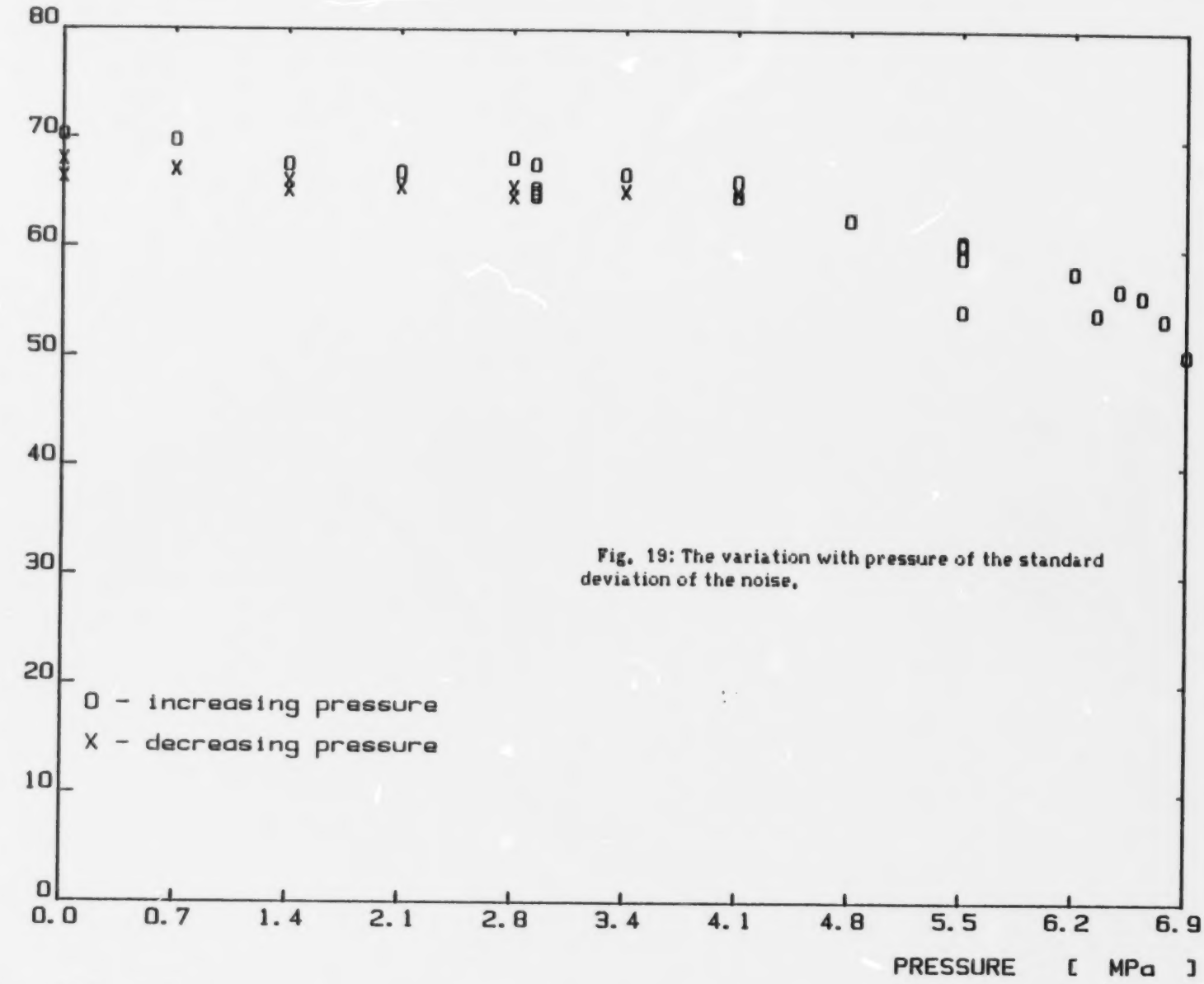

Fig. 19: The variation with pressure of the standard deviation of the noise.

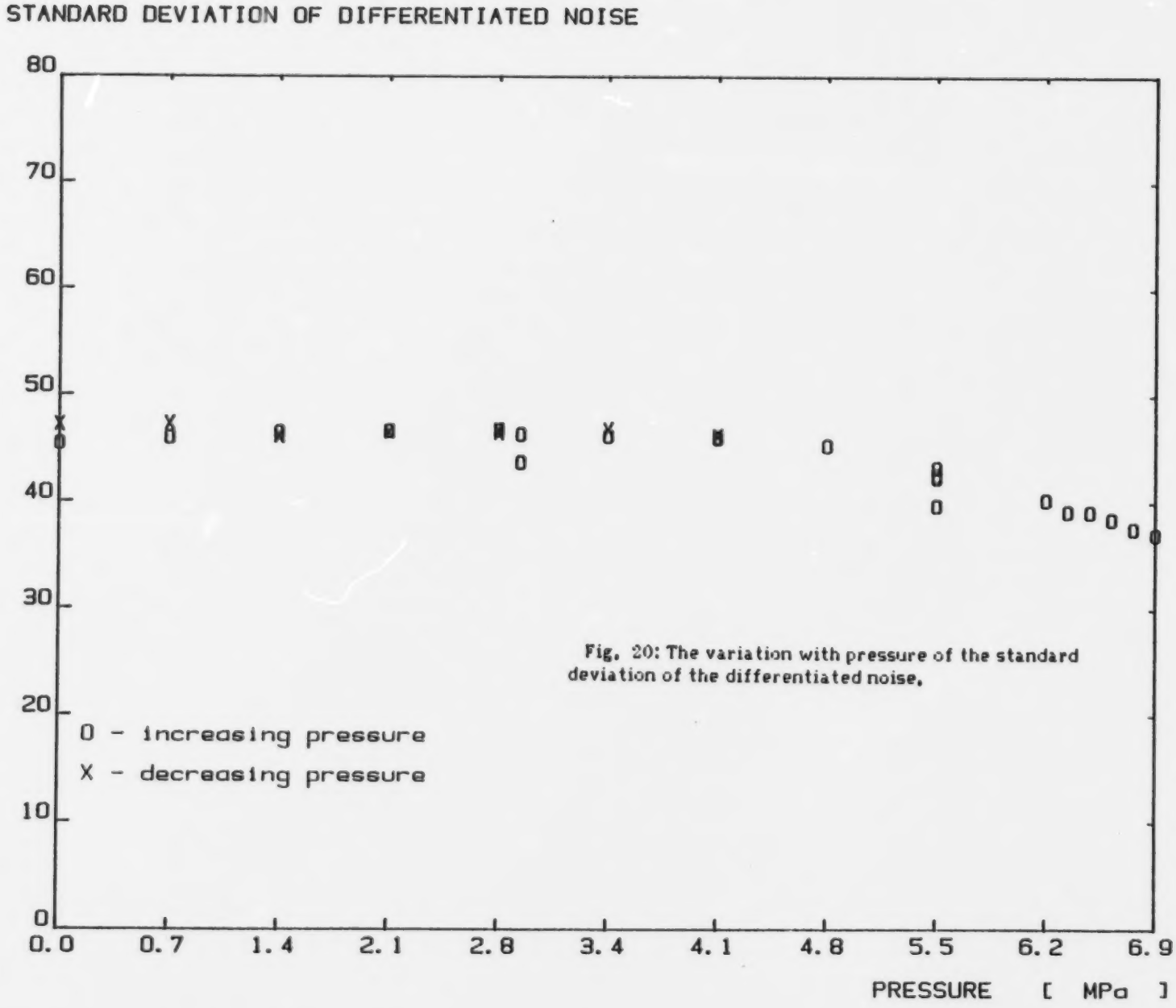

Fig. 20: The variation with pressure of the standard deviation of the differentiated noise.

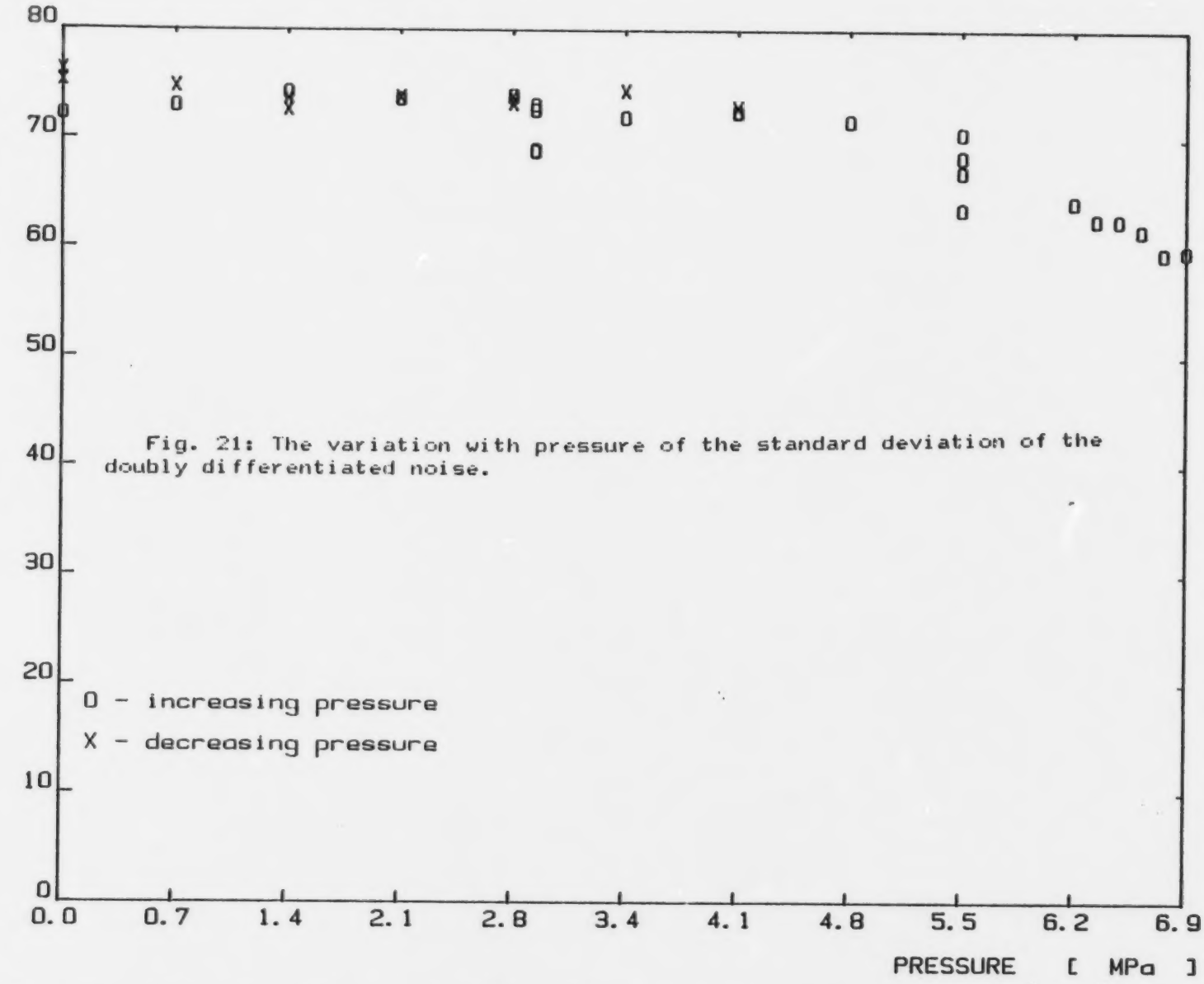

Fig. 21: The variation with pressure of the standard deviation of the doubly differentiated noise.

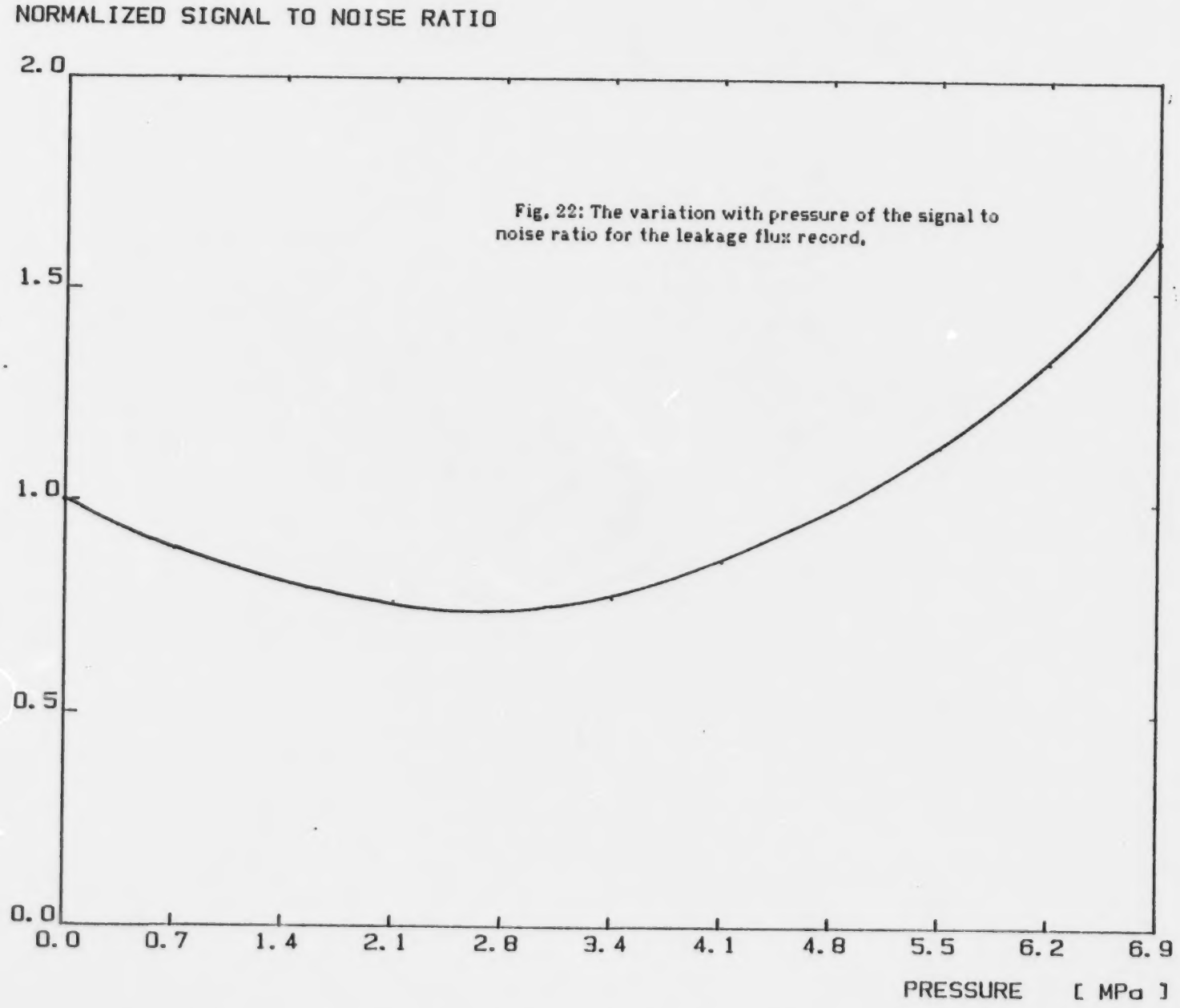

Fig. 22: The variation with pressure of the signal to noise ratio for the leakage flux record.

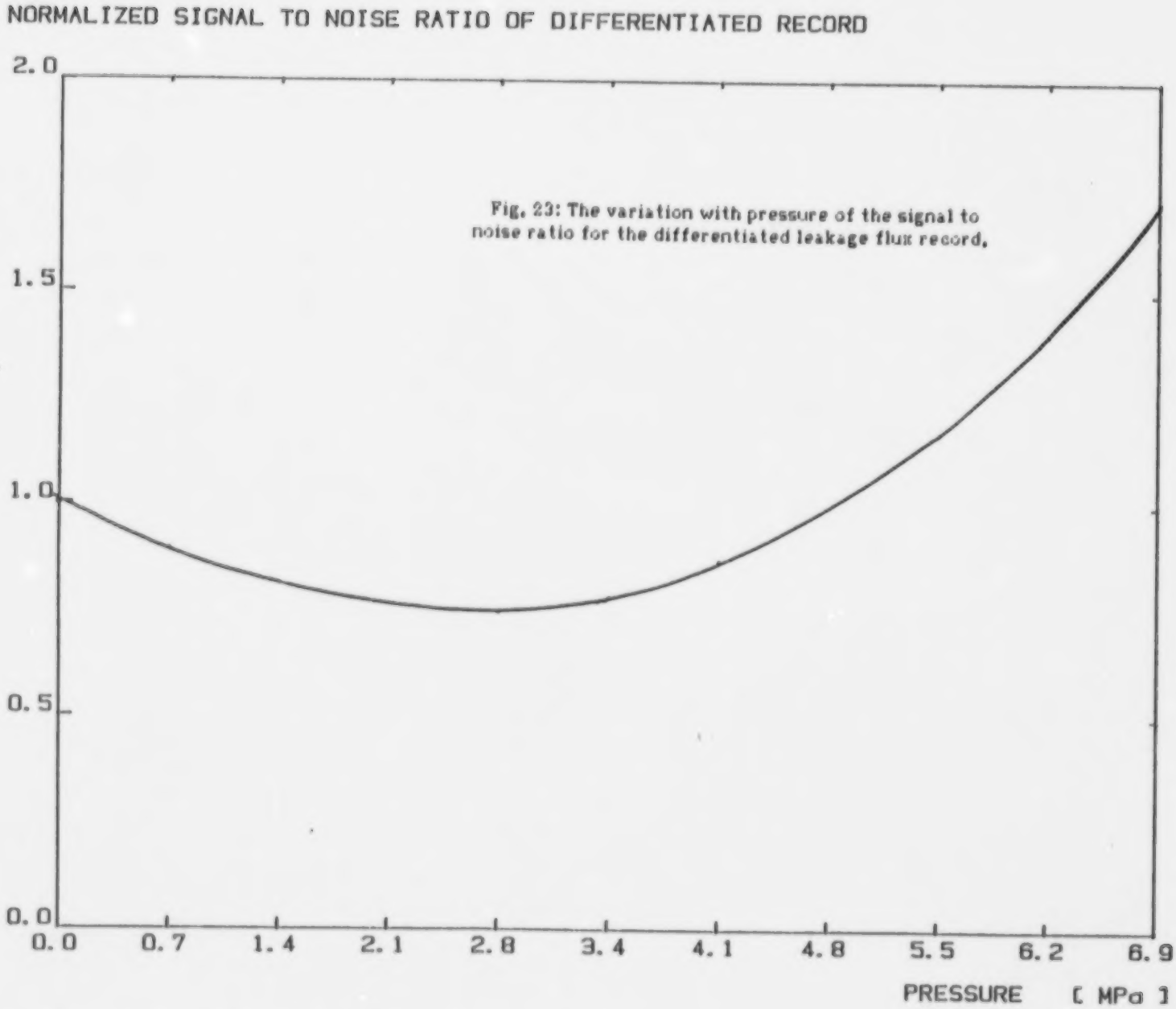

Fig. 23: The variation with pressure of the signal to noise ratio for the differentiated leakage flux record.

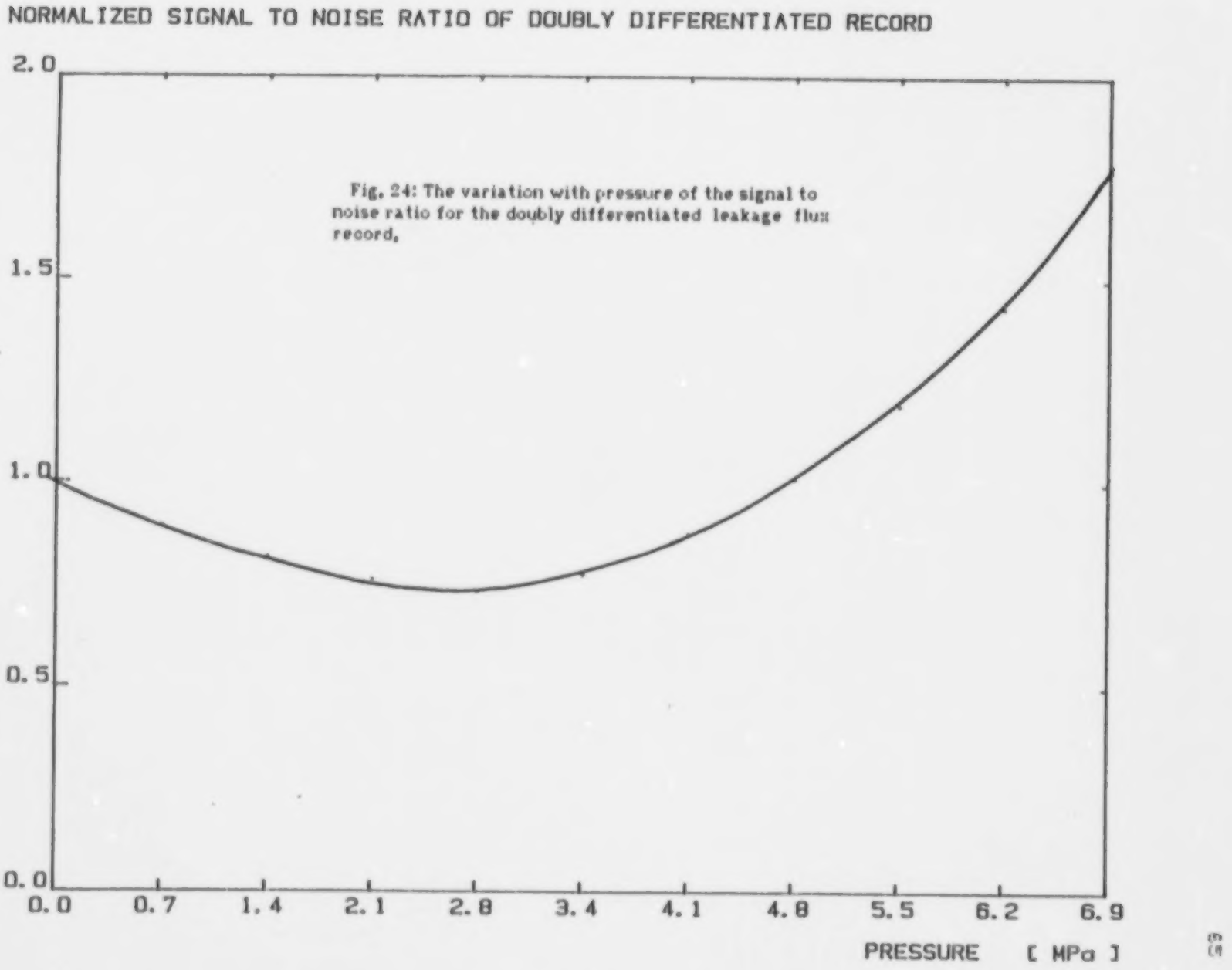

Fig. 24: The variation with pressure of the signal to noise ratio for the doubly differentiated leakage flux record.

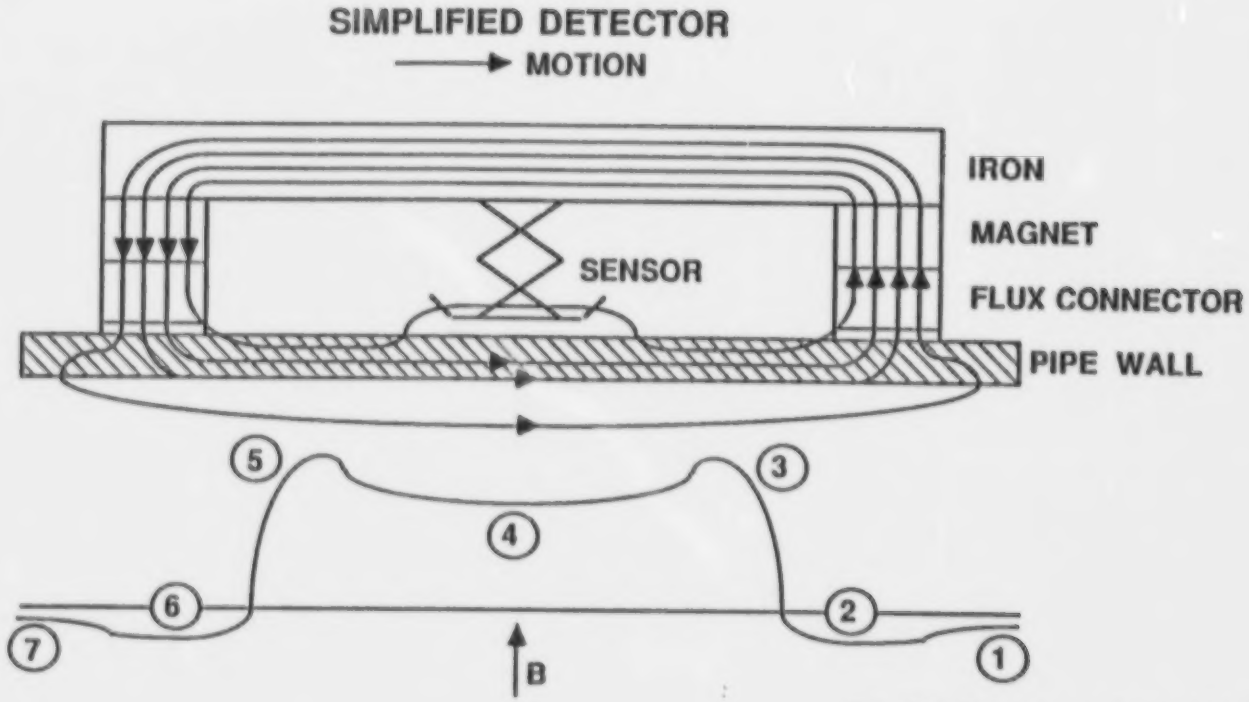

Fig. 25: Simplified magnetic leakage flux detector and corresponding profile of the axial component of the field in the pipe wall. As the detector passes over a given section of pipe it experiences first of all a small reverse field, [2], then a high forward field at the flux connector, [3], followed by a slightly reduced field due to spreading of the flux toward the center of the detector, [4], then another peak field at the trailing flux connector [5] which is followed by another slight reverse field, [6].

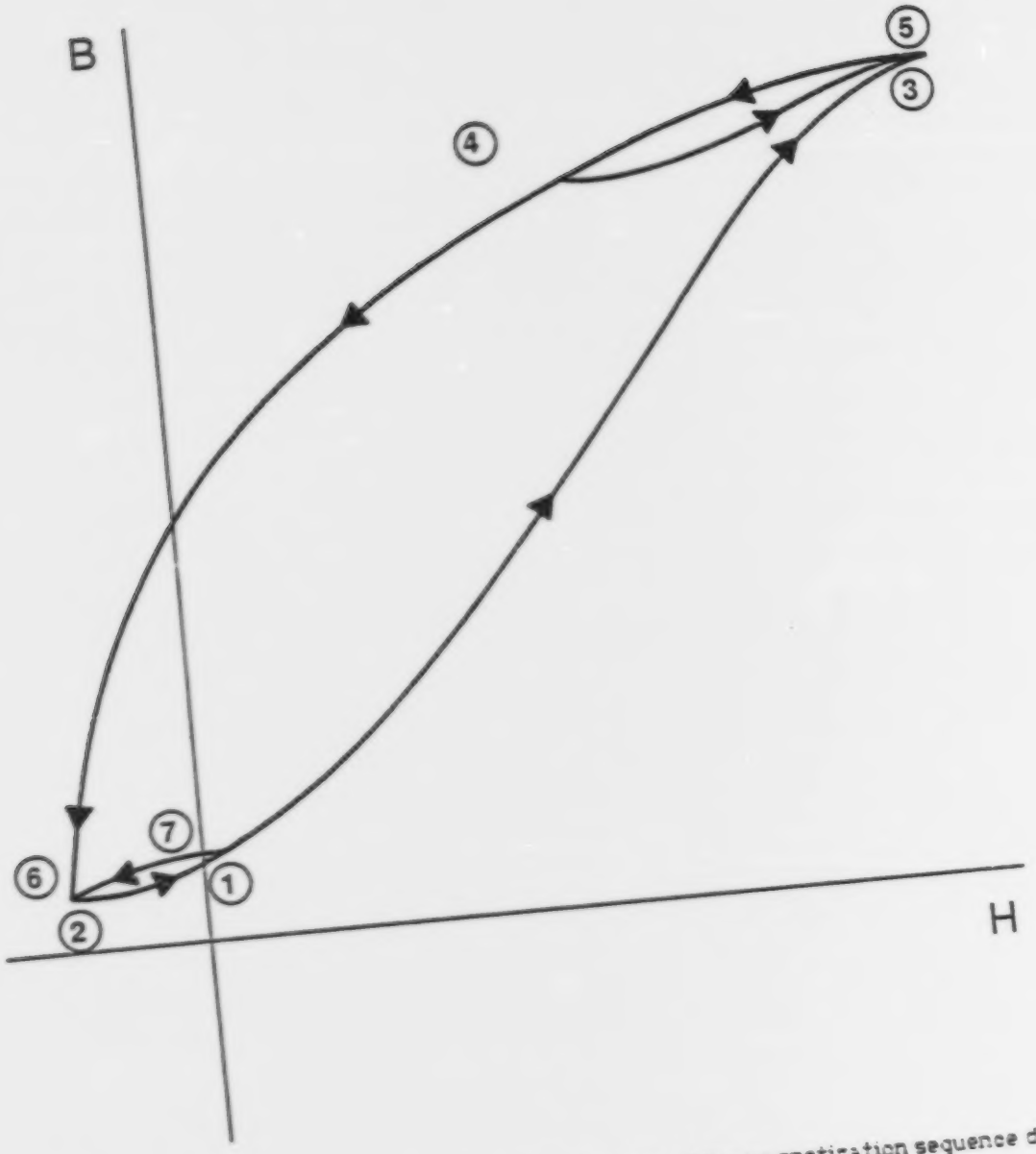

Fig. 26: B – H plot of the magnetization sequence due to the axial field variation shown in Fig. 25.

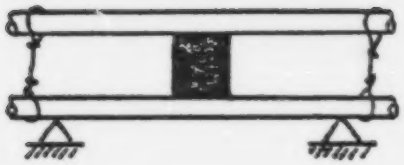

Fig. 27: "The Nutcracker" Two pipes bent against each other ove a central spacer

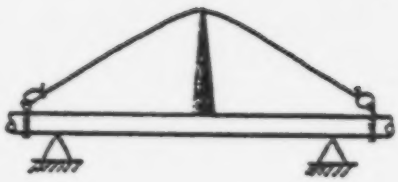

Fig. 28: "The Bow" A single pipe used as a member of a simple truss

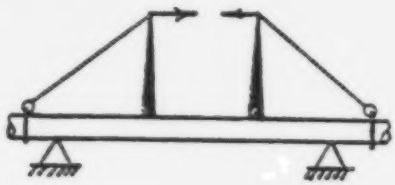

"The Bow", two columns

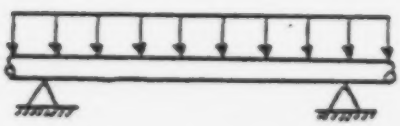

Fig. 29: A pipe loaded by its own weight

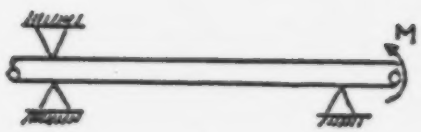

Fig. 30: A pipe loaded by applying a moment at one end

Fig. 31: Cantilevered pipe with fixed end

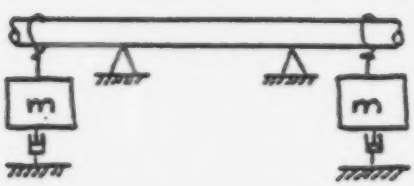

Fig. 32: Supported pipe loaded with weights. Positions of supports and weights may be interchanged.

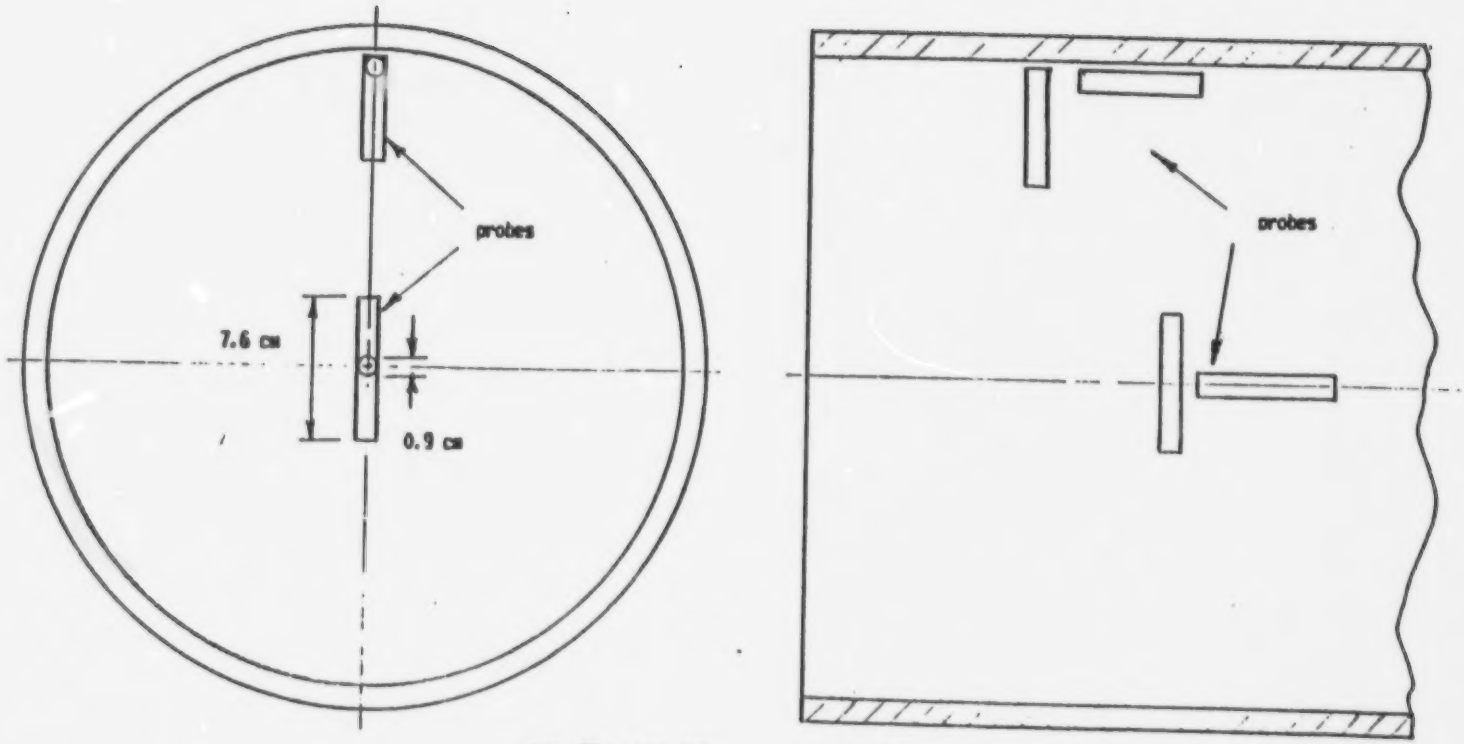

Fig. 33: Cross section of pipe showing suggested positions of magnetometer probe

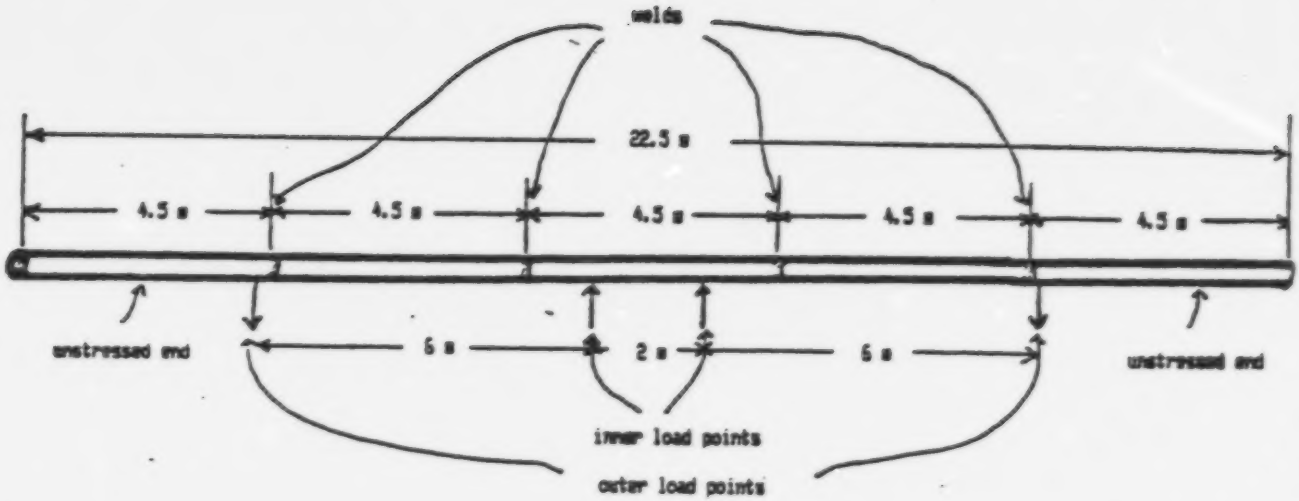

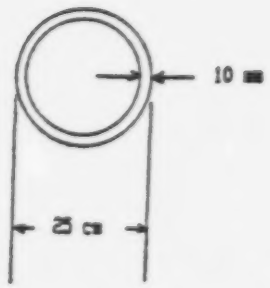

Fig. 34: Suggested pipe dimensions for either the "two-column bow" or the "deloadable weight" loading schemes.

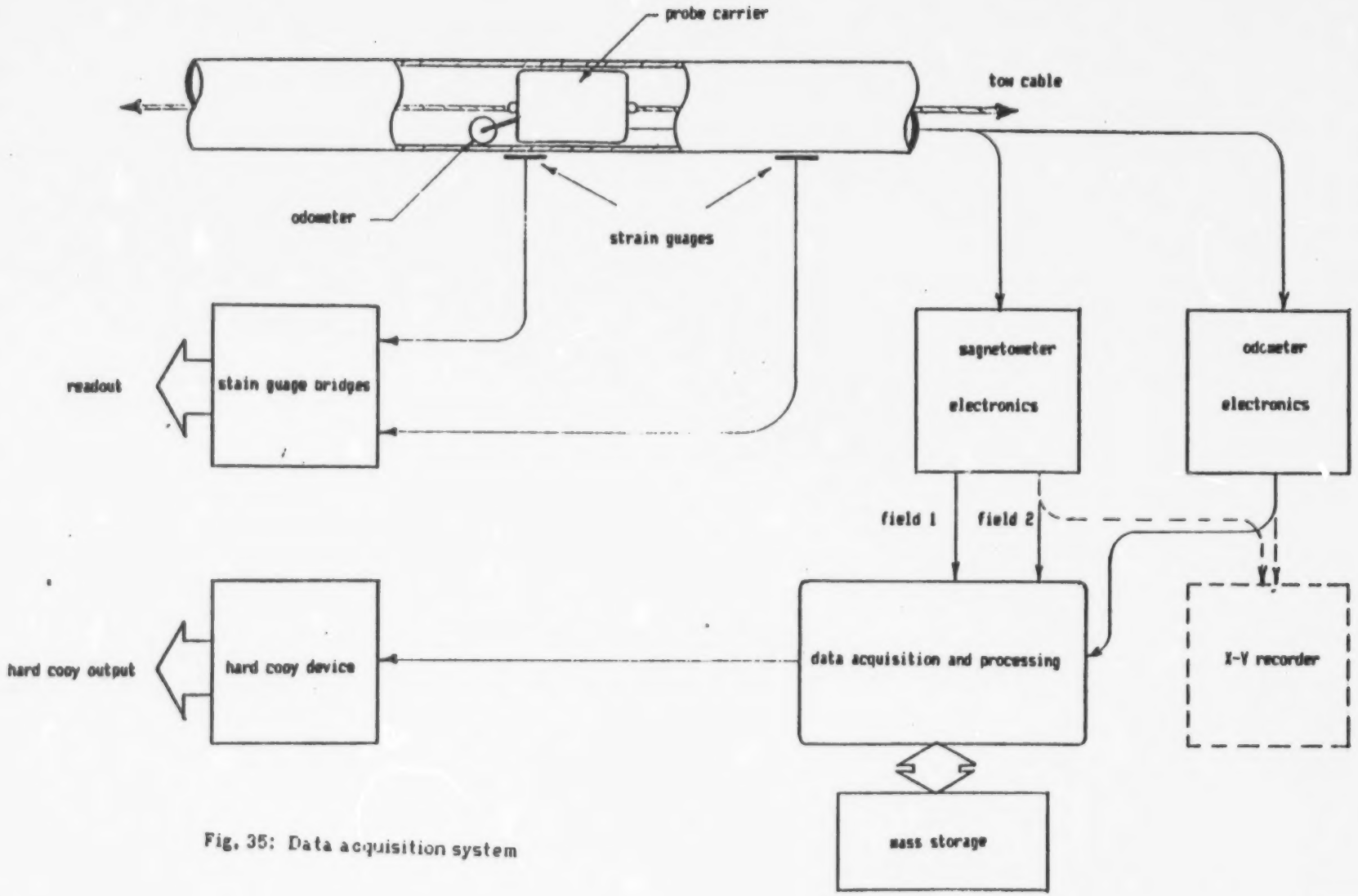

Fig. 35: Data acquisition system

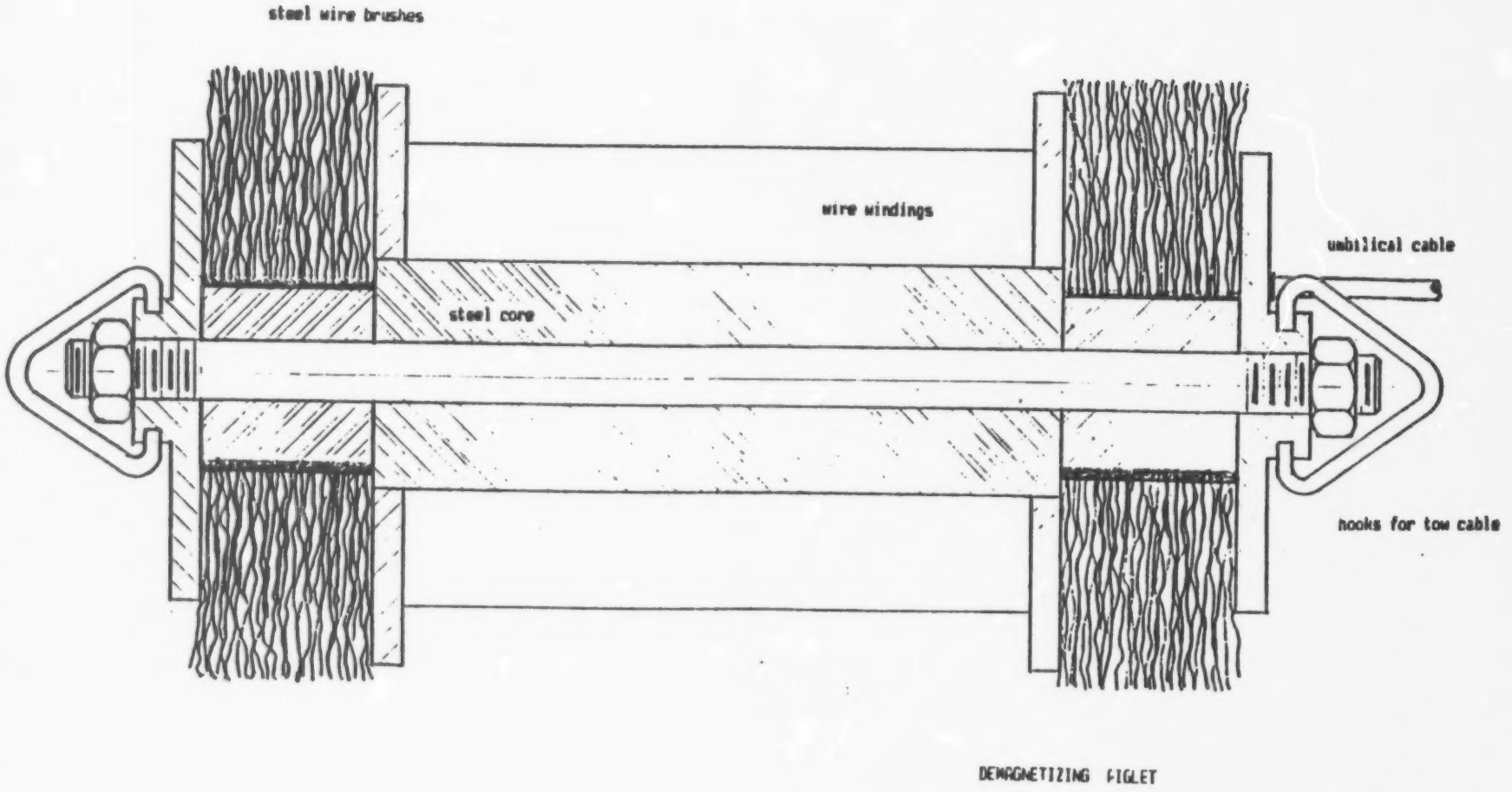

Fig. 36: Magnetizing/Demagnetizing piglet

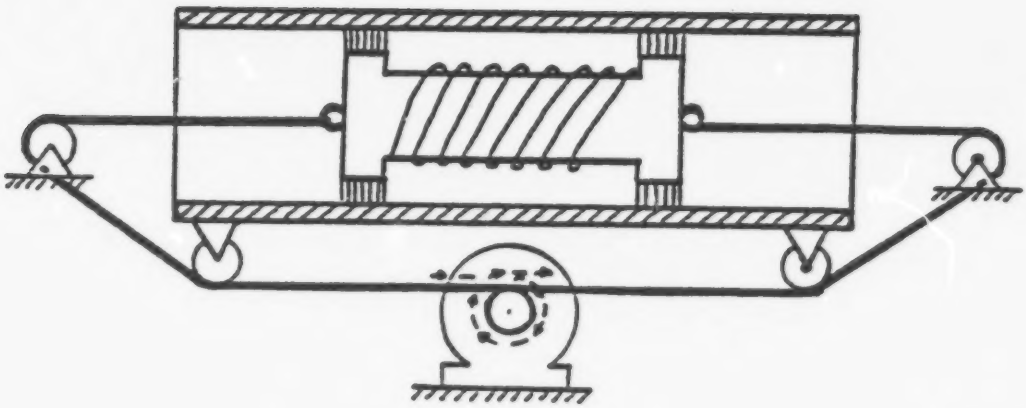

PULL THROUGH SYSTEM

Fig. 37: Pull-through system for instrumentation and demagnetization

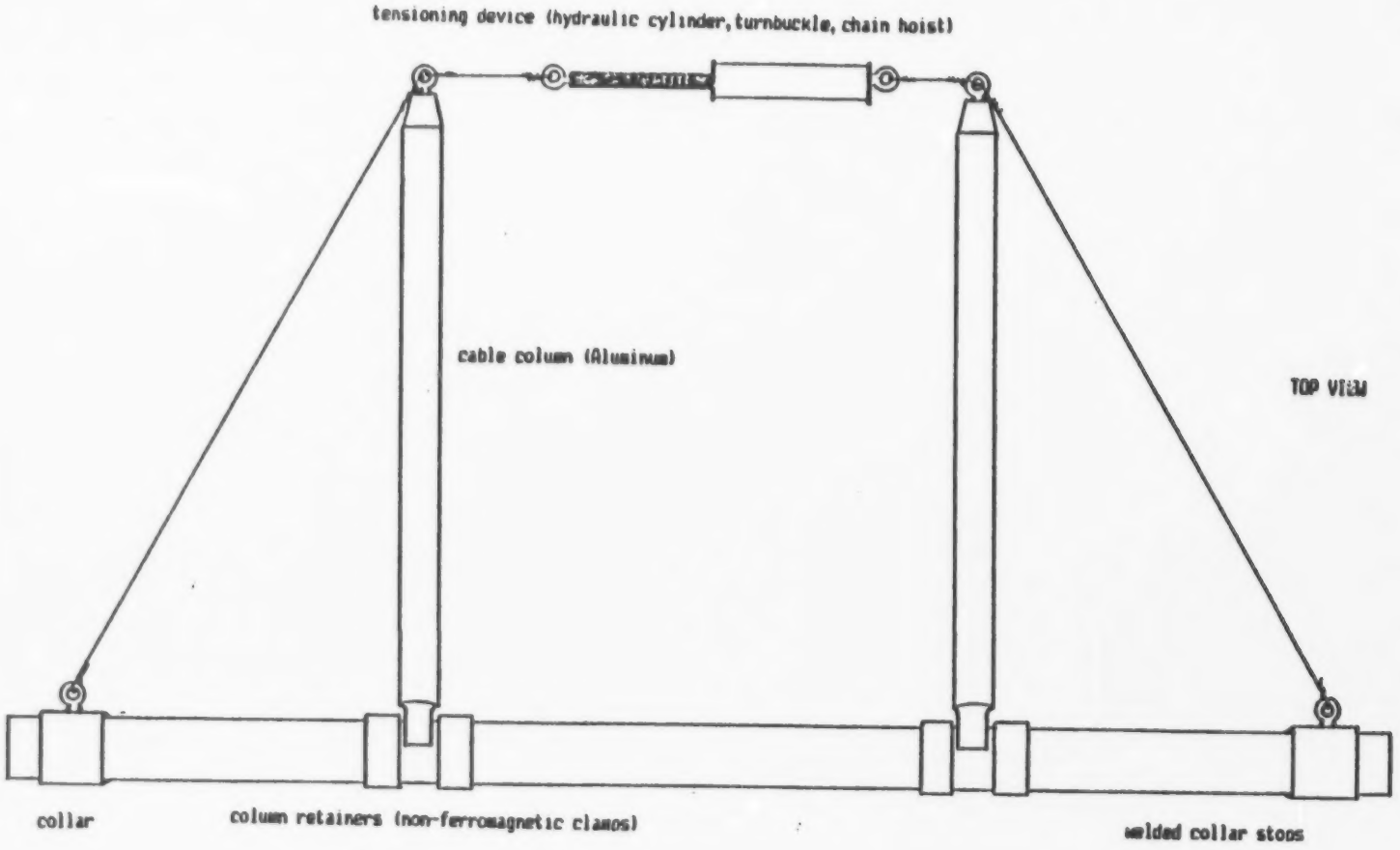

Fig. 12 Detailed Sketch of the "Bow"

Fig. 38: The two column bow – detail

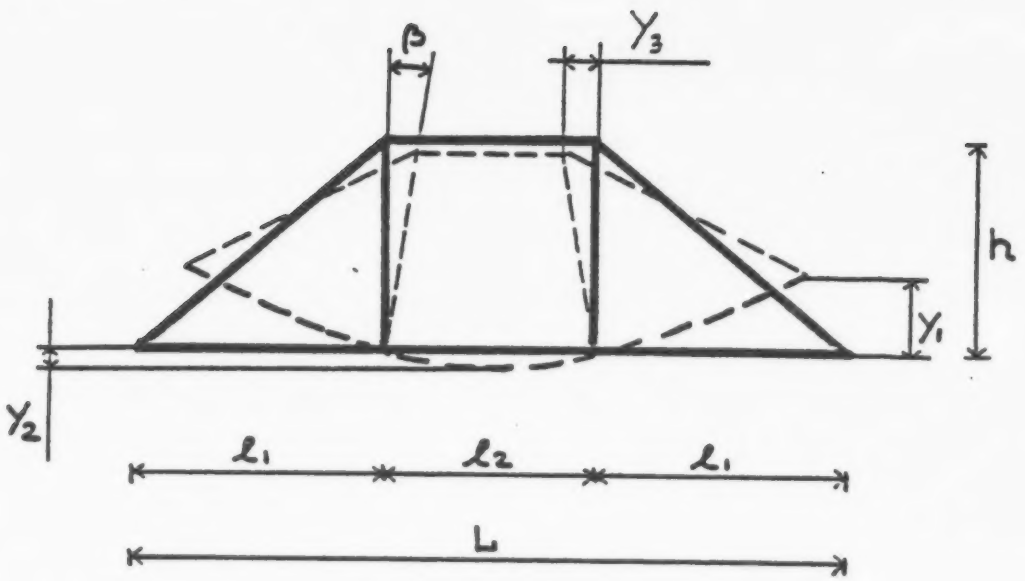

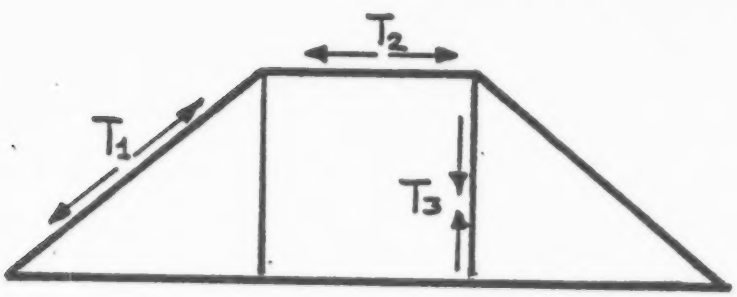

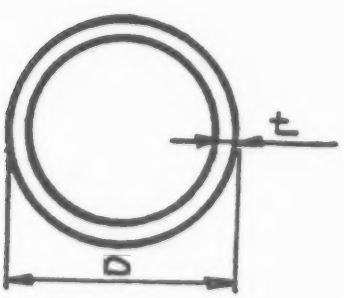

Fig. 39: Diagram of loads and dimensions for the two column bow loading scheme

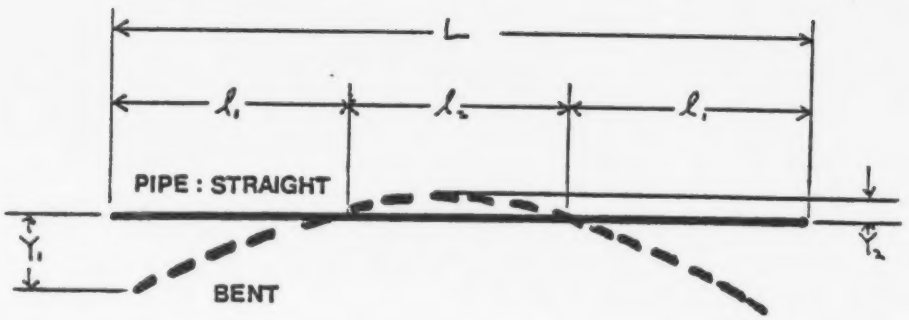

DIMENSIONS & DEFLECTIONS

LOADS

Fig. 40: Diagram of loads and dimensions for the deloadable weight loading scheme

APPENDIX A

EFFECT OF STRESS ON MAGNETIZATION AND MAGNETOSTRICTION IN PIPELINE STEEL*

D.L. Atherton and J.A. Szpunar
Department of Physics, Queen's University
Kingston, Ontario K7L 3N6, Canada

Abstract

Measurements of the effects of stress on the initial magnetization curve of a sample of 1% Mn pipe line steel and on its reversible component are presented. Stress-induced changes in the reversible and irreversible magnetization components are shown. Examples of magnetization changes induced by tensile and compressive stress cycles of various amplitudes and at different fields are given. Magnetostriction measurements made on the same sample under various tensile and compressive stresses measured along annysteretic and initial magnetization curves are included. A simple interpretation is suggested based on the assumption that stress changes the alignments of magnetic domain easy axes with respect to the strain.

Introduction

Our previous investigations of the effects of stress on magnetization of pipe lines[1,2,3] have encouraged us to study specimens of pipe line steel in order to determine the effects of stress on magnetization and magnetostriction.

Low field changes in magnetoelastic properties have already been discussed by Birss et al[4]. They demonstrated that for a range of carbon steels that have been subjected to various metallurgical treatments the magnetization-stress curves are asymmetrical with respect to tension and compression. An understanding of the magnetization changes and magnetostatic and magnetoelastic interactions between defects is however difficult especially in construction steel where inclusions, pearlite and cementite structures and also texture contribute to the complexity of such interactions. Microstructure is responsible for the variety of the domain structures observed in steel. Szpunar and Szpunar[5] have classified domain structures in construction steel using four types of domain patterns. The observed domain configurations are complex and the proportion of different types of domains changes with the grain size. Stress will obviously modify such domain structure. To predict such changes we use the well known relation for energy assuming that a uniform tension of magnitude σ is applied in the crystal direction.

$$E = K_1(\alpha_1^2\alpha_2^2 + \alpha_2^2\alpha_3^2 + \alpha_3^2\alpha_1^2) - \frac{3}{2}\lambda_{100}\sigma(\alpha_1^2\gamma_1^2 + \alpha_2^2\gamma_2^2 + \alpha_3^2\gamma_3^2)$$

$$- 3\lambda_{111}\sigma(\alpha_1\alpha_2\gamma_1\gamma_2 + \alpha_2\alpha_3\gamma_2\gamma_3 + \alpha_3\alpha_1\gamma_3\gamma_1).$$

where α_1, α_2, α_3 are the directional cosines of the magnetization directions and the γ_1, γ_2, γ_3 are the directional cosines of the stress. Thus to the crystal energy is added a term $\sigma\lambda/1$ known as a magnetoelastic energy. Since this energy is a function of the product $\lambda\sigma$ we may expect that a crystal which has positive magnetostriction when deformed by tension will behave like a crystal having negative magnetostriction but deformed in compression. In line pipe steel the magnetocrystalline energy is a dominant part of the total energy. K_1 is high and the easy magnetic direction is <100>. For steel $\lambda\sigma$ is positive for tension and the corresponding energy term will be a minimum when the orientation of the domain magnetizations is parallel to the direction of the stress. If the $\lambda\sigma$ product is negative, as in compression tests, the energy minimum corresponds to a domain magnetization orientation which is normal to the direction of the compressive stress. An understanding of the effect of stress on magnetization of pipe steel is important not only because of the need for fundamental knowledge of magnetization processes but also because it may help to facilitate the magnetic detection of stress.

Experimental Results

1% Manganese line pipe steel has been subjected to tensile and compressive stresses. Magnetization changes and magnetostriction have been measured. The experimental apparatus has been described previously[6]. Reversible components of magnetization have been determined by assuming that small reversible changes in magnetization can be summed and that each magnetization state of the specimen is achieved as a result of the reversible and irreversible magnetization changes. An example of the method used for an unstrained sample is presented in Fig. 1.

Fig. 2 shows the magnetization changes caused by tension and compression applied at a low field of 1kA/m. The magnetization is separated into reversible and irreversible components. Tensile stress increases the magnetization more than compressive stress. The changes in the irreversible components are much higher than in the reversible components. An increase in magnetization with compression or tensile stress is observed at low fields; however, at higher fields the situation becomes more complex. This is indicated by Fig. 3 which gives initial magnetization curves measured for zero stress and stresses of -500 kPa and 500 kPa. There are three transition points which indicate that at various field strengths the effect of stress on magnetization can be very different. This problem is further illustrated in Fig. 4 where stress induced changes in magnetization for three different values of the field strength are presented. The specimen was initially demagnetized then magnetized to the indicated field then tensile stresses of 200, 400 and 600 MPa were applied in three stages. Each stress was relaxed to zero before the next higher stress value was applied. The specimen was then demagnetized and similar compressive stresses applied. The increase in magnetization with tensile stress at low fields contrasts with the decrease at high fields. The

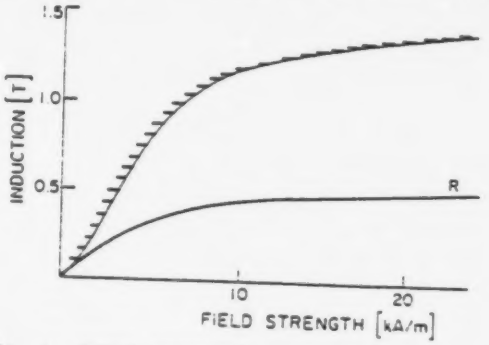

Fig. 1: Initial magnetization curve showing the small field reversals used to separate the reversible component (R).

*Research supported by Canadian National Research Council (IMRI) and Department of Energy, Mines and Resources (CANMET).

transition is gradual and is illustrated in Fig. 5.

Any interaction between stress and magnetization cannot be properly understood without an analysis of the influence of stress on magnetostriction. Magnetostriction measurements have been made on the same specimen along anhysteretic magnetization curves and the results are presented in Figs. 6 and 7. We observe that tensile strain shifts the magnetostriction towards the negative direction and a stress of about 400 MPa is enough to suppress the initial positive value. Compressive stress has a smaller impact on the shape of the magnetostriction versus induction curves. Magnetostriction measurements made traditionally along the initial magnetization curve are relatively similar as seen from Fig. 8.

Discussion

We have measured magnetomechanical and magnetostrictive effects on the same sample and we have separated the reversible and irreversible components for magnetization although this has not yet been done for all processes. We believe that this will be necessary before any thermodynamic correlations can be attempted. Clearly our results show that the interactions between stress and magnetization are complex. Only elementary conclusions can be drawn as yet.

From Fig. 3 we see that the reversible component constitutes a significant portion of the total magnetization. For the specimen examined we observe that tensile stress increases the magnetization at low fields and decreases the magnetization at high field. As we have discussed already tensile stress changes the

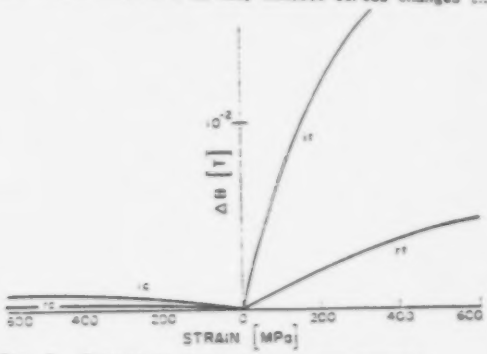

Fig. 2: Changes in reversible and irreversible magnetization components caused by tension (rt, it) and by compression (rc, ic) applied at a field of 1 kA/m.

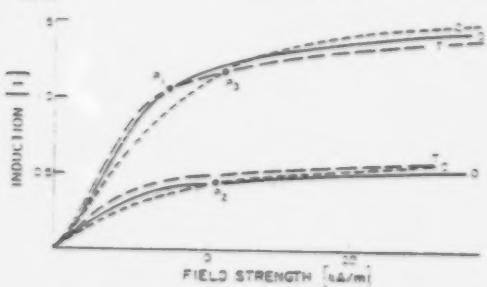

Fig. 3: Effects of tension (T) and compression (C) on the unstressed (O) initial magnetization curve and its reversible component.

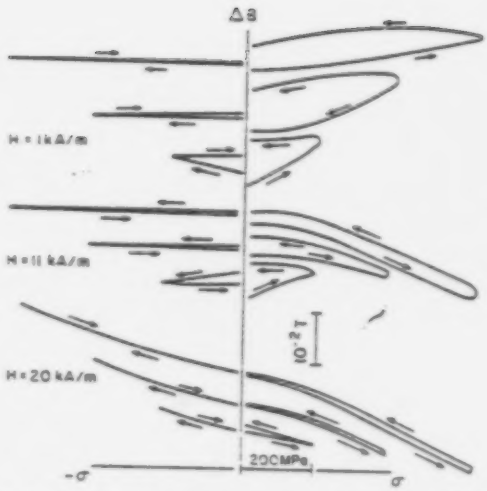

Fig. 4: Changes in magnetization caused by cycles of increasing tension or compression at various fields. The sample has been demagnetized between each stress reversal or change in field.

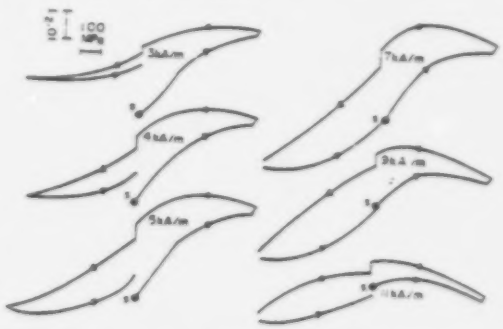

Fig. 5: Changes in magnetization due to a cycle of first tension then compression applied at various fields.

distribution of domain wall orientations to give more domain walls aligned with the stress axis. 180° domain walls are the first to be moved if oriented parallel to the direction of stress and consequently a slight increase in the field strength will give a higher increase in specimen magnetization than that obtained without tensile strain. Compressive stress should have the opposite effect. This agrees with our experimental observations for both total and reversible magnetization changes. At high field strength, between 29 and 30 kA/m, we observe that the magnetization which can be obtained with the specimen under compression is higher than the magnetization which is observed with the specimen under tension, although we have observed previously that both tend toward the same saturation magnetization[7]. A possible explanation is that compressive stress has forced a preferential orientation of domain magnetizations perpendicular to the direction of stress. At higher fields such a distribution of the magnetization vectors is more likely to be changed by rotational processes than for a distribution characterized by preferential

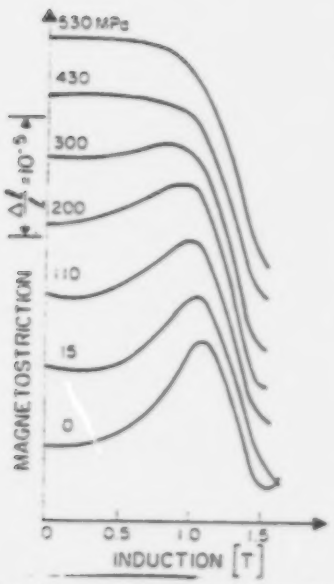

Fig. 6: Magnetostriction measured along the anhysteretic magnetization curve for various tensile stresses.

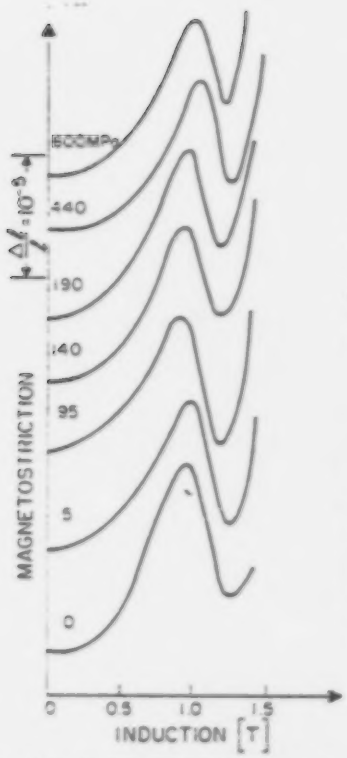

Fig. 7: Magnetostriction measured along the anhysteretic magnetization curve for various compressive stresses.

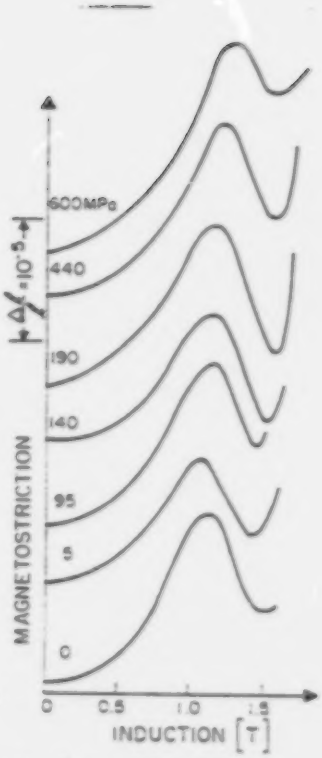

Fig. 8: Magnetostriction measured along the initial magnetization curve for various compressive stresses.

magnetization orientations along the direction of tensile stress. This is most likely responsible for the greater magnetization (at 20 kA/m) seen for the specimen under compressive stress than for the unstressed specimen. We have also observed that tension has a significant impact on magnetization as well as on magnetostriction. Compression does not seem to affect these properties as much.

This same assumption of the effect of stress on the distribution of domain orientations, if correct, may be used to explain our magnetostriction results. Fig. 6 demonstrates clearly the changes in the specimen's magnetostrictive characteristics caused by tensile stress. Since tensile stress increases the number of domains aligned parallel to the stress axis, a movement of 180° domain walls appears to contribute to the change in magnetization especially at low field. Such a process is not accompanied by magnetostrictive strain. Fig. 7 shows however that compression does not significantly affect magnetostriction although the high stress magnetostrictive maxima are shifted toward higher field due to the increased relative importance of rotational magnetization processes.

A more detailed qualitative interpretation of these results will be given in a further paper.

References

[1] D.L. Atherton and A. Teitsma, J. Appl. Phys., 53(11), p. 8130, Nov. 1982.

[2] D.L. Atherton, L.W. Coathup, D.C. Jiles, L. Longo, C. Welbourn and A. Teitsma, IEEE Trans. Magn. MAG-19(4) p. 1564, July 1983.

[3] D.L. Atherton, C. Welbourn, D.C. Jiles, L. Reynolds and J. Scott-Thomas, IEEE Trans. Magn. MAG-20(6), p. 2129, Nov. 1984.

[4] R.R. Birss, C.A. Faunce and E.D. Isaac, J. Phys. D, 4, p. 1080, 1971.

[5] J.A. Szpunar and B. Szpunar, IEEE Trans. Magn. MAG-21(6), p. 2613, Nov. 1985.

[6] D.C. Jiles, D.L. Atherton, H.T. Lassen, D. Noble, J. deVette and T. Astle, Rev. Sci. Instrum., 55(11), p. 1843, Nov. 1984.

[7] L.G. Dobranski, D.C. Jiles and D.L. Atherton, J. Appl. Phys., 57(1), p. 4229, April 1985.

APPENDIX B

ANALYSIS OF THE IREVERSIBLE PROCESSES OF MAGNETIZATION IN STEEL*

J. A. Szpunar, D. L. Atherton and B. Szpunar
Department of Physics, Queen's University,
Kingston, Ont., K7L 3N6, Canada

ABSTRACT

Magnetization changes are due to both reversible and irreversible processes. Preisach diagrams can be used to represent irreversible changes but a reversible component must be added to give the total magnetization change. We show that the reversible magnetization component can be separated experimentally by incremental field reversals. It is a function of M, H and the magnetic history. The remaining irreversible magnetization changes can be represented on a Preisach diagram. Experimental and calculated hysteresis loops, using reversible and irreversible components, are shown for a 1% Mn steel.

* Research supported by Canadian Department of Energy, Mines and Resources (CANMET) and National Research Council (IMRI) and by Natural Sciences and Engineering Research Council.

INTRODUCTION

The problem of representing arbitrary hysteresis paths in ferromagnetic materials is complex and numerous models have already been suggested. It is difficult to develop a theoretical understanding of these processes because crystallographic structure, grain structure, grain orientation and impurities make it very difficult to describe analytically the magnetostatic and magnetoelastic interactions between structural elements of the polycrystalline solids. In this paper we examine certain ideas of the Preisach approach to hysteresis in order to analyse the reversible and irreversible parts of magnetization changes in polycrystalline steel. In spite of an extensive literature on Preisach type models[1,2] this problem has not been studied. We believe that an understanding of the representation of reversible and irreversible processes is crucial for users of this popular representation of magnetization processes.

In the Preisach model the polycrystalline material is divided into parts and the magnetic property of each part is characterized by rectangular hysteresis loops. Such loops are in general shifted from the system origin and are characterized by two switching fields at which magnetization changes from state I to state II and vice-versa.

The assumption that each element of a ferromagnet is characterized by a hysteresis loop is equivalent to assuming that the magnetization is irreversible. Reversible processes can only be described within this model if we assume that the loop is reduced to a line i.e $H_a=H_b$. We may consider therefore that reversible changes are concentrated along the a=b line. It is however impossible to obtain information on the density of such degenerate loops. Experimentally measured Preisach diagrams may contain information about the reversible part included with a total magnetization changes. But information about the reversible part cannot be extracted. Further if such Preisach diagrams are used to generate the magnetization of materials which have well defined magnetic history errors can occur because the method of calculating magnetization in materials is correct only for irreversible processes and cannot account for the reversible part. Generaly speaking this reversible part depends on the magnetic history and is a function of H and M.

EXPERIMENTAL

A sample of 1% Manganese pipeline steel has been examined. The specimen shows relatively high remanence of 1.2 T. Standard equipment described previously in reference 3 is used. The specimen, having dimensions (70x24x24) mm^3 is placed tightly between the poles of the magnet. There was no need to account for the external demagnetizing effect in this since both B and H are measured. In order to obtain information for the Preisach diagram we first demagnetize the specimen then magnetize to H_{max} and then measure the descending magnetization curve to $-H_{max}$. Then, the specimen is remagnetized to H_{max} and, in the next step, the magnetization is set to point P at H_1 on the descending remanence curve, as shown in Fig.1. From there the field is increased and the ascending magnetizing curve is measured. Fig.1 shows this procedure and examples of ascending magnetizing curves are presented in Fig.2. Ascending curves represent the sum of the reversible and irreversible changes in the magnetization of the specimen. In order to estimate the contribution of the reversible changes a small reverse field -dH is applied when the ascending curves are being measured. An example is given in Fig.3. Since the magnetization changes generated by the fields dH and -dH are the same we assume that the total change in the magnetization dM consists from two parts dM_r and dM_i. Thus,

$$dM_i = dM - dM_r$$

Only M_i can be predicted from the Preisach diagram since it describes only the irreversible processes. Such a diagram must be calculated from the irreversible component of the magnetization. In order to separate this irreversible component from the total change in magnetization we have followed the same procedure for all ascending curves. Small incremental reversible changes were summed up to give the reversible $M_r(H)$

$$M_r(H) = \int_0^H \frac{dM_r(H)}{dH}\, dH$$

The reversible part was measured as a function of the field strength and changes in this part are illustrated in Fig.4. The reversible part measured this way represents usually (10-20)% of the total magnetization. In the next step we have calculated the irreversible ascending curves and used these curves to calculate the Preisach diagram. The Preisach diagram is expressed as a distribution function p(a,b), where p(a,b)dadb is the probability of having elements with parameters between a and a+da and b and b+db.

The results are represented in Fig.5 which demonstrates that there is a strong maximum of the p(a,b) function. The histogram along the line OC is given separately in Fig.6. Fig.5 indicates that the elementary hysteresis curves are distributed approximately symmetricaly with respect to H=0 with most of them having their ascending switching fields around H_c=3kA/m.

DISCUSSION

The Preisach diagram calculated from the irreversible magnetization curve can be then used to obtain any arbitrary irreversible magnetization path in a magnetic material. This is done according to the following formula, which expresses the irreversible descending magnetization curve as

$$M_i(H) = \int_{a=-H_{max}}^{H_{max}} \int_{b=-H_{max}}^{H_{max}} M_{II}\, p(a,b)\, da\, db - \int_{a=-H_{max}}^{H_{max}} \int_{b=H_{max}}^{H} M_I\, p(a,b)\, da\, db$$

or the ascending magnetization curve as

$$M_i(H) = -\int_{a=-H_{max}}^{H_{max}} \int_{b=-H_{max}}^{H_{max}} J_I\, p(a,b)\, da\, db + \int_{a=-H_{max}}^{H} \int_{b=-H_{max}}^{H_{max}} J_{II}\, p(a,b)\, da\, db$$

As an example we have calculated hysteresis loops for various values of H_{max}. Since these loops represent M_i only, namely the irreversible processes, they do not agree well with the experimental curve. As we can see in Fig.7a the calculated hysteresis loops are much flatter than the experimental loops. The agreement is however relatively good if the reversible part is added to the irreversible changes calculated from the Preisach diagram. The same procedure is used for other hysteresis loops and the agreement with the experiment is satisfactory, as shown in Fig.8.

When studying the magnetic characteristics of the sample it is obviously

necessary to distinguish between the reversible part of the magnetization and the irreversible part. The contribution of the reversible part of the magnetization depends not only on the value of B and H but also on the previous magnetic history. In order to illustrate this we may represent the reversible fraction of the magnetization for ascending magnetization curves, obtained as shown in Fig. 1, in the same format as the Preisach diagram (Fig.9). We see that this reversible contribution changes, both as a function of the field strength and also as a function of the field from which the ascending magnetization has been measured. It also depends on the sequence of reversals or magnetic history. Figs. 4 and 10 show that the greatest contribution to the reversible fraction of the total magnetization is observed at low positive fields. This is also apparent from Fig. 9, for which reversible magnetization components have been determined for elemental areas $dH_a dH_b$ measured along ascending magnetization curves similarly to the Preisach diagram determination. The most rapid increase in the total magnetization is also observed at these low positive fields. In the Preisach diagram for the irreversible magnetization we observe a strong maximum at a precisely defined field strength at which there is a rapid increase in the irreversible component of the magnetization. The contribution of the reversible component however does not change much (Fig.9). It should be noted that the results given in Fig.9 should not be compared with the Preisach diagram since they cannot be used for calculation of hysteresis. Fig 9 is a convenient representation of the reversible part for the given field reversal sequence only.

If the magnetic history of the specimen is destroyed by careful demagnetization and then the initial magnetization curve is measured the contribution of the reversible fraction to the total magnetization is a function of H.

Such measurements are presented in Fig.10 and can be used to separate these two factors. As a result, see Fig.11, we observe that the reversible fraction constitutes a high percent of the total magnetization at a very low field and that the contribution of this fraction decreases rapidly to 20 percent with increasing field strength. A gradual increase of the irreversible part is observed at high field strength, above the knee of the magnetization curve. This increase is attributed to the increasing role of rotation processes, which may have a significant reversible component.

The large contribution of the reversible processes at low field strength is probably due to a number of factors. We believe that the initial increase in the magnetization is possible under the influence of an incremental increase in the field strength, because certain domain walls are shifted from their thermodynamic equilibrium position in the grain and such shifts may occur without pinning. Further an increase in the magnetization at low field occurs for these domain walls which are already pinned. All domain walls which have moved and which have contributed to an increase in the magnetization have to be finaly pinned by various inhomogeneities, for example the grain boundaries, cementite inclusions, small pearlite grains and non metallic inclusions. Being pinned they can still contribute to an increase in the reversible magnetization by elastic deformation of the domain wall. A quantitative description of this phenomena will be given in a seperate paper.

FIGURE CAPTIONS

Fig.1 A major hysteresis loop to saturation with the ascending magnetization curve. The shaded region indicates the area where domains have switched from state II to state I upon lowering the field from H_{max} to H_1 and subsequently have switched from state I to state II by increasing the field from H_1 to H_2.

Fig.2 Typical ascending curves (a) and curves showing the reversible magnetization components described subsequently (b).

Fig.3 An ascending curve showing the elementary reversible changes in the magnetization. The change in the magnetization of the specimen is composed from two parts, reversible M_r and irreversible M_i.

Fig.4 Reversible portions of the magnetization measured along ascending magnetization curves.

Fig.5 The Preisach diagram for irreversible processes.

Fig.6 A histogram illustrating the density of the elements having the hysteresis loops $H_a=-H_b$ i.e along the line OC on Fig 5.

Fig.7 Hysteresis loops calculated from the Preisach diagram
(a) illustrating the irreversible processes only,
(b) with the reversible fraction added.

Fig.8 Hysteresis loops calculated from the irreversible Preisach diagram with added reversible parts (points) compared with measured hysteresis loops (continous lines).

Fig.9 The contribution of the reversible part of the magnetization measured along ascending magnetization curves.

Fig.10 Initial magnetization curves (a) measured, (b) irreversible component (c)reversible component.

Fig.11 The reversible component of the magnetization (as a percent of the total magnetization) plotted as a function of the field strength (a) and as a function of the total magnetization (b).

REFERENCES

1. F.Preisach, "On Magnetic Aftereffect", Zeitschrift fur Physik, Vol. 94, pp. 277-302, 1935.

2. R. M. Del Vecchio, "An Efficient Procedure for Modeling Complex Hysteresis Processes in Ferromagnetic Materials", IEEE Trans. on Magnetics, Vol. MAG-16, No. 5, pp. 809-811, Sept. 1980.

3. D.C. Jiles, D.L. Atherton, H.I. Lassen, D. Noble, J. deVette and T. Astle, "Microcomputer-based system for control of applied uniaxial stress and magnetic field," Rev. Sci. Instrum. Vol. 55, No. 11, pp. 1843-1848, Nov. 1984.

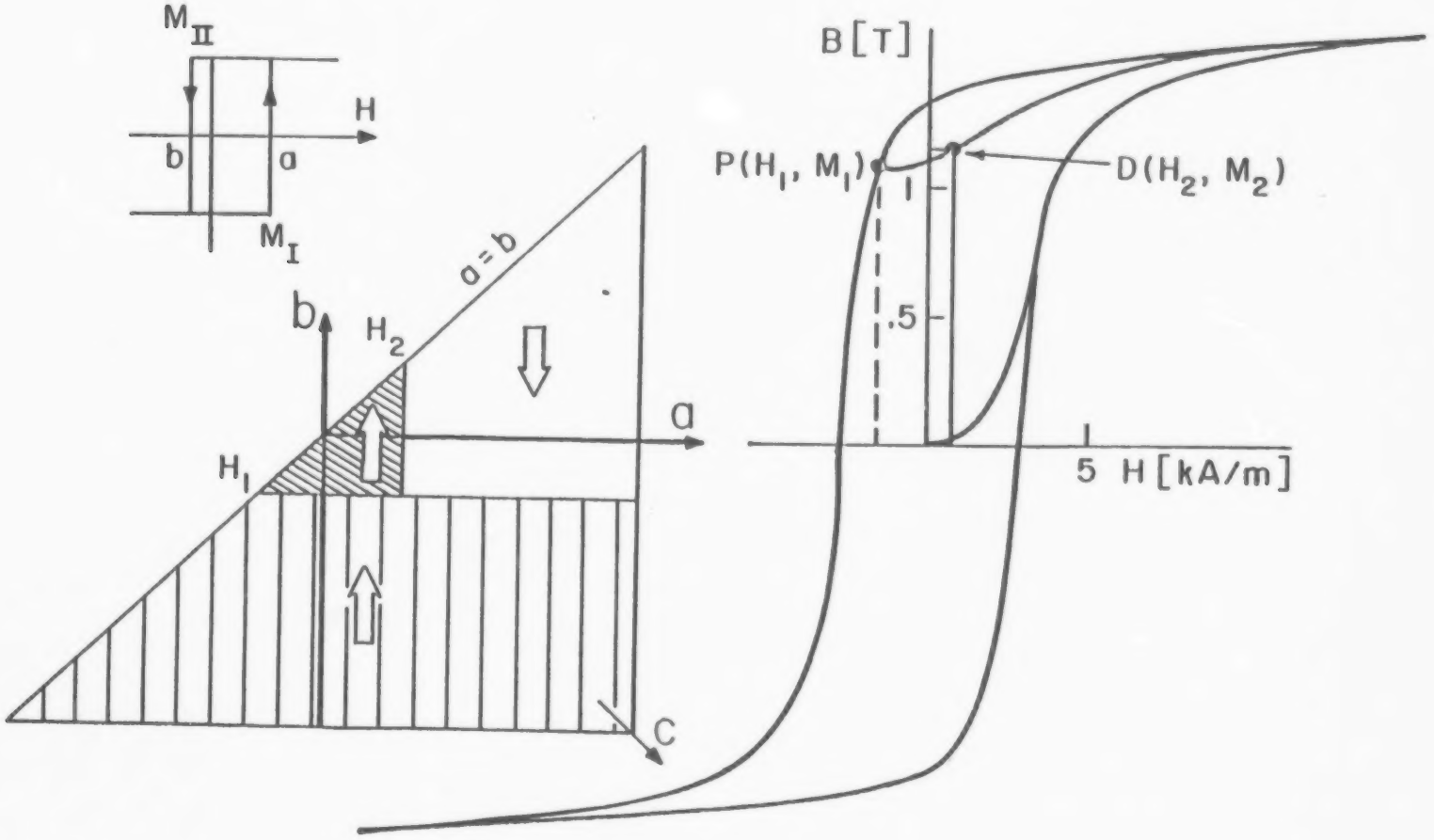
M_II
H
b
a
M_I
a=b
b
H_2
H_1
a
C
B[T]
P(H_1, M_1)
D(H_2, M_2)
1
.5
5 H[kA/m]

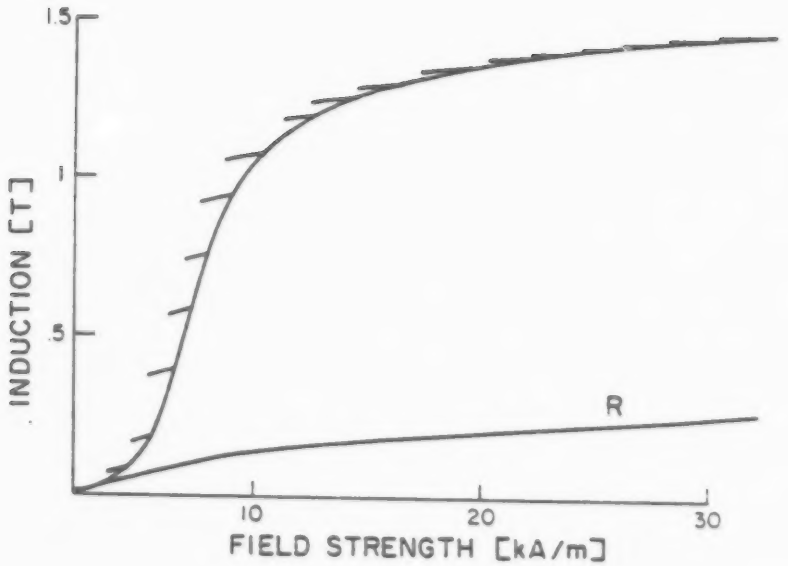

Fig 2

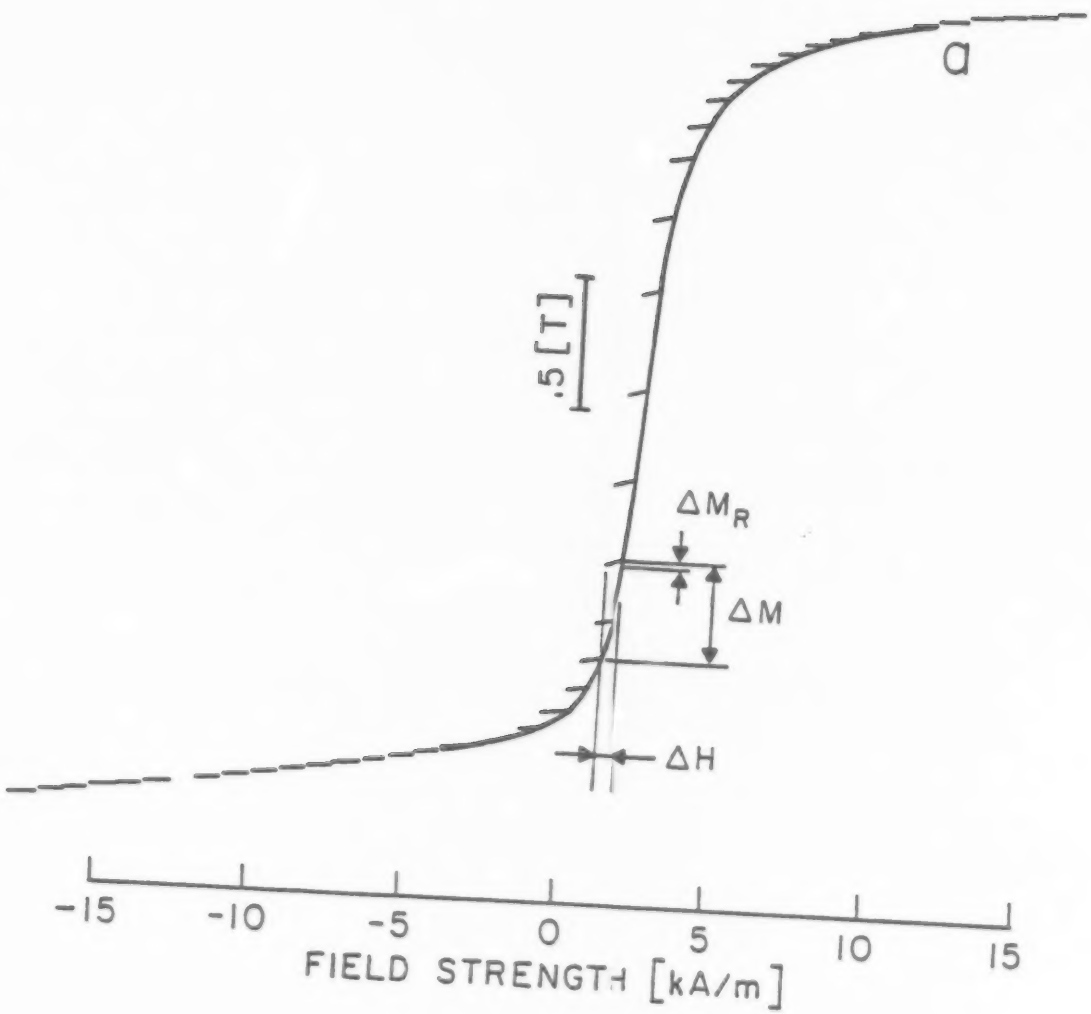

Fig 3.

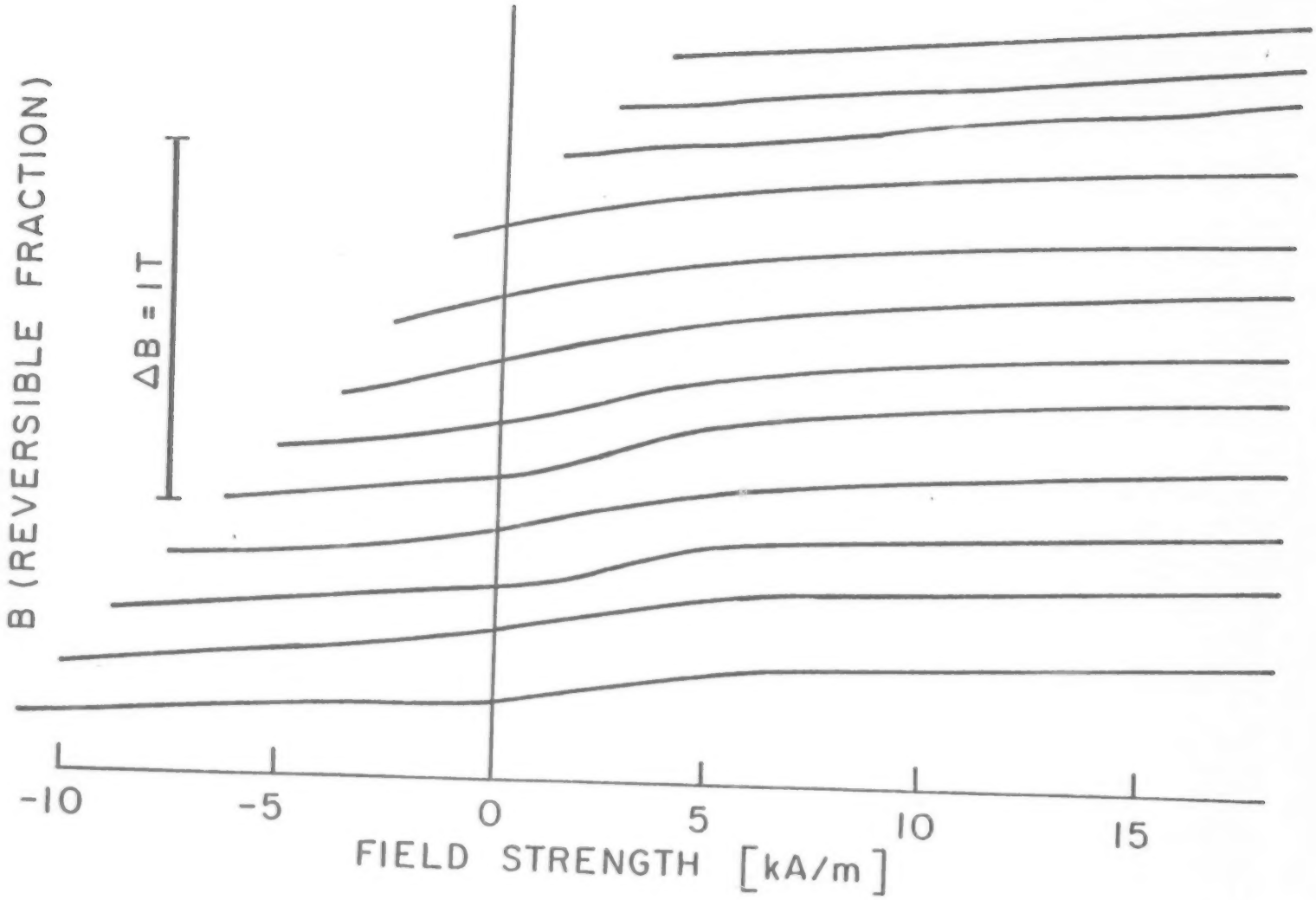

Fig 9

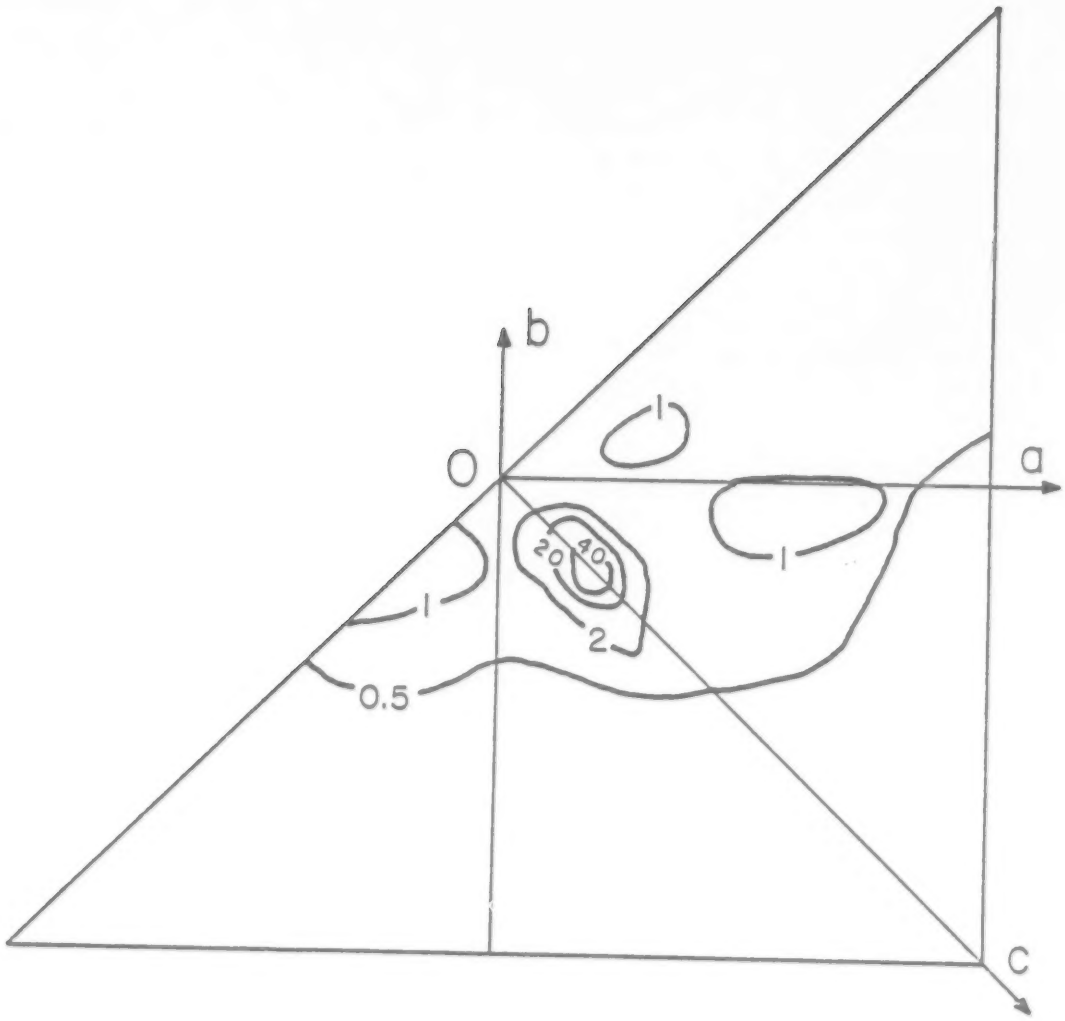

Fig 5

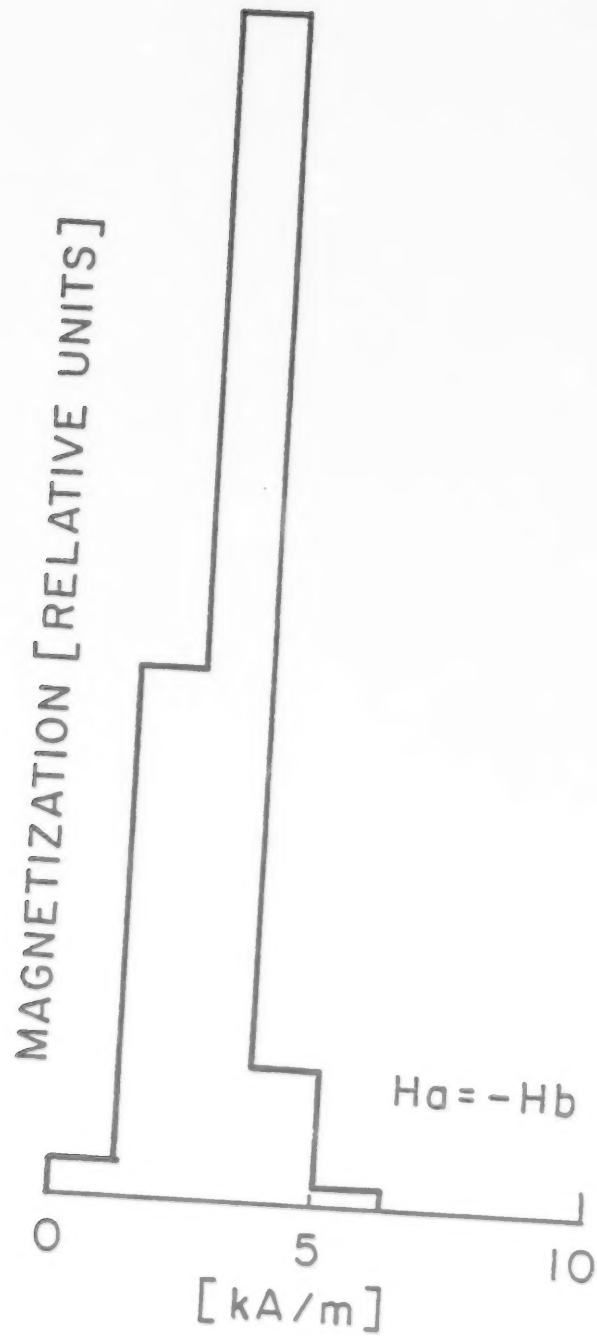

Fig 6

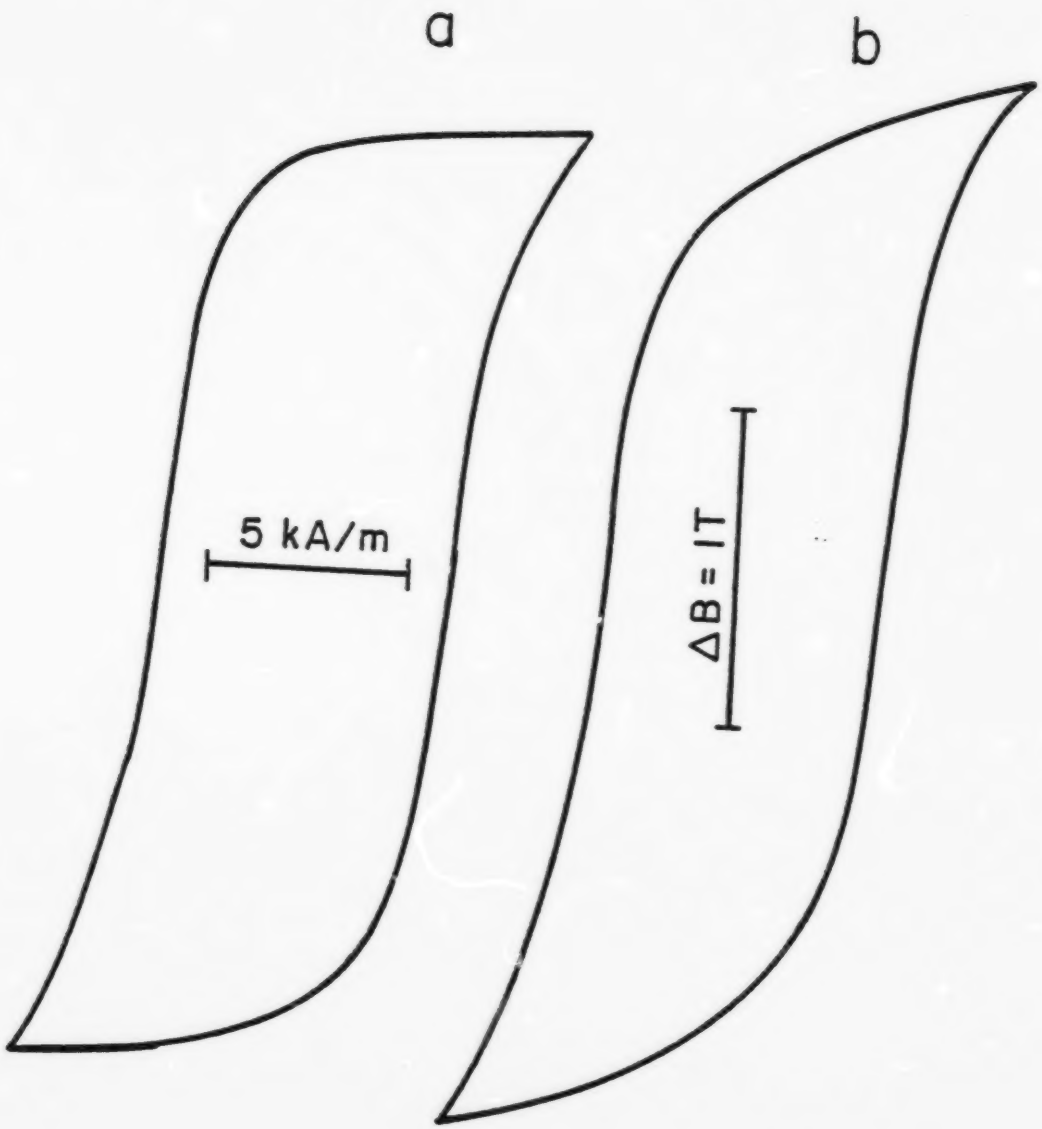

Fig 7

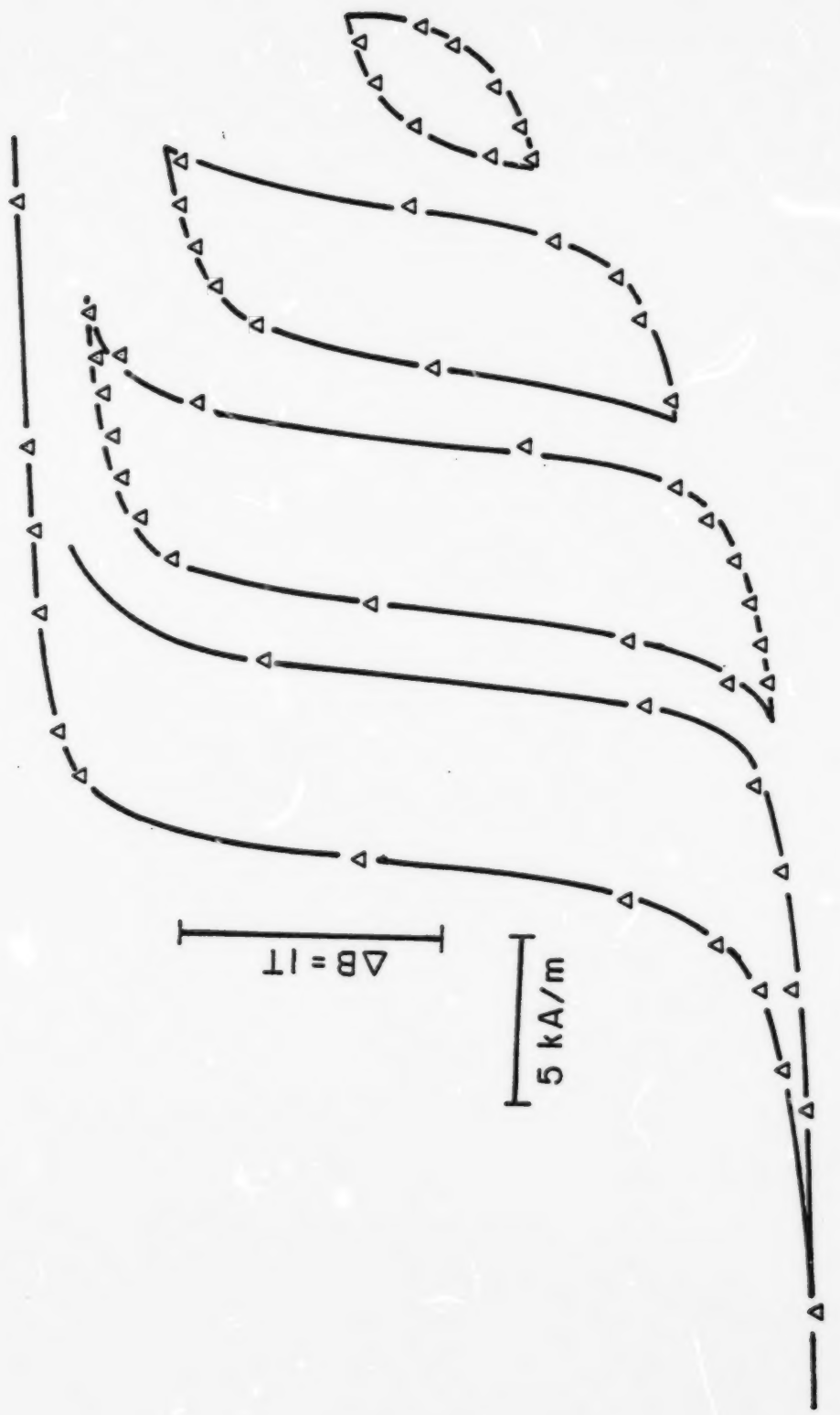

Fig 8

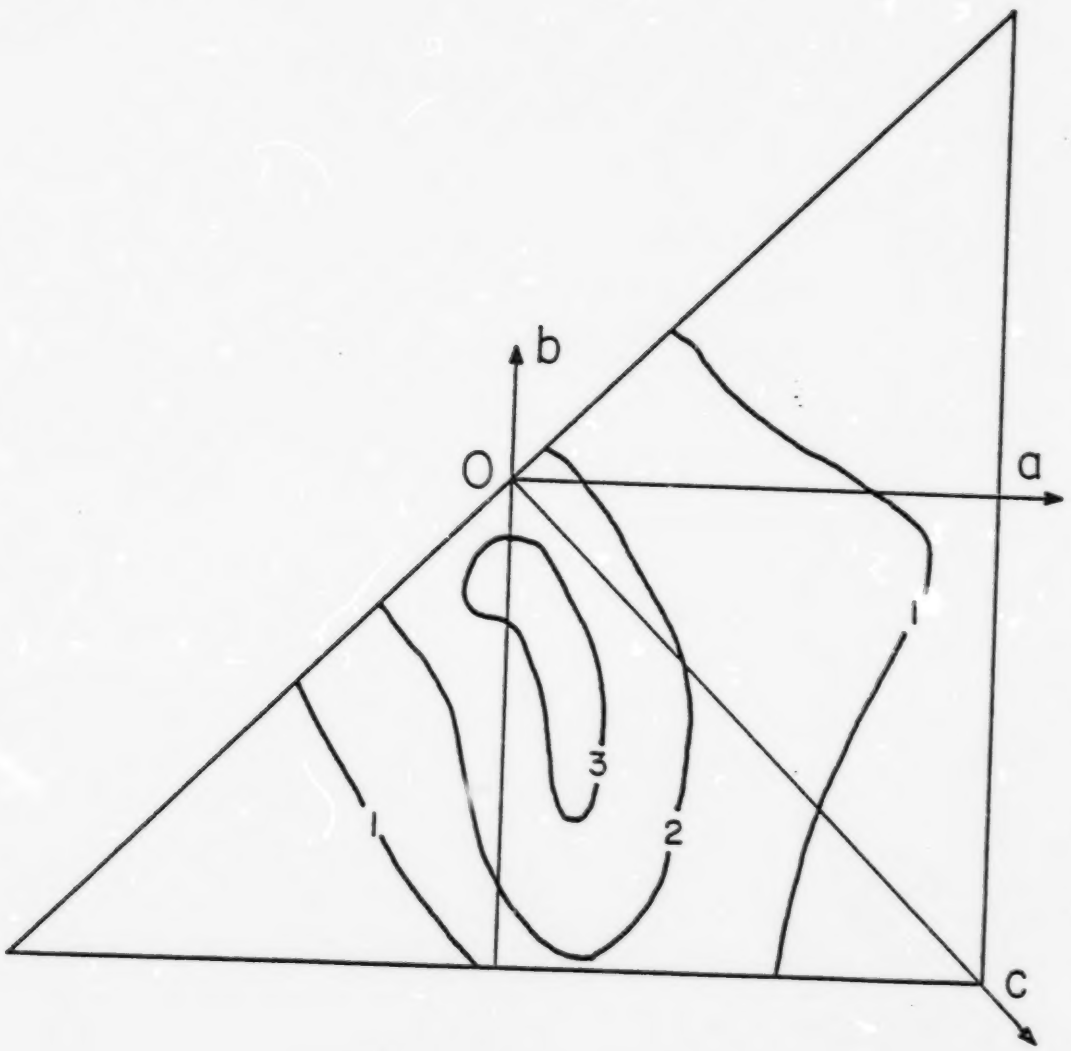

Fig 9

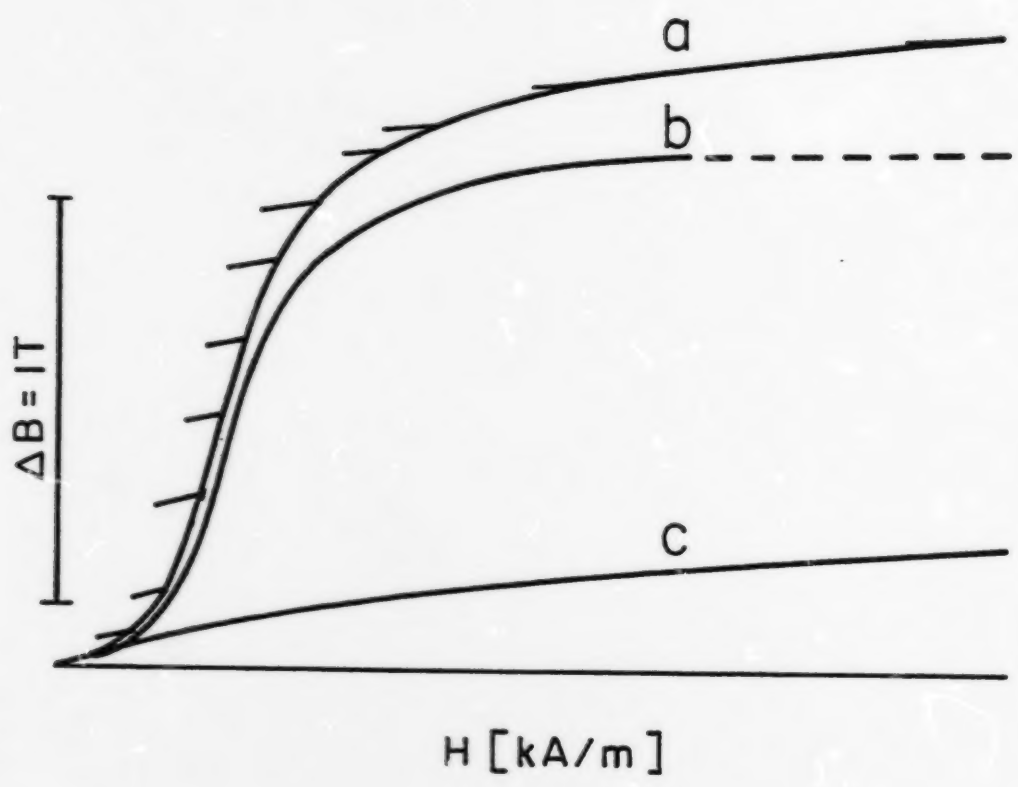

Fig 10

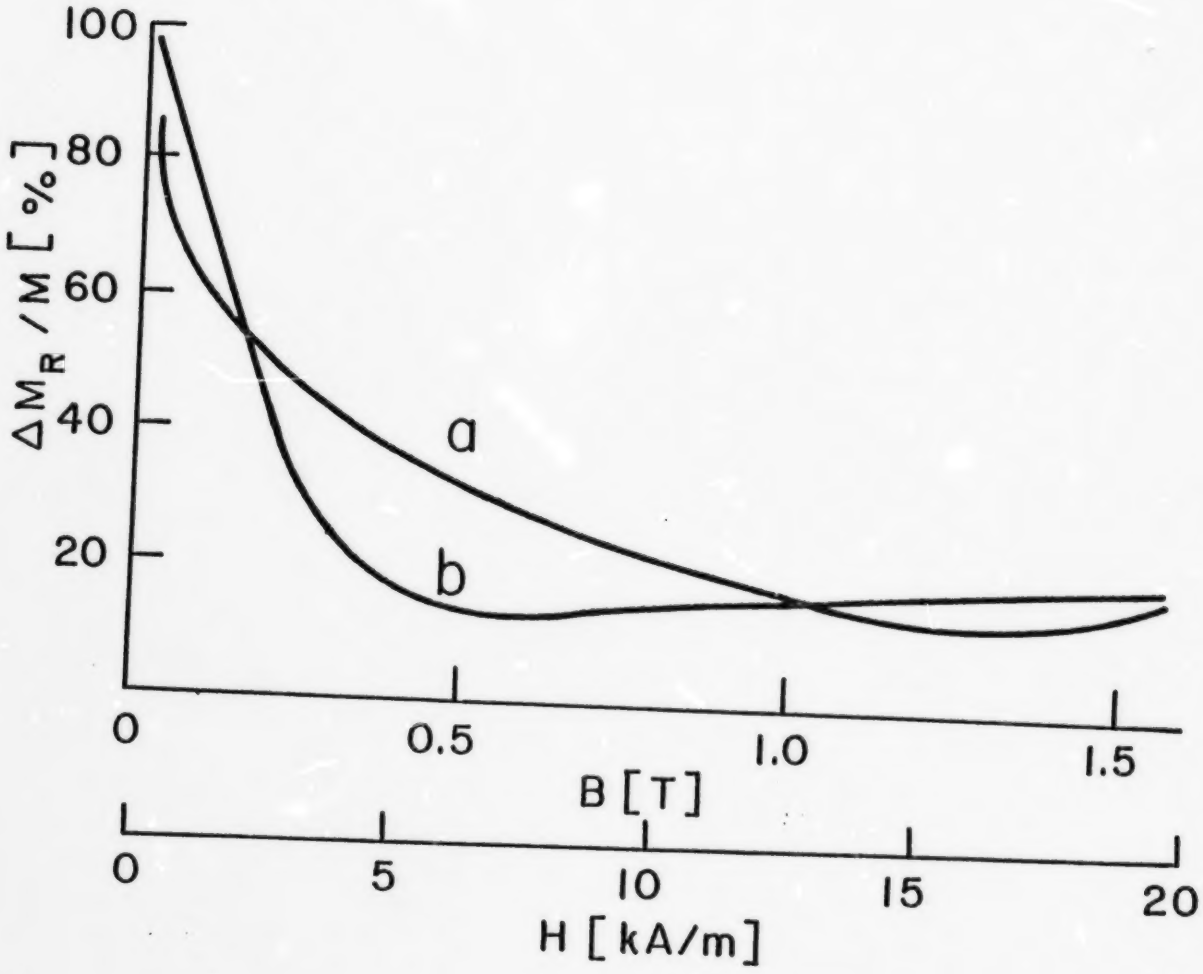

Fig 11

APPENDIX C

1

A new approach to Preisach diagrams*.

D.L. Atherton, Barbara Szpunar, J.A. Szpunar
Physics Department, Queen's University, Kingston,
Ontario, K7L 3N6, Canada

Abstract.

Magnetization processes are complex. A simple Preisach diagram can describe only the irreversible component of magnetization. We introduce here an extended Preisach model including a reversible magnetization component given by a Langevin function which describes low field experimental hysteresis loops very well. We also show that there is a family of anhysteretic curves dependent on the amplitude and form of the AC used to generate them and the turning points on the M-H plane.

* Research supported by Natural Sciences and Engineering Research Council and by contract from National Research Council (Industrial Materials Research Institute) and Department of Energy Mines and Resources (CANMET).

1. INTRODUCTION.

Preisach diagrams are a convenient way of depicting the complicated processes and sequences of magnetization[1]. The ferromagnet is envisaged as a set of elementary interacting domains with rectangular magnetization loops with varying coercivities. The interaction between domains is represented by shifting the origins of the elementary domain magnetization loops. The weak point of the theory is that, in order to perform any calculation, it is necessary to know the distribution function which describes the density of different types of domains with different magnetization loops. This must be measured experimentally[2,3]. Everett[4] worked independently of Preisach to produce a rather similar formulation which did however include the distribution functions. Work on Preisach diagrams which appeared after 1950 when the domain theory of magnetism had been reviewed by Kittel[5] made a big further step toward the better understanding of Preisach diagram representations and their restrictions[6,7,8].

The problem is further complicated because these theories do not include reversible processes such as domain wall bowing. The consequence of this is that, for considerations such as initial susceptibilities, it is necessary either to use distribution functions which have very high values close to the origin or to make some other adjustment such as Del Vecchio has done[9]. Preisach diagrams are however useful in describing the irreversible processes occuring during magnetization and in recording the sequence of significant turning points describing the magnetization history.

Here we propose modifications to avoid these problems and then show how these diagrams can be used to show anhysteretic magnetization and anhysteretic curves. We extend the concept of the anhysteretic magnetization curve to families of anhysteretic curves including anhysteretic curves for minor or asymmetric magnetization loops.

2. PREISACH DIAGRAMS.

On the Preisach model ferromagnetic material is considered to consist of elementary domains which have rectangular hysteresis loops. These are characterized by the switching fields which set the magnetization up (H_a) or down (H_b) corresponding to the direction of the magnetic field, as shown in Fig.1. The Preisach diagram, shown in Fig.2, represents the area of interest for H_a and H_b. By increasing the magnetic field, H, the elementary domains whose critical switching field is lower or equal to the applied field and which were magnetized in the direction opposite to the field reverse their direction to align with the applied field. With decreasing magnetic field domains which are already magnetized in the direction of the field and whose reverse switching field is greater or equal to the current magnetic field reverse their direction of magnetization.

This description of the magnetization process is in accord with the concept of magnetization by domains switching abruptly at their threshold fields as evidenced by Barkhausen jumps.

Preisach diagrams are a convenient way of depicting the processes and turning points involved in magnetic history.

A fundamental concept or assumption of great importance which underlies Preisach type models is that each domain can be characterized by uniquely defined upper and lower switching fields. This implies that between any pair of upper and lower field reversal points the domains which are switched will always be the same or that between any pair of turning points the same set of domains from the ensemble will be switched. This enables us to state that between any pair of turning points a uniquely predetermined fraction of the domains will be operational and that the remaining fraction will be effectively locked or hidden and can play no part in changes in magnetization between these turning points.

In order to clarify the picture we present several examples of elementary hysteresis loops and their corresponding Preisach diagram processes on Figs.3,4 and 5.

3a. THE DISTRIBUTION FUNCTION.

The weakness of the Preisach diagram representation is that in order to describe any hysteresis loop we need to know the distribution function. This can only be found experimentally. As we show subsequently, if a simple finite distribution function is assumed this leads to zero initial susceptibility. In order to obtain finite initial susceptibilities we have to consider distribution functions which have very high values at low fields. Examples show that the function can be complicated[3].

Another serious limitation which causes discrepancies between experimentally measured and calculated hysteresis loops is that a distribution function which does not change during the processes of magnetization is assumed. This implies that hysteresis loops should always close at the end of any complete cycle. Experimentally slight non-closure may be detected particularly at the completetion of the first loop before a large loop has become stablized. Differences may also be noted between the magnetizations at the turning points of small amplitude Rayleigh loops between fields of the same amplitude. The Preisach diagram representation of hysteresis gives rise to restrictions on the shape of minor loops as demonstrated by the the examples shown in Fig.6. The minor loops I,II,III are defined by the same triangle on the Preisach diagram (Fig.6b) and additionally, from the symmetry of the distribution function[6], it follows that loops IV and V on Fig.6a must be similar to loops I,II,III but rotated by 180 degree.

Everett[4] realised these possible difficulties fully and tried to introduce a universal distribution function which would be a good average approximation for both ascending and descending curves. He pointed out the following difficulties in the theory. Firstly the concept of the distribution function assumes that the characteristics of a given domain are independent of the state of its neighbours. Secondly the distribution function is limited only to two possible domain states with magnetization up or down thus precluding consideration of domain orientation. Finally time dependent processes are not included.

Woodward and Della Torre[8] found a criterion for materials which can be represented well by Preisach diagrams. They claim that only materials which are statistically stable can be adequately described by a Preisach diagram representation. Statistical stability means that if any elementary domain changes its characteristic fields b and a to b',a', there must be a corresponding change for some other domains parameters from b',a' to b,a.

3b. EVERETT FUNCTIONS.

In order to determine the distribution function from experimental measurements changes of magnetization due to changes of the applied field are measured. Everett proposed[7] a function which is related simply to the magnetization changes and the distribution function (p(a,b)).

$$E(H_1,H_2)=\int_{H_1}^{H_2} da \int_{H_1}^{a} db\ p(a,b)$$

This represents the integral of the distribution function over the triangular region of the Preisach diagram. In Figs.3b, 4b and 5b we present Preisach diagrams for the initial curve, the upper branch of the saturation major hysteresis and the lower branch of the saturation major hysteresis loop. It is clear that the corresponding changes of magnetization can be represented by the Everett function. The initial curve (Fig.3) is simply:

$$M_i(H)=0.5*E(-H,H)$$

The upper branch at point H with the hysteresis loop with turning point at H_1 (Fig.4) is:

$$M_u(H)=M_i(H_1)-E(H,H_1)$$

The corresponding lower branch at point H for the same loop is (Fig.5):

$$M_l(H)=M_u(-H_1)+E(-H_1,H)$$

The above relationships show that, when there is hysteresis, magnetization depends not only on the applied magnetic field but also on the history.

Enderby[10] introduced a useful notation whereby any hysteresis loop can be represented by the pattern of the turning points, for example:

$$M(H)= M(0^{A}{}_{B}{}^{C}{}_{D}.....H)$$

for which the corresponding magnetization curve and the Preisach diagram are depicted on Fig.7.

Del Vecchio defined rules[2] for abreviating the pattern to the significant turning points only or "forgetting" overwritten loops. He stated that if H is on the upper or lower branch of the hysteresis loop and is correspondingly higher than any previous upper turning point or is lower than some lower turning point we can truncate the pattern at this point with the H value at this point. Explicitly;

Rule 1: If H is in an upper position and exceeds the prior H_n in an upper position, replace that H_n by H, terminating the sequence.

Rule 2: If H is in a lower position and is lower than the prior H_n in a lower position, then replace that H_n by H, terminating the sequence.

4. INITIAL AND ANHYSTERETIC MAGNETIZATION CURVES.

Hysteretic magnetization represents processes where domains are in a local minimum energy configuration. To obtain the magnetization curve which represents the global minimum energy configuration we have to superimpose at every point an AC field whose amplitude decays slowly to zero. The magnetization curve thus obtained is called the anhysteretic curve. It is widely used in recording[11,12]. A simple question arises regarding any dependence of the anhysteretic curve on the superimposed AC. It is generally considered that, in order to obtain the global minimum energy of the anhysteretic, it is only necessary to apply AC of sufficient amplitude. Preisach diagrams give a different answer. The resulting anhysteretic curve depends greatly on the type of AC field pattern used, not only on the maximum amplitude but also on the way it changes with time. The dependence of the quality of recording on the maximum amplitude of the AC-bias was noticed early and is known as under bias if the amplitude of AC oscillation is too small and over bias if the amplitude of AC oscillation is too big. However the effect of the bias amplitude on the quality of recording has been neglected previously in Preisach model discussions. We consider this now. In Fig.8a we show the symmetrical oscillation which is usually used in magnetic recording. This type of oscillation is also used for demagnetizing the recording medium and, as evident from Fig.8b, the Preisach diagram with the DC field equal to zero gives the demagnetized state.

In our further discussion of the anhysteretic curve we assume a constant distribution function for simplicity. This assumption is a good approximation for the irreversible magnetization fraction in the low field Rayleigh region[13] as shown later.

In Fig.9 we give the family of anhysteretic curves corresponding to the upper and lower branches of a magnetization curve and the initial curve. As seen from the corresponding Preisach diagrams of Fig 10, if the amplitude (A) of AC bias field plus the DC field (H) is lower than the maximum field (H_m) we obtain different Preisach diagrams for different points on the hysteresis loop instead of one principal curve corresponding to large amplitude AC bias field giving over bias.

We now discuss the influence of the form of oscillation on the shape of the ahysteretic curve and propose a special type of oscillation which, for a constant distribution function, gives a linear anhysteretic magnetization curve. Fig.11 shows this special type of alternating field decay. In Fig.12 and 13 we depict the corresponding Preisach diagrams. In Fig.14 we show anhysteretic curves for minor loops starting from the initial magnetization curve which correspond to the Preisach diagram of Fig.13a and the anhysteretic curve for the saturation major loop corresponding to the limiting case ($H_m=H_s$) of the Preisach diagram in Fig.13a. For comparison we also show on Fig.14 the initial curve for the same constant distribution function. The maximum deviation from the anhysteretic curve occurs at 50% of the turning point fields. We also present anhysteretic curves for minor loops from the upper branch of the hysteresis loop in Fig.15 and in Fig.16 anhysteretic curves for the minor loops of the lower branch curve. The corresponding Preisach diagrams are shown in Fig.13. By assuming a constant distribution function we can find the analytic equation for the magnetization curves for different regions of the hysteresis loop. These are presented in Table 1.

We therefore propose that there is not a single unique anhysteretic curve but rather a family of anhysteretic curves. The principal anhysteretic curve represents the situation where the entire domain ensemble has been driven to a minimum energy state for the DC bias field under consideration. Points on it are obtained by using a symmetric AC bias field with an initial amplitude sufficient to switch all domains however, as we have shown above, it is not only the amplitude of the AC bias which determines the final state but also the form of oscillation used (symmetric or asymmetric). It is therefore not possible to give a unique definition of the form of AC oscillation needed to drive the magnetization to the global minimum equilibrium value. Other techniques, such as the application of very high intensity ultrasound, might also be used to drive all the domain magnetization vectors to their global equilibrium state by supplying external energy to overcome the effect of pinning sites. Other possibilities include large amplitude stress cycling or thermal cycling.

Most hysteresis loops depend on previous magnetic history, i.e. the sequence of turning points, which can be represented on Preisach diagrams. The Preisach diagram concept is that between any two turning points only a fraction of the domain ensemble is operational, the remainder being locked or hidden. We can therefore define an equilibrium distribution of domain magnetization vectors for the operational fraction of the domain ensemble, as defined by the turning points, and for a particular field (between the limiting turning points). This gives rise to families of anhysteretic curves depending on the limiting turning points on the M-H plane or on the amplitude and form of AC bias used since these define the fraction of domains being operated on to obtain their local minimum equilibrium energy states.

5.REVERSIBLE MAGNETIZATION.

Preisach diagrams with elementary rectangular hysteresis loops of finite width describe only irreversible processes. The consequence of this is that the initial susceptibility is zero, which is, of course, contrary to experimental observation.

The distribution function must be determined experimentally. It is obtained by measuring changes in magnetization which, by definition, include both reversible and irreversible contributions. Bate[3] has shown an experimental distribution function describing experimental magnetization curves for fine magnetic particles. Although the agreement with experimental results is very good the procedure is not very useful as both reversible and irreversible processes have been considered together and the distribution function gives little information about the physical processes occuring during magnetization.

In order to obtain more information about reversible and irreversible magnetization contributions we consider small changes of the magnetic field. In Fig.17 an example of a Rayleigh hysteresis loop is given. We see that the shape of the hysteresis loop and the initial curve are in agreement with the shape of the loop and initial curve obtained using a constant distribution function (Fig.14) but the slope of the magnetization curve near to the turning points corresponding to the upper and lower branches of the hysteresis loop and near to the origin of the initial curve are finite and equal to the initial susceptibility. This contrasts with the simple Preisach diagram result where the slope is equal to zero due to neglecting the reversible part. What are these reversible processes? Globus proposed[14] a simple model of domain wall bowing to describe reversible processes in polycrystalline materials. The reversible part is linearly dependent on the magnetic field. This result supports our conclusion that in analysing magnetic processes by Preisach diagrams we should first separate the reversible part of the magnetization which, for low fields, can be described by the equation:

$$M_{rev} = (\text{Initial susceptibility}) * H$$

Then the remaining irreversible part can be described by a more regular distribution function which, for low magnetic field, can even be a uniform distribution. The Preisach model combined with the separate model for the reversible part we will call the extended Preisach model. In the next section we demonstrate the application of this model to the description of magnetization processes in steel.

6. THE EXTENDED PREISACH MODEL.

In order to study the contributions of reversible and irreversible processes we have chosen a steel sample.

In Fig.18 we show the reversible magnetization component extracted by using small field reversals. This reversible part can be described well over a wide range of the magnetic field by a Langevin function which, of course, describes rotational processes. Even domain wall bowing is actually a local rotational process due to interactions between spins along the domain wall. There is no critical field for this processes as demonstrated by the nonzero value of the recoil permability.

All processes which require a finite critical field we define as being irreversible processes. They can be represented by a Preisach diagram. The distribution function for this simple hysteresis mechanism depends on the distribution of defects which lock the domain walls in certain positions and also on the texture which describes the distribution of easy axes in crystallites and thus characterizes the distribution of the locally applied effective external field at the grain. In a material with randomly distributed defects which are not strongly textured and with a random interaction field with nearest domains, as in the low field region, we would expect that a constant distribution function should be a good description of the elementary irreversible processes. In Fig.19a,b we show the experimental hysteresis loops for steel. Fig.20a shows that ascending curves can cross the initial curve with different slopes at the crossing points (O,X on Fig.20a). This demonstrates that, although major hysteresis loops can be described well by simple equations or functions, an arbitrary pattern of magnetization processes must include information about the previous magnetic history. Preisach diagrams are one of the possible ways of describing this magnetization history.

In Fig.20a,b we show that our improved model can describe any pattern of magnetization processes well with only four parameters. The reversible part is shown on fig.20c and is described by the equation:

$$M_{rev}=xM_sL[(H+\alpha M)/a]$$

where x represents proportion of the reversible part, $L[(H+\alpha M)/a]$ is the Langevin function. From examination of experimental curves for a wider range of magnetic field we note that the reversible part shows some small hysteresis. This arises because it is dependent on the mean field which is dependent on the total magnetization which demonstrates hysteresic behavior. The irreversible part is presented for the initial curve and a major loop in Fig.20d. It demonstrates a parabolic behavior due to the constant distribution function assumed.

Our theoretical hysteresis loops have been obtained using a microcomputer and a Pascal program. In spite of the general belief that calculations using Preisach models are time consuming we obtained the plots shown in only a few minutes.

7.CONCLUSIONS.

Preisach diagrams are very useful in describing locked and operational fractions during magnetization processes. They are particularly useful in the interpretation of recording processes, especially anhysteretic curves. We have also used Preisach diagrams to show that the anhysteretic is not unique and that it is in fact dependent on both the amplitude and form of the AC bias, the turning points or the fraction of the domain ensemble which is being driven to equilibrium.

The Preisach model describes irreversible processes quite well but reversible processses also contribute to magnetization changes and should be considered. We have therefore extended the Preisach model to include a reversible magnetization contribution.

Preisach diagram representation is the only theory at the moment which can represent the dependence of the complicated magnetization curves on the previous history, however they cannot describe the full details of real processes, for example minor loops which, according to the simple Preisach model, should always close.

Preisach diagrams are only useful for some materials. They do not represent the real physical situation where any arbitrary domain configuration can be found but, by means of the distribution function, they give us some information about the interaction between domains.

TABLE 1.

Analytic formulae for the magnetization curves using a constant distribution function. H_∞ is the saturation field, M_∞ the saturation magnetization, H_m the turning point for the major loop, H_1,H_2 the minor loop turning points and H the current value of the applied magnetic field.

Type of curve.	: Equation describing M - H dependence. for a constant distribution function
Initial curve:	$M/M_\infty = H^2/H_\infty^2$
Anhysteretic curve for the saturation major loop:	$M/M_\infty = H/H_\infty$
Anhysteretic curve for a major loop:	$M/M_\infty = H_m*H/H_\infty^2$
Anhysteretic curve for an upper branch minor loop:	$M/M_\infty = (H_m*H_m+2H_m*H_1-H_1*H_2+H*(H_2-H_1))/(2H_\infty*H_\infty)$
Anhysteretic curve for a lower branch minor loop:	$M/M_\infty = (H_2*H_2+H_1*H_2-(H_\infty-H_2)*2+H*(H_2-H_1))/(2H_\infty*H_\infty)$

FIGURE CAPTIONS.

Fig.1 The magnetization curve for an elementary domain. H_a and H_b are the critical switching fields. H_m, the shift of the origin of the hysteresis loop, represents the interaction between domains. H_c is half of the difference in the switching fields (zero point coercivity).

Fig.2 The Preisach diagram representing the physical regions of the fields causing swiching up (H_a) and down (H_b).

Fig.3a The initial magnetization curve.

Fig.3b The Preisach diagram for the initial cuve.

Fig.4a The upper branch of the saturation hysteresis loop.

Fig.4b The Preisach diagram for the upper branch of the saturation hysteresis loop.

Fig.5a The lower branch of the saturation hysteresis loop.

Fig.5b The Preisach diagram for the lower branch of the saturation hysteresis curve.

Fig.6a Minor loops which, on the Preisach model, should all be similar.

Fig.6b The Preisach diagrams for the minor loops shown on Fig.6a.

Fig.7a Hysteresis curves for a complicated pattern (see text).

Fig.7b The Preisach diagram for the complicated pattern shown in Fig.7a.

Fig.8a Symmetric AC bias oscillation as used in magnetic recording shown for a particular value of DC field.

Fig.8b The Preisach diagram for the anhysteretic curve obtained with large amplitude AC bias field. The corresponding diagram with zero DC field represents the demagnetization process.

Fig.9 A family of anhysteretic curves obtained using a constant distribution function and a symmetric AC bias field.

Fig.10 The Preisach diagrams for symmetrical AC bias corresponding to:
a).the anhysteretic curve for the initial magnetization curve,
b).the anhysteretic curve for the upper branch of the magnetization curve,
c).the anhysteretic curve for the lower branch of the magnetization curve.
H_m is the maximum total field or the magnitude of the symmetric turning point fields in case c. H is the DC bias field and A the amplitude of the AC bias.

Fig.11 A sequence of oscillations which generates a linear anhysteretic curve when used with a constant distribution function.

Fig.12 The Preisach diagram for the anhysteretic curve for the saturation major hysteresis loop and the sequence of oscillations shown on Fig.11.

Fig.13 Preisach diagrams for the anhysteretic curves for the oscillation sequence depicted in Fig.11 corresponding to:
a). the anhysteretic curve for a minor loop originating from the initial curve (see Fig.14),
b). the anhysteretic curve for a minor loop originating from an upper branch curve (see Fig.15),
c). the anhysteretic curve for a minor loop originating from a lower branch curve (see Fig.16).

Fig.14 The anhysteretic magnetization curves using a constant distribution function and the AC bias shown on Fig.11 depicting:
full line - the anhysteretic curves for minor loops (corresponding to the Preisach diagram of Fig.13a),
dotted line - saturation major hysteresis loop,
broken line - the initial magnetization curve.

Fig.15 Upper branch minor loops using a constant distribution function and the corresponding anhysteretic curve for the oscillation sequence shown in Fig.11 and the Preisach diagram of Fig.13b.

Fig.16 Lower branch minor loops using a constant distribution function and the corresponding anhysteretic curves for the oscillation sequence shown on Fig.11 and the Preisach diagram of Fig.13c.

Fig.17 An example of the initial magnetization curve and hysteresis loop in the Rayleigh low field region.

Fig.18 The reversible magnetization component (R) extracted from the total magnetization (T) by using small field reversals.

Figs.19 a) experimental ascending curves and minor loops,
b) experimental demagnetization curves for steel.

Fig.20 Theoretical: a) ascending curves and minor loops,
b) demagnetization curves,
c) reversible part,
d) irreversible part.

REFERENCES

1. F. Preisach, "On Magnetic Aftereffect", Zeitschrift fur Physik, Vol.94, pp.277-302, 1935.

2. R.M. Del Vecchio, "An Efficient Procedure for Modelling Complex Hysteresis Processes in Ferromagnetic Materials", IEEE Trans. on Magnetics, Vol.MAG-16, pp.809-811, 1980.

3. G. Bate, "Statistical Stability of the Preisach Diagram for Particles of gamma-Fe_2O_3", J. Appl. Phys., Vol.33, pp.2263-2269, 1962.

4. D.H. Everett,"A General Approach to Hysteresis - Part 3. A Formal Treatment of the Independent Domain Model of Hysteresis", Trans. Faraday Soc. pp.1077-1096, 1953.

5. C. Kittel, Phys. Rev., Vol.70, pp.965-71, 1946, Ibid., Vol.73, pp.810-11, 1948, "Physical Theory of Ferromagnetic Domains", Rev.Mod.Phys., Vol.21, pp.541-83, 1949.

6. G. Biorci and D. Pescetti, "Analytical Theory of the Behaviour of Ferromagnetic Materials," Il Nuovo Cimento, Vol.7, No.6, pp.829-842, 1958.

7. D.H. Everett, "A General Approach to Hysteresis - Part 4. An Alternative Formulation of the Domain Model", Trans. Faraday Soc., Vol. 51, pp.1551-1557, 1955.

8. J.G. Woodward and E.Della Torre, J. Appl. Phys., Vol.31, pp.56-62, 1960.

9. R.M. Del Vecchio, "The Inclusion of Hysteresis Processes in a Special Class of Electromagnetic Finite Element Calculations", IEEE Trans. on Magnetics, Vol. MAG-18, pp.275-284, 1981.

10. J.A. Enderby,"The Domain Model of Hysteresis, Part 1. Independent Domains", Trans. Faraday Soc., Vol.51, pp.835-848, 1955.

11. G. Schwantke, "The Magnetic Tape Recording Process in Terms of the Preisach Representation", J. Audio Eng. Soc., Vol.9, pp.37-47, 1961.

12. F. Jorgensen, "The Complete Handbook of Magnetic Recording", TAB Books Inc., Blue Ridge Summit, PA, 1980 .

13. Rayleigh, Lord, "on the Behaviour of Iron and Steel under the Operation of Feeble Magnetic Forces", Phil. Mag., Vol.5, No.23, pp.225-248, 1887.

14. A. Globus and R. Valenzuela, IEEE Trans. Magnetics, Vol.MAG-11, pp.1300, 1975.

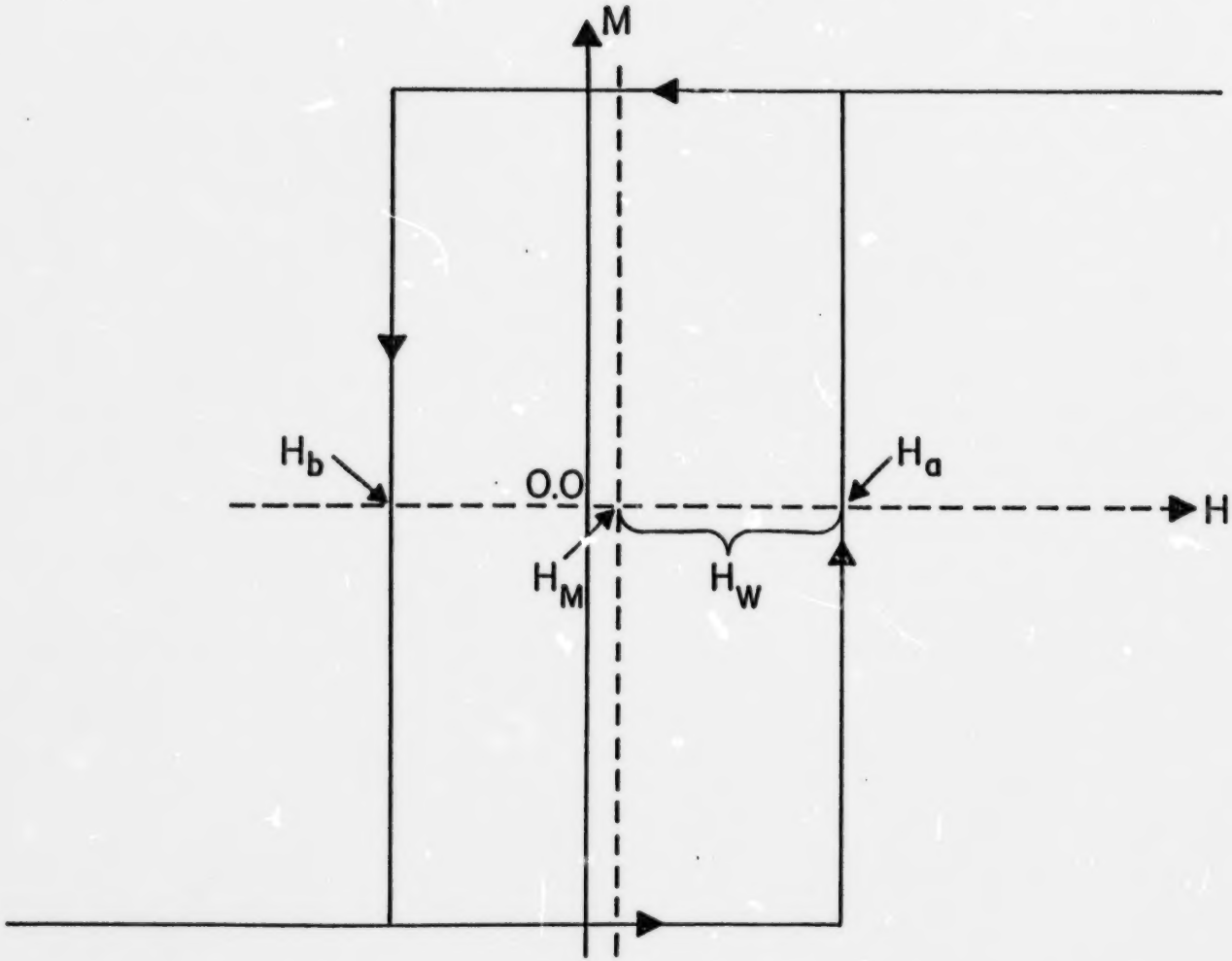

Atherton Szpunar & Szpunar Fig 1

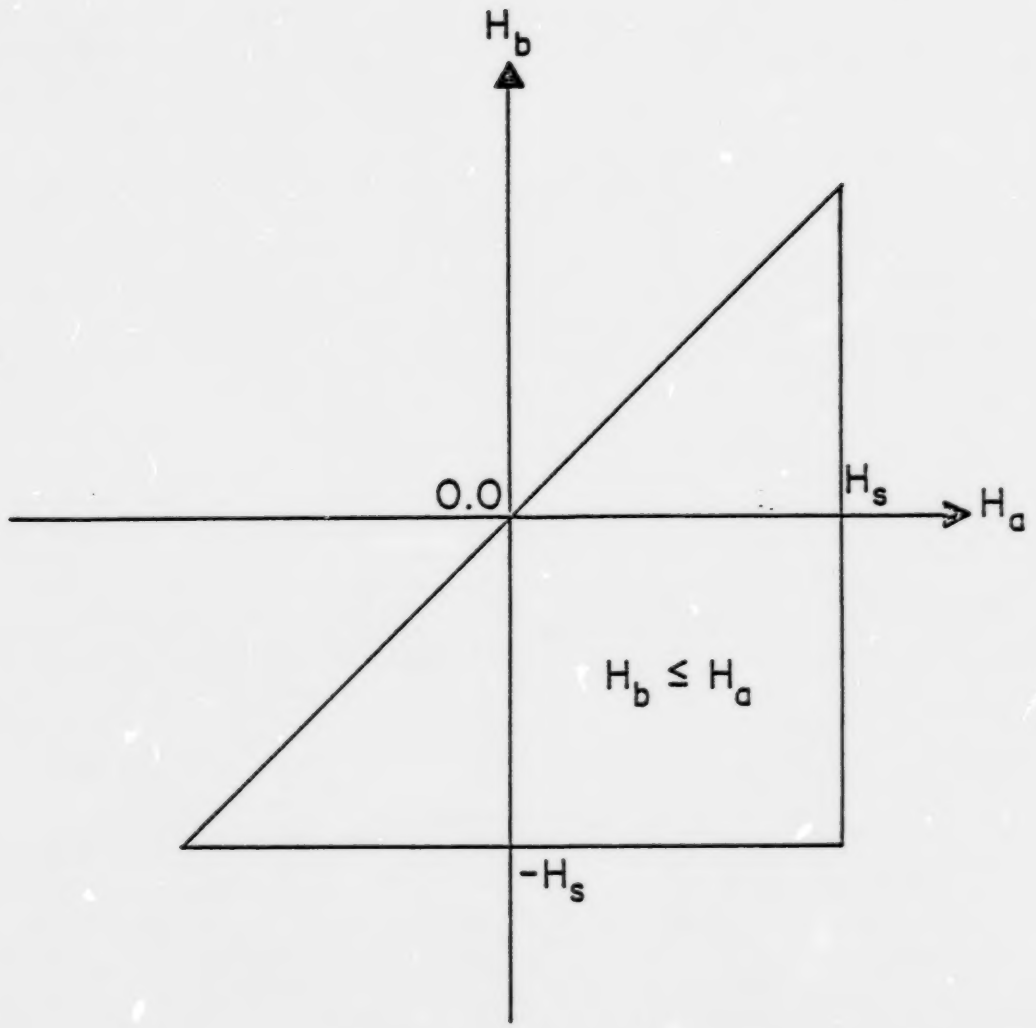

Athertón, Sizpuras & Sizpura- Fig 2

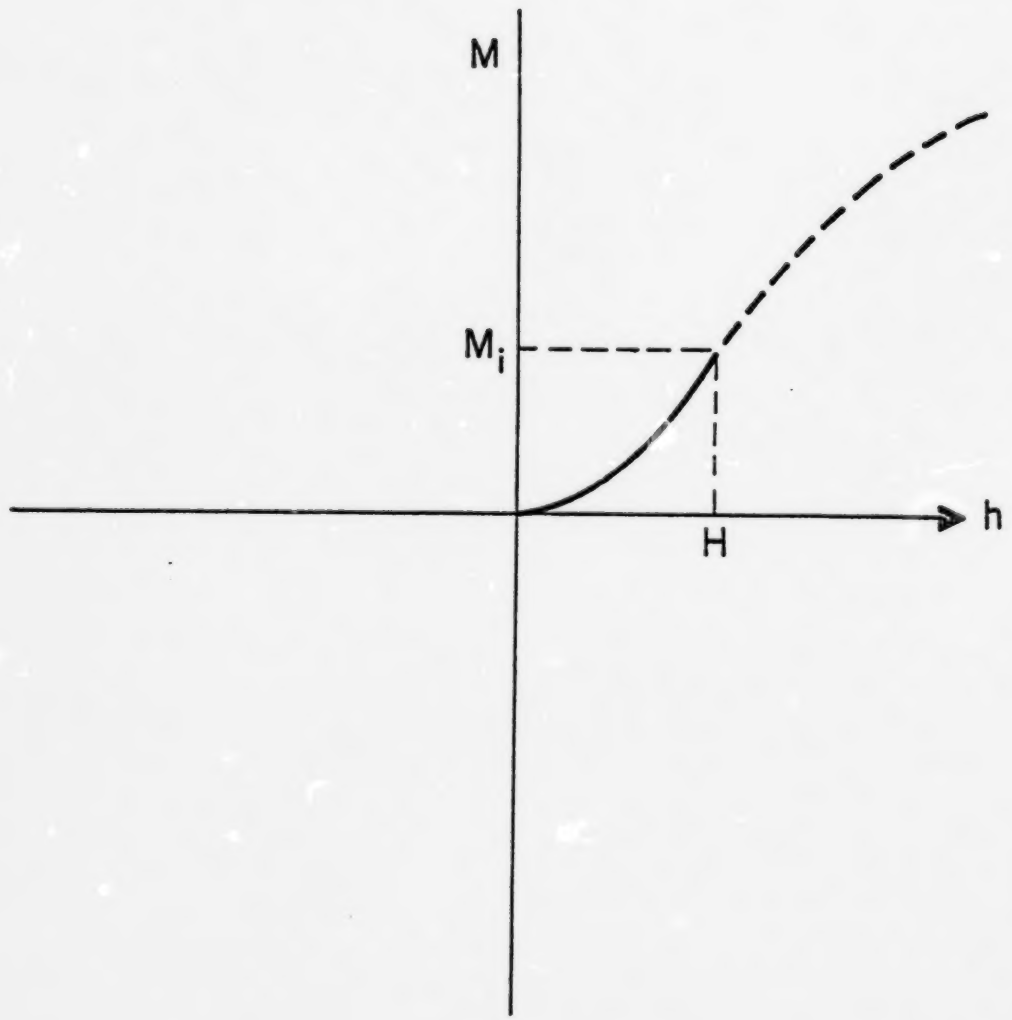

Athestoa, Lepura: aSzpura

Fig 3a

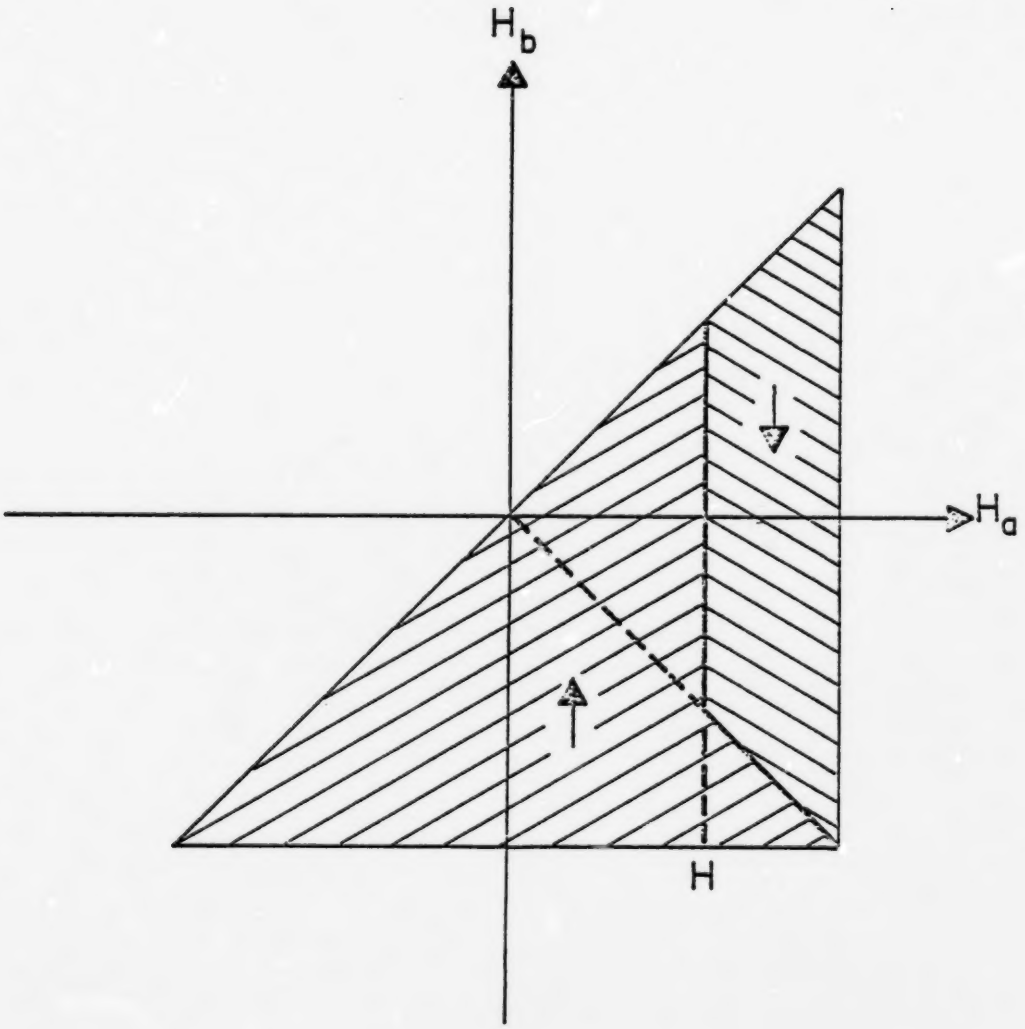

Atherton, Lupura Lupura Fig 3 b

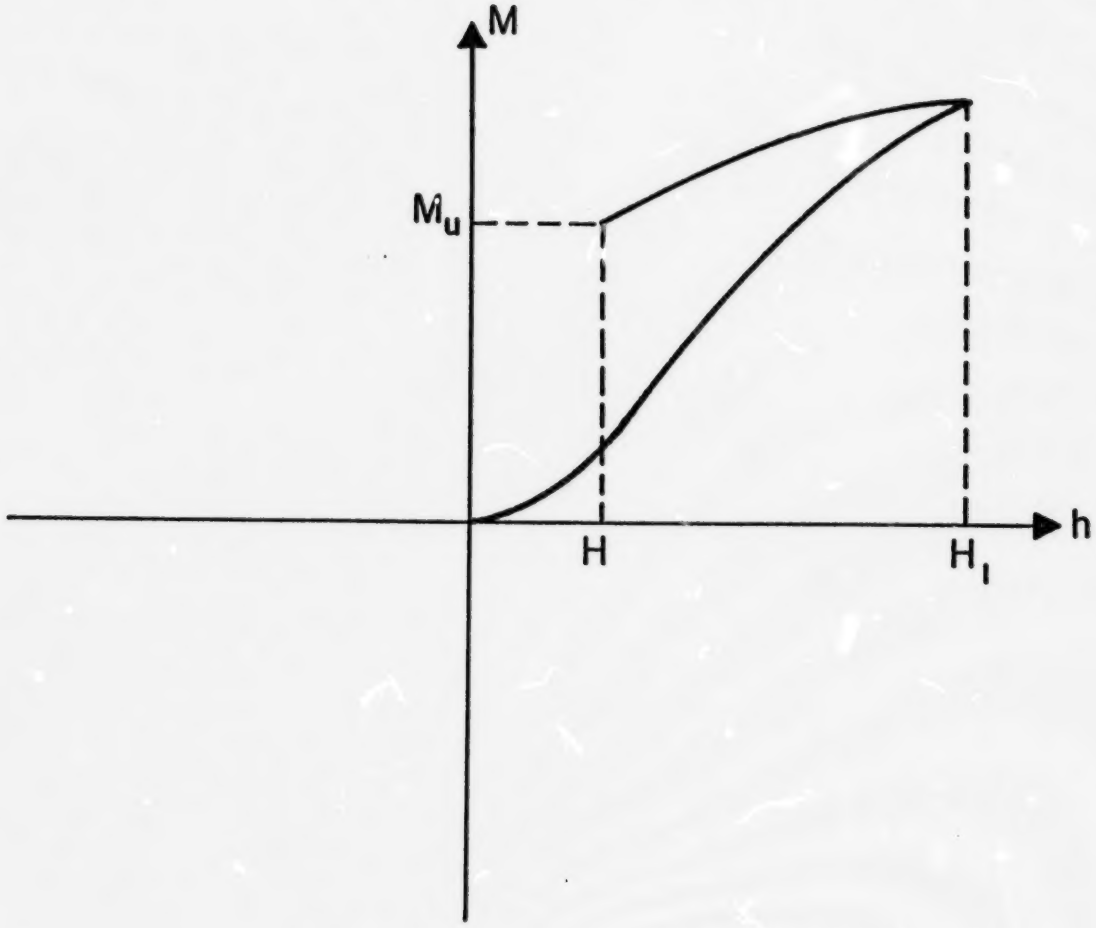

Athetön, Szparas a Szparat Fig 4a

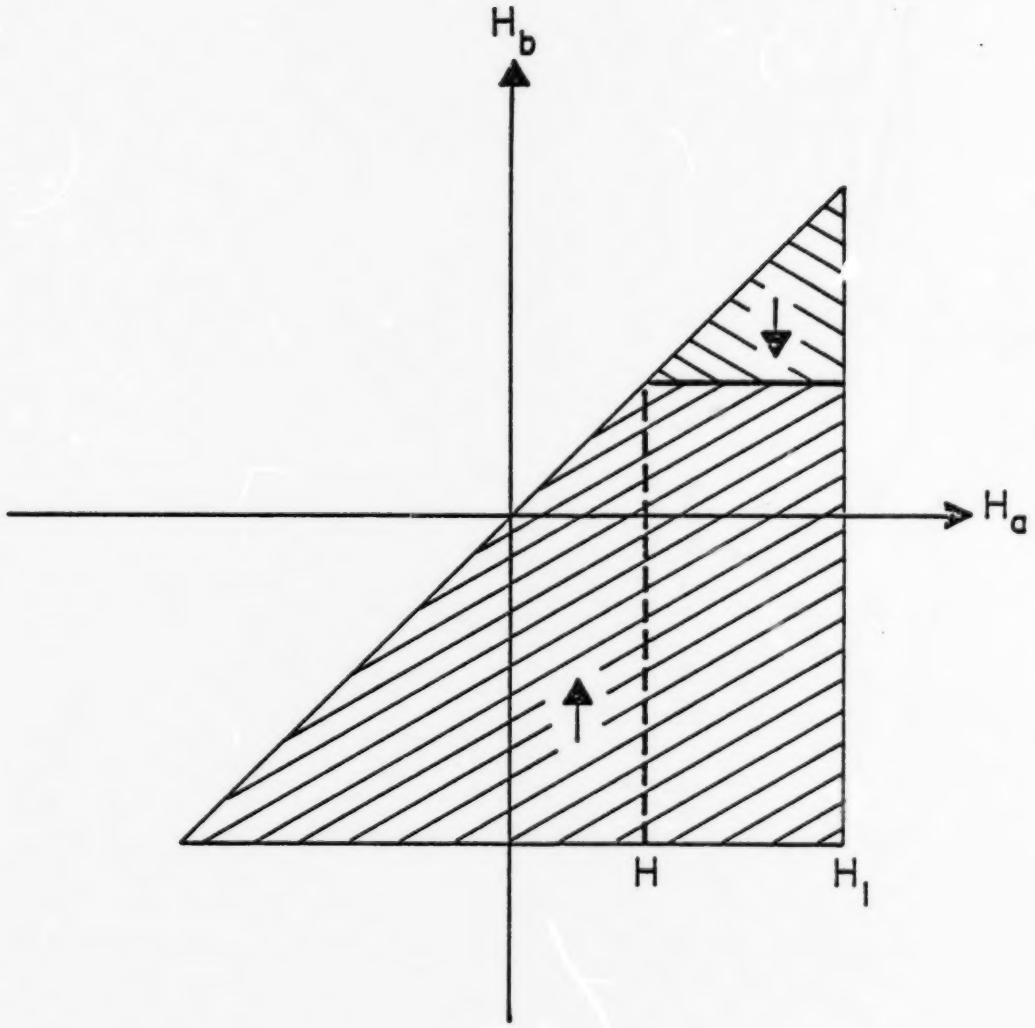

Alheton, Szpuras a Szpuras Fig 4.6

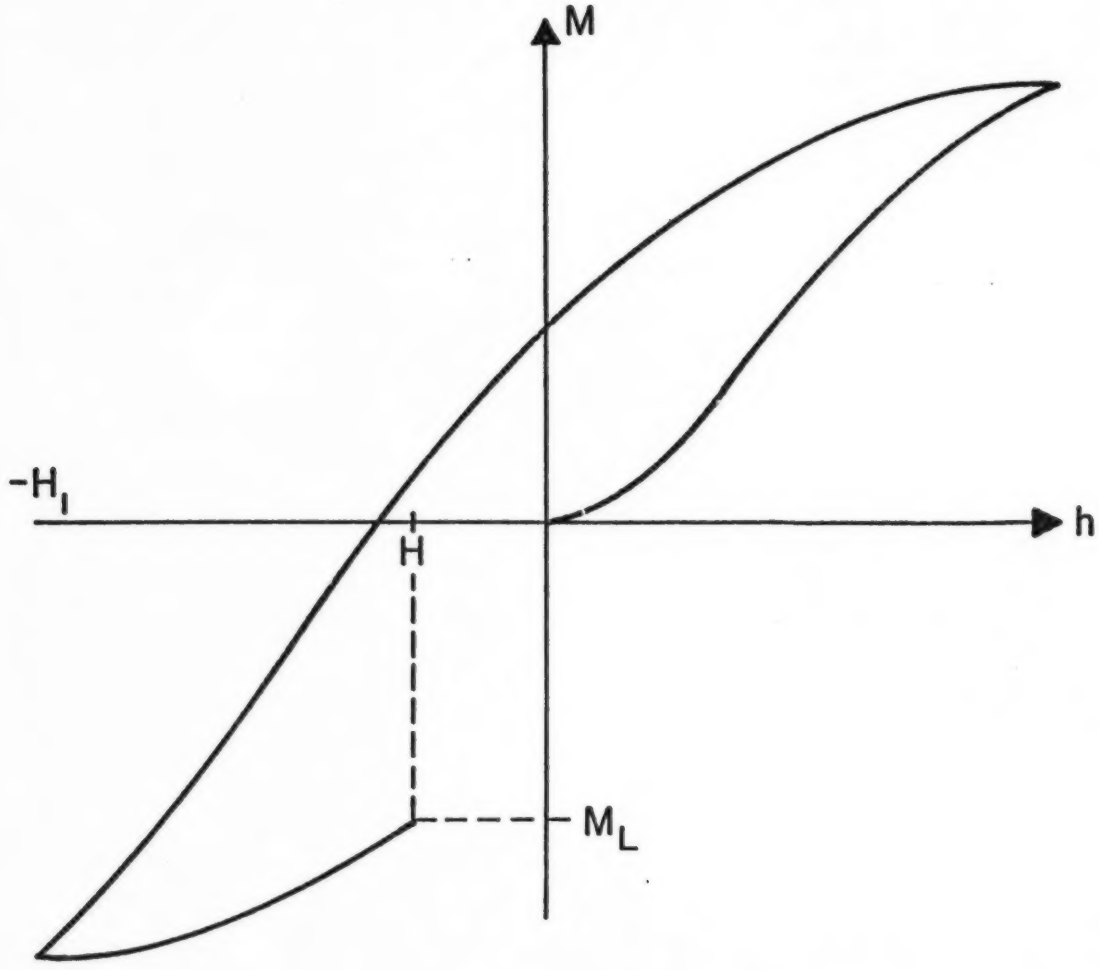

Atherton, Szpurar & Szpurar Fig 5a

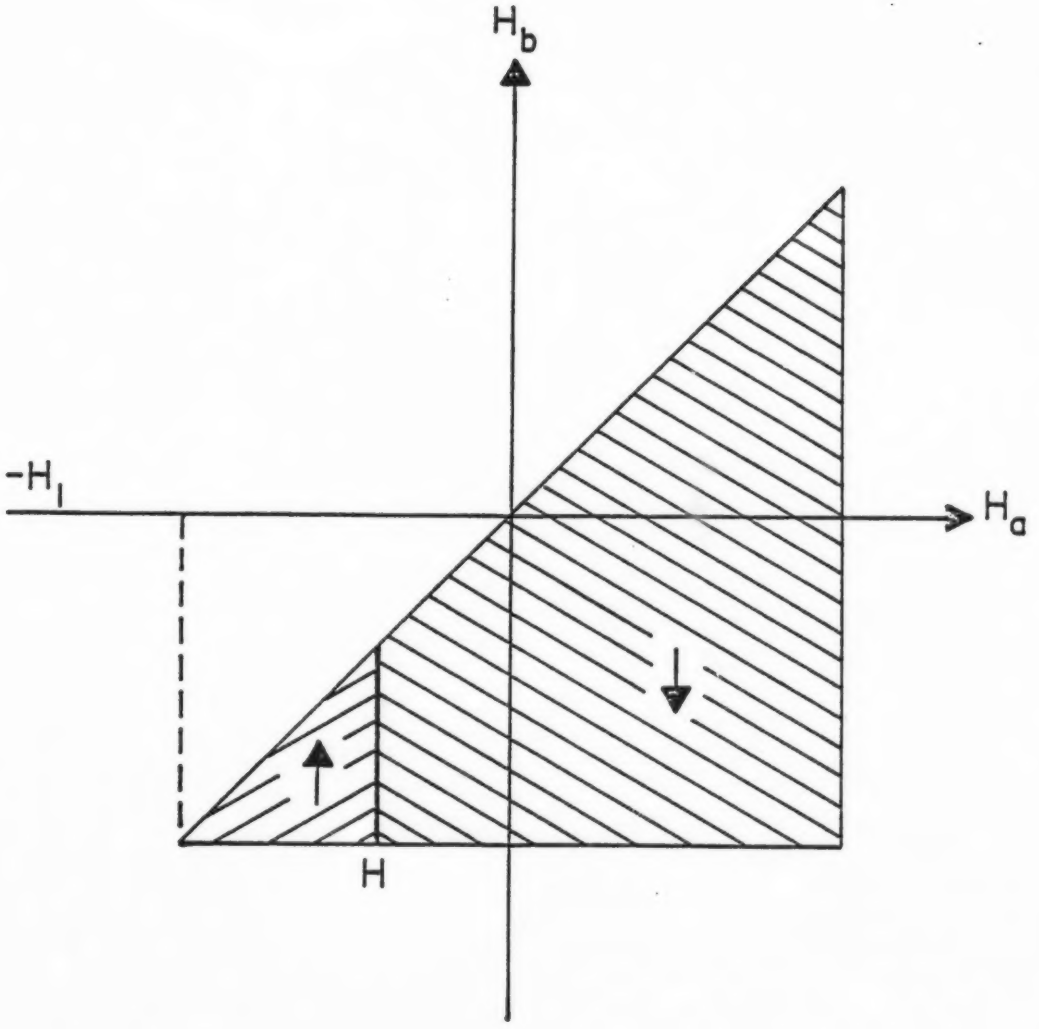

atherton, Szpunar & Szpunar Fig 5b

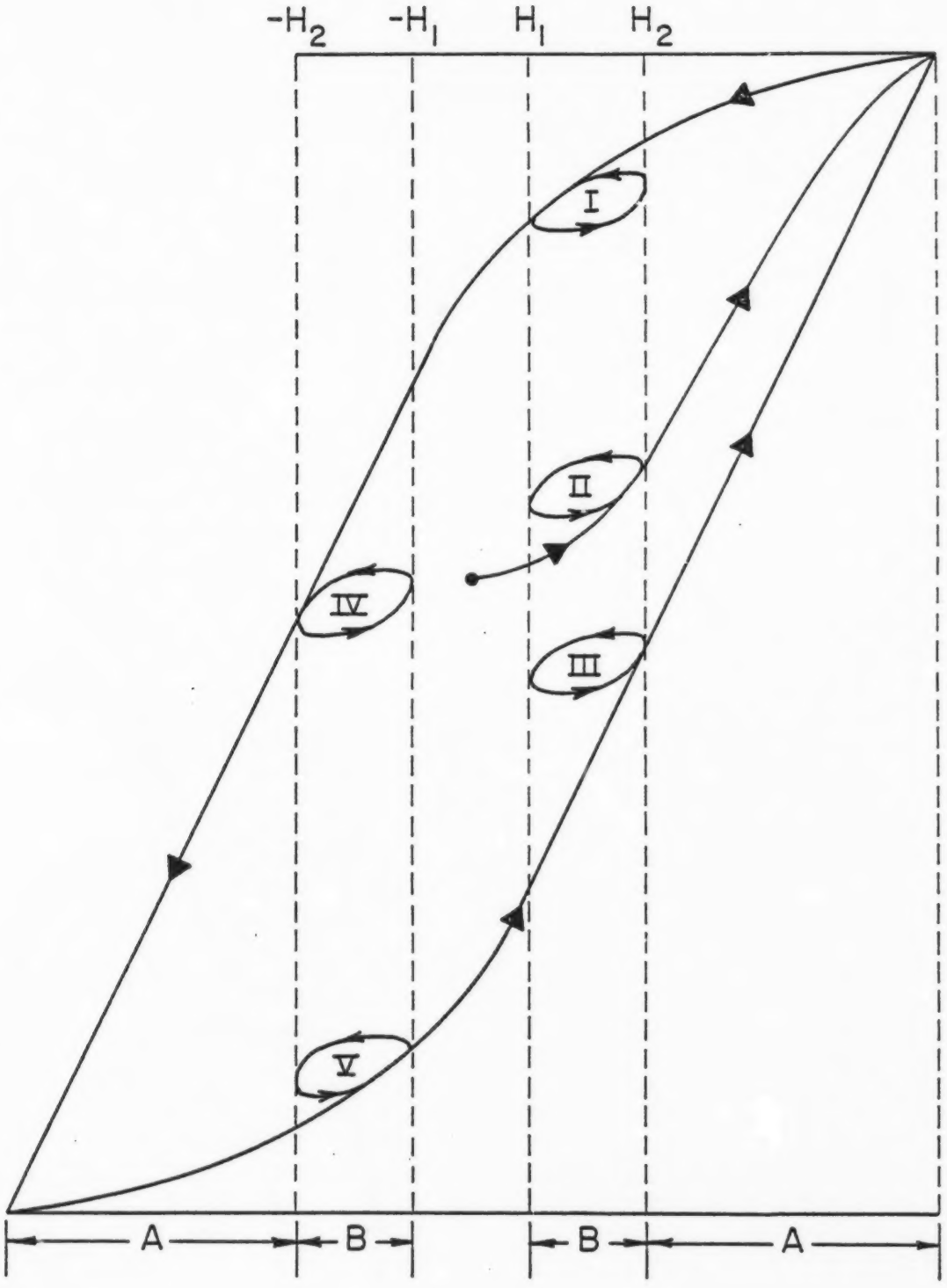

atherton, 2z pura & 2zpura Fig 6a

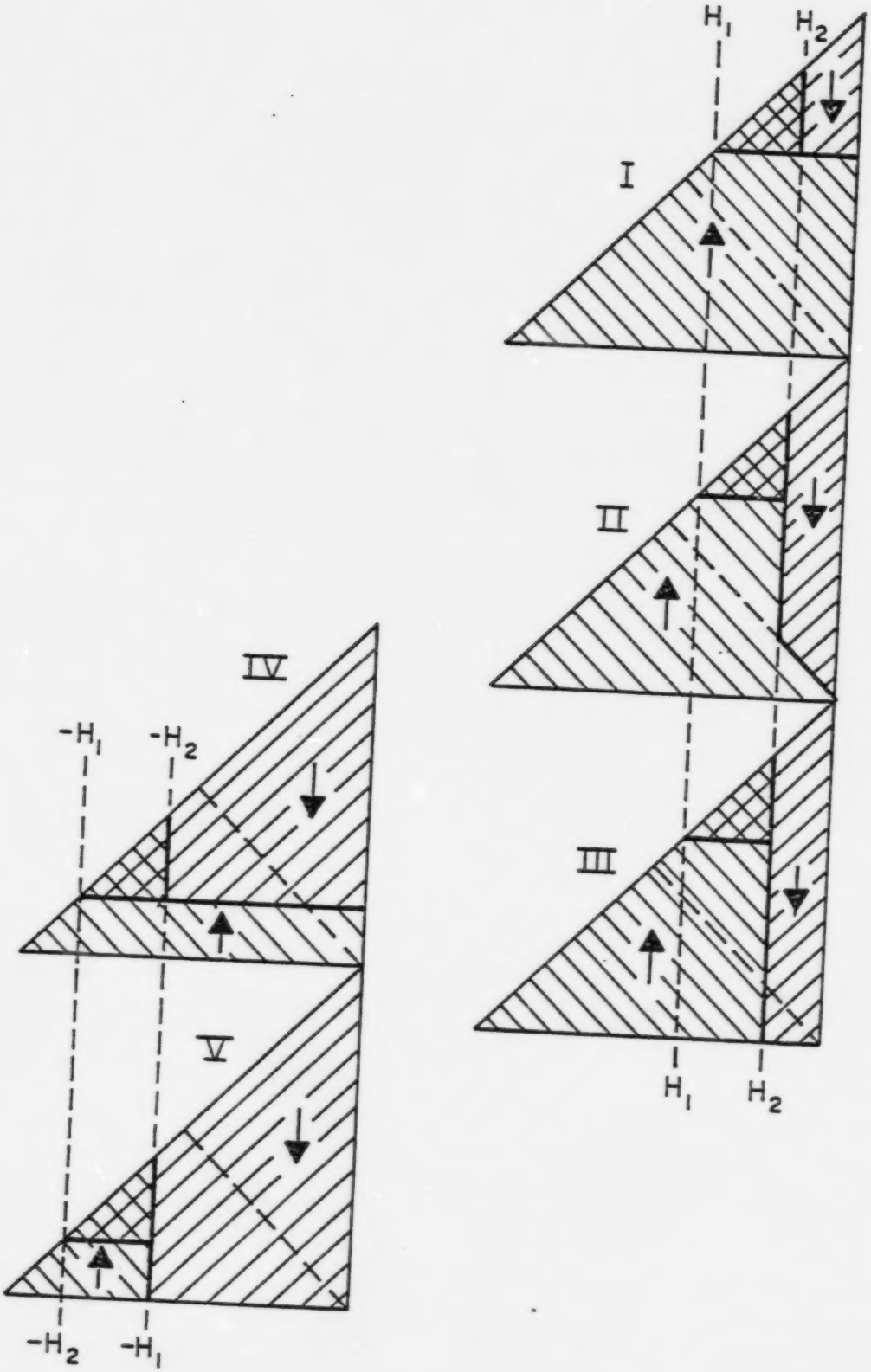

Atherton, Sherwood & Simpson Fig 6b

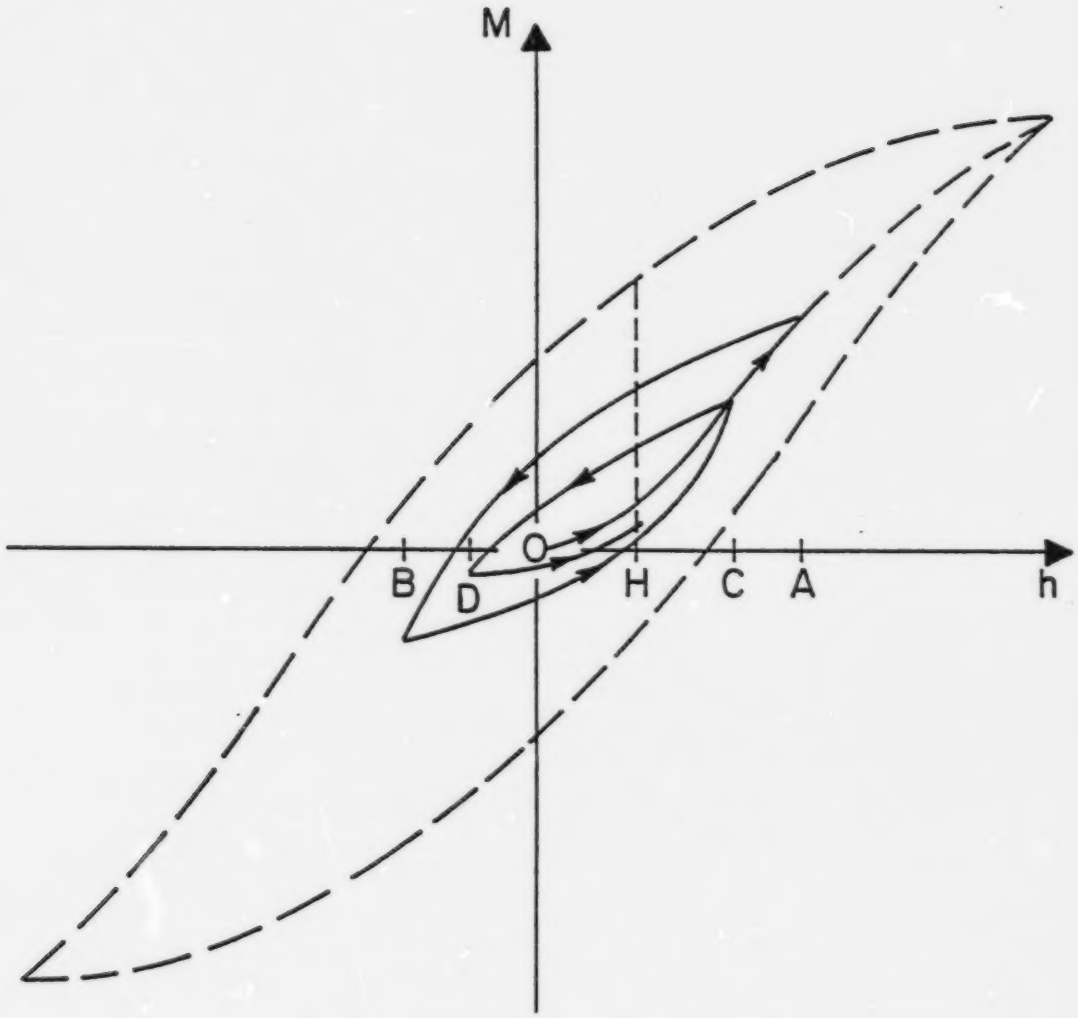

atherton, Szpura a Szpura Fig 7a

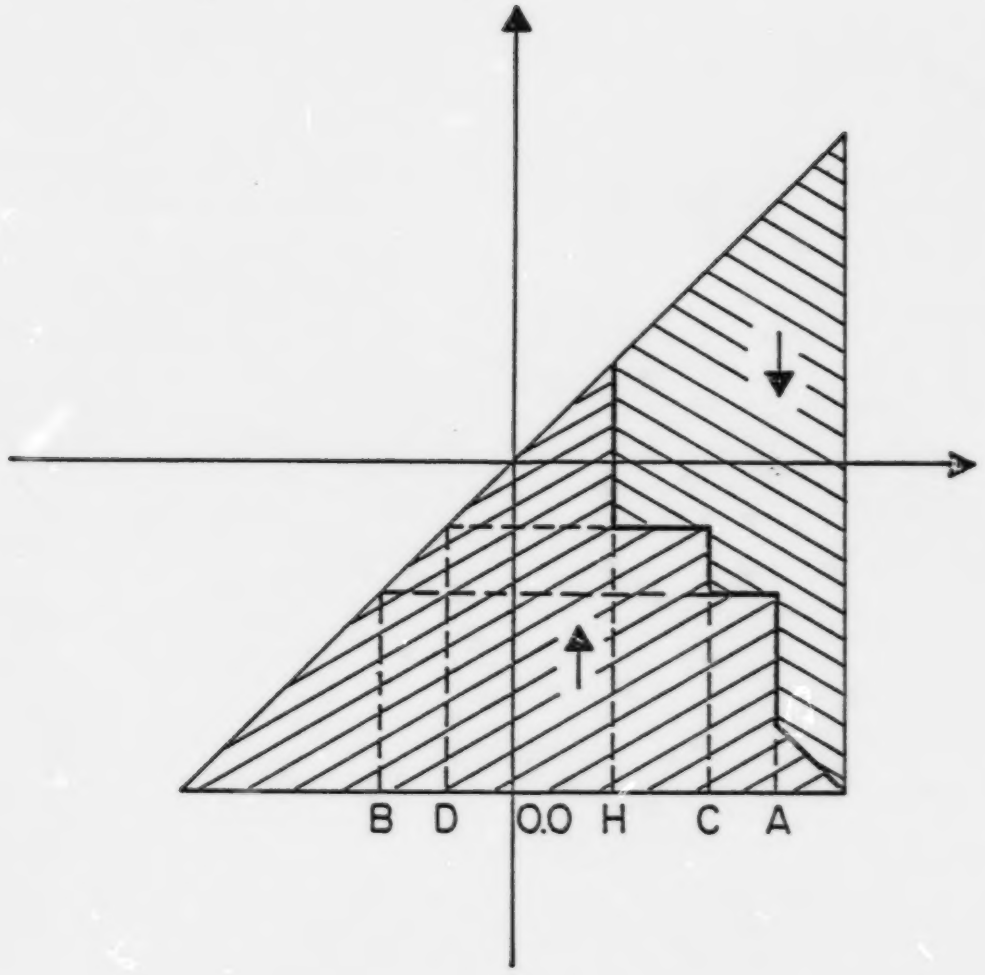

Atheter., Szpura = Szpura Fig 7b

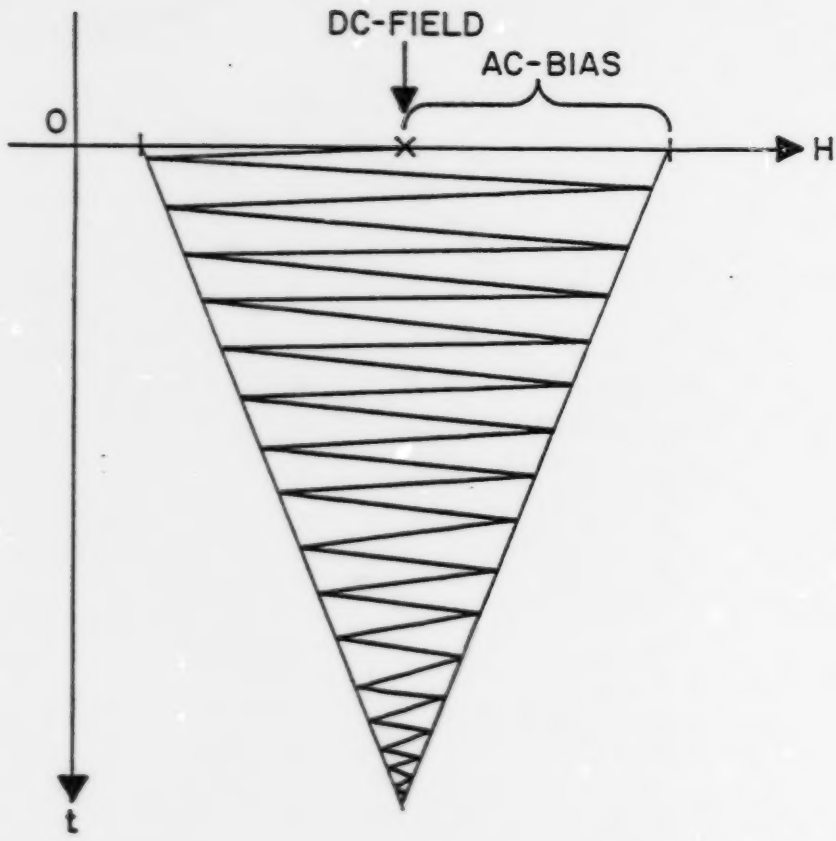

Atherton, Szpunar & Szpunar Fig 8a

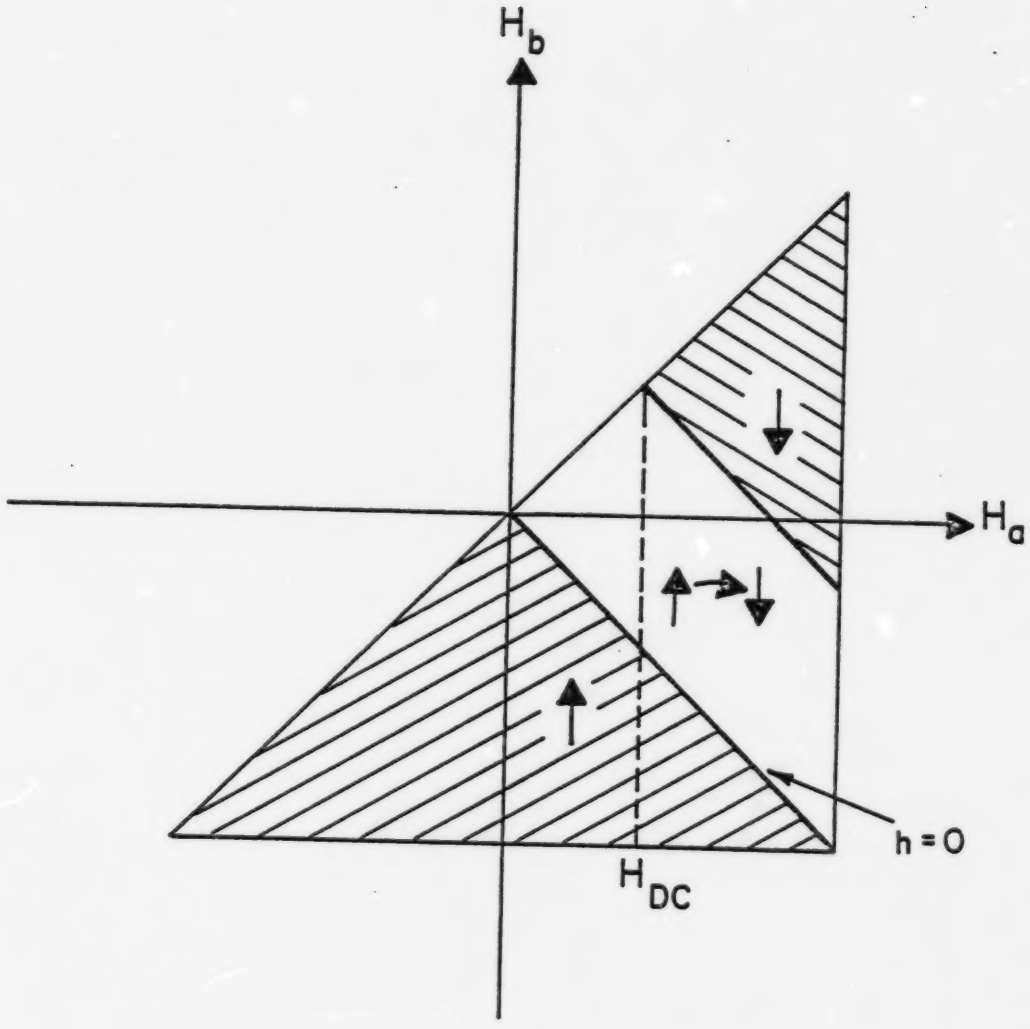

Wharton, Szpunar & Szpunar Fig 8.6

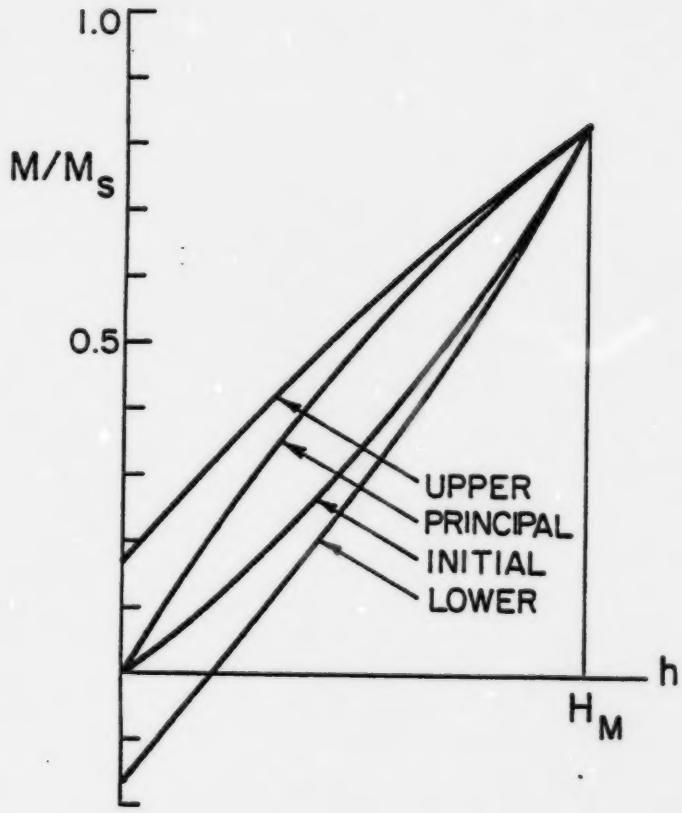

Atherton, Szpunar & Szpunar. Fig 1

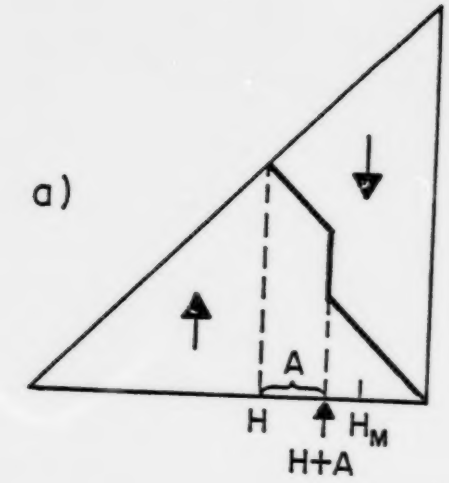
a)
A
H
H+A
H_M

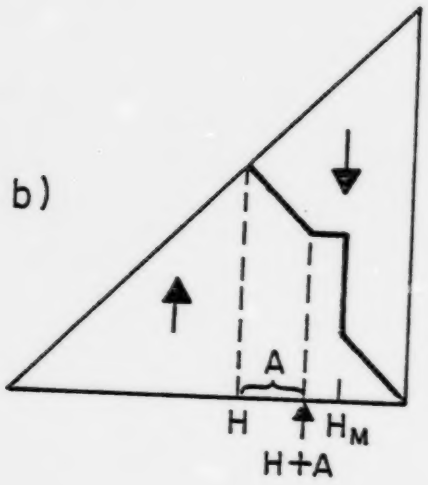
b)
A
H
H+A
H_M

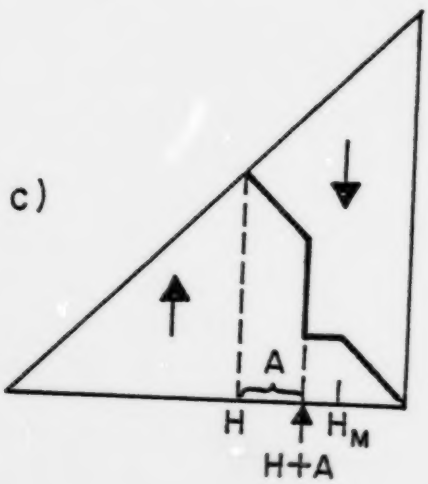
c)
A
H
H+A
H_M

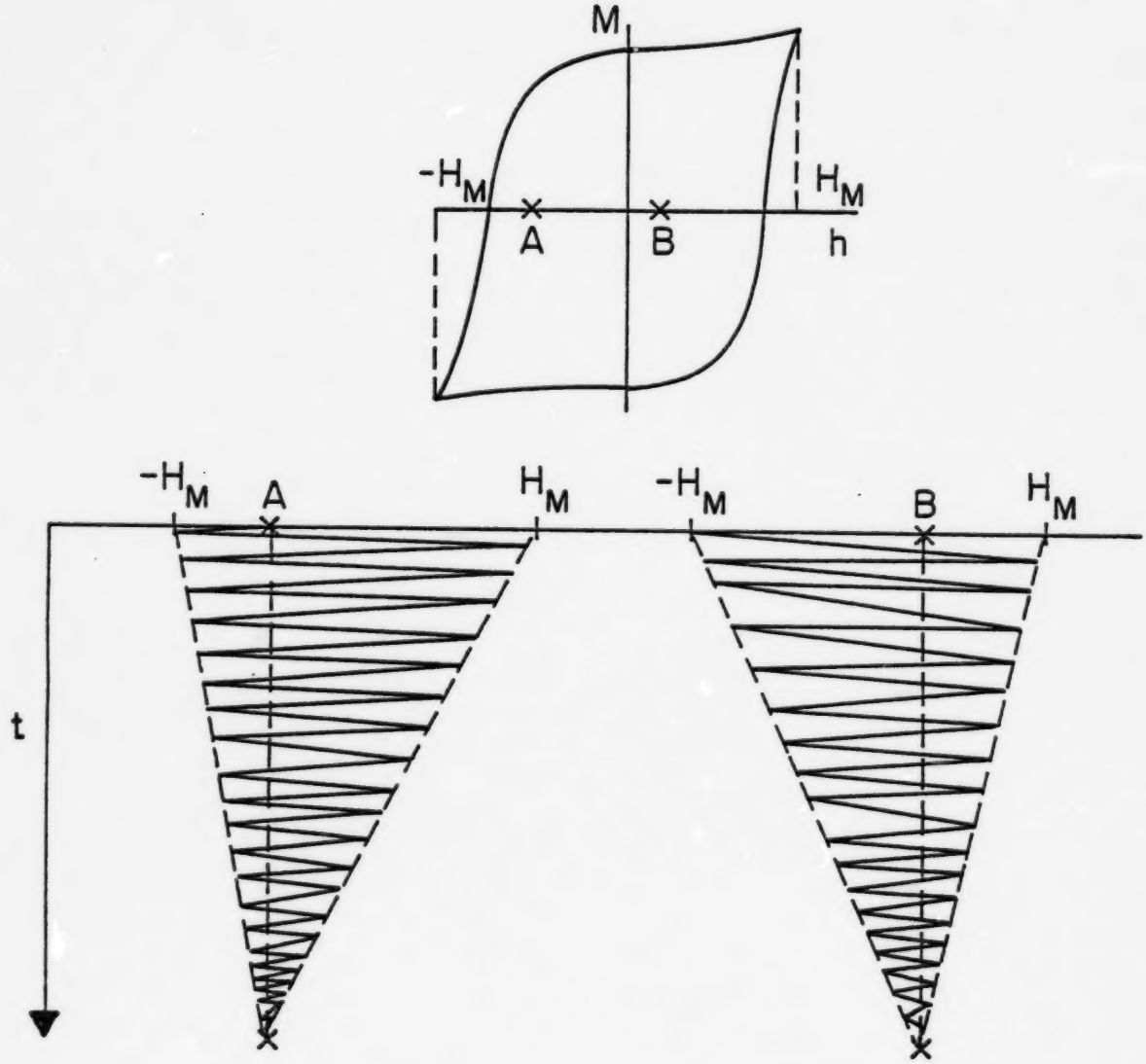

Athelon, Szpura a Szpura - Fig 11

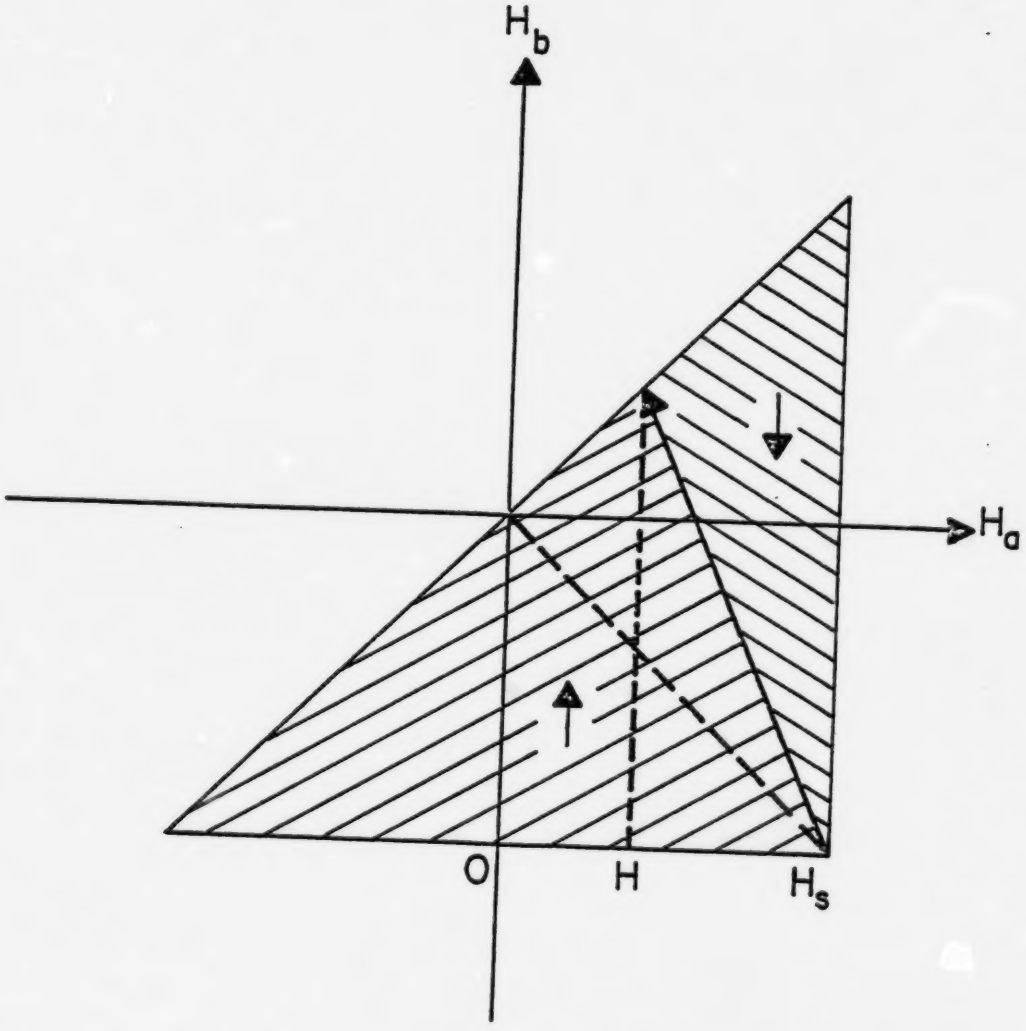

Athorton, Szpura a Szpura- Fig 12

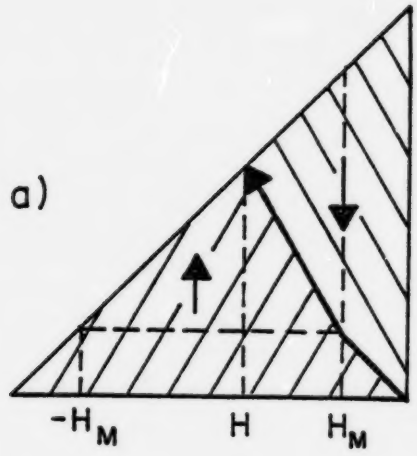

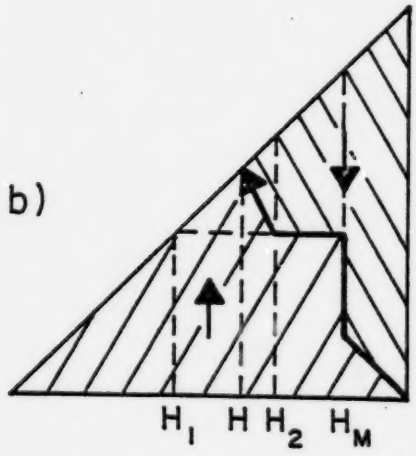

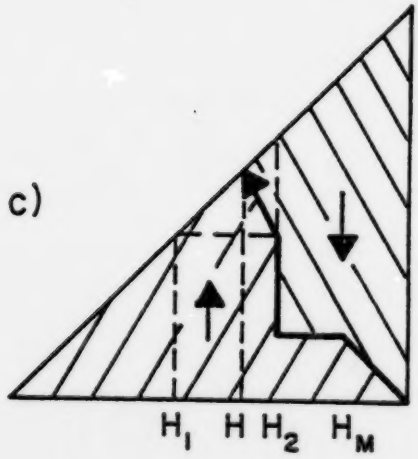

Alteration, separar a S2 pura Fig 13

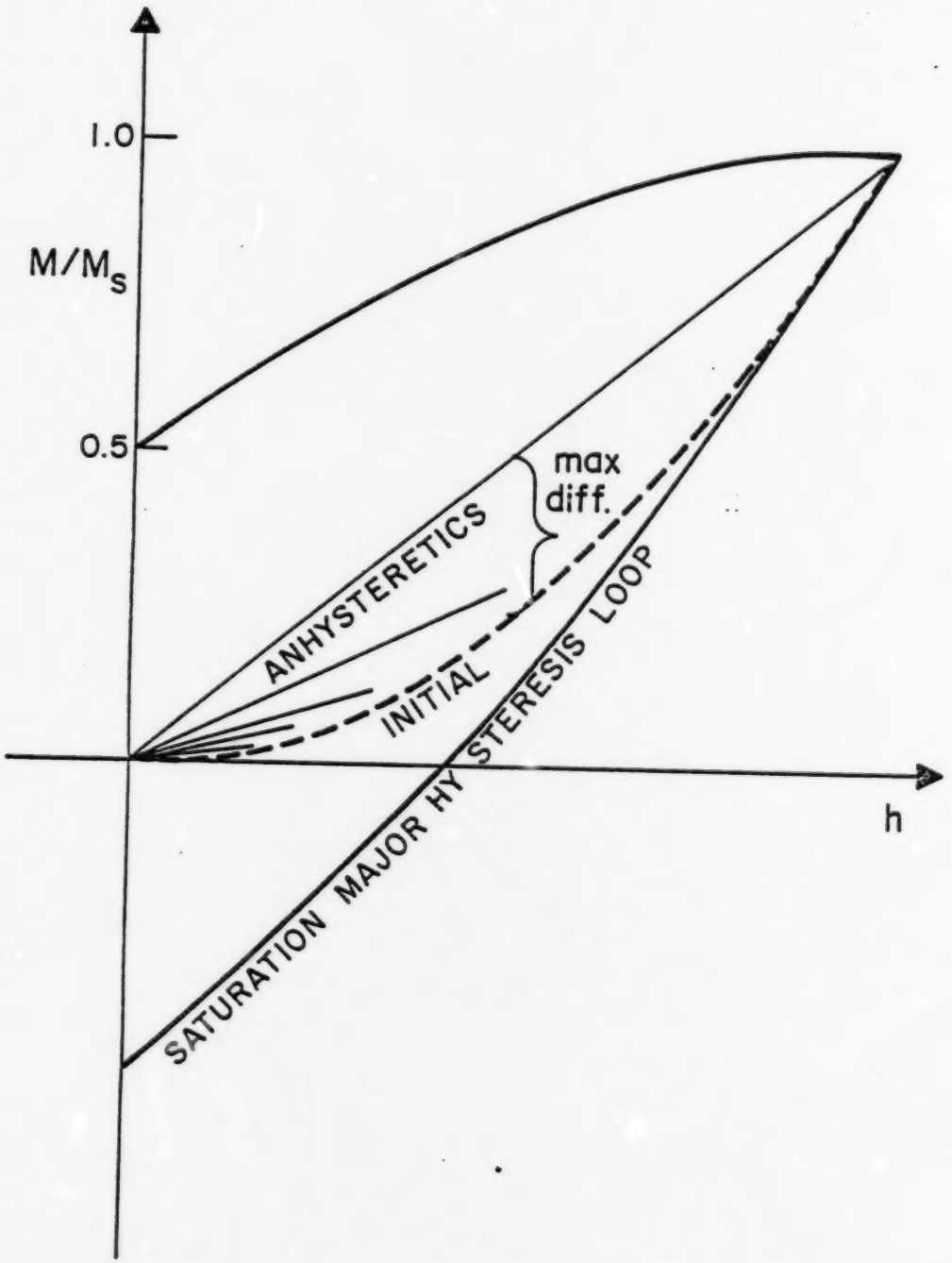

Allen, Szpura & Szpura Fig 14

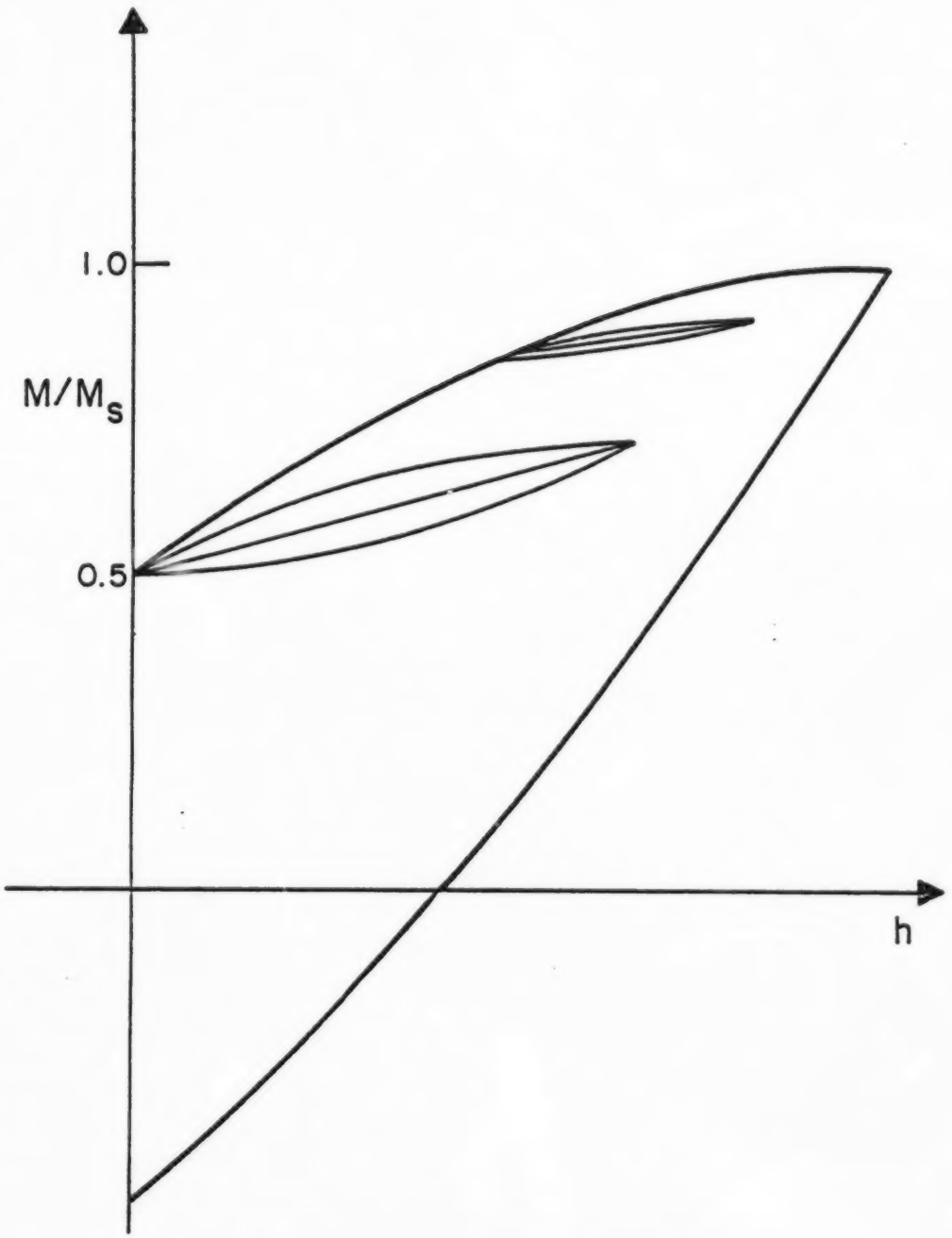

atherton, Szpura a Szpura Fig 15

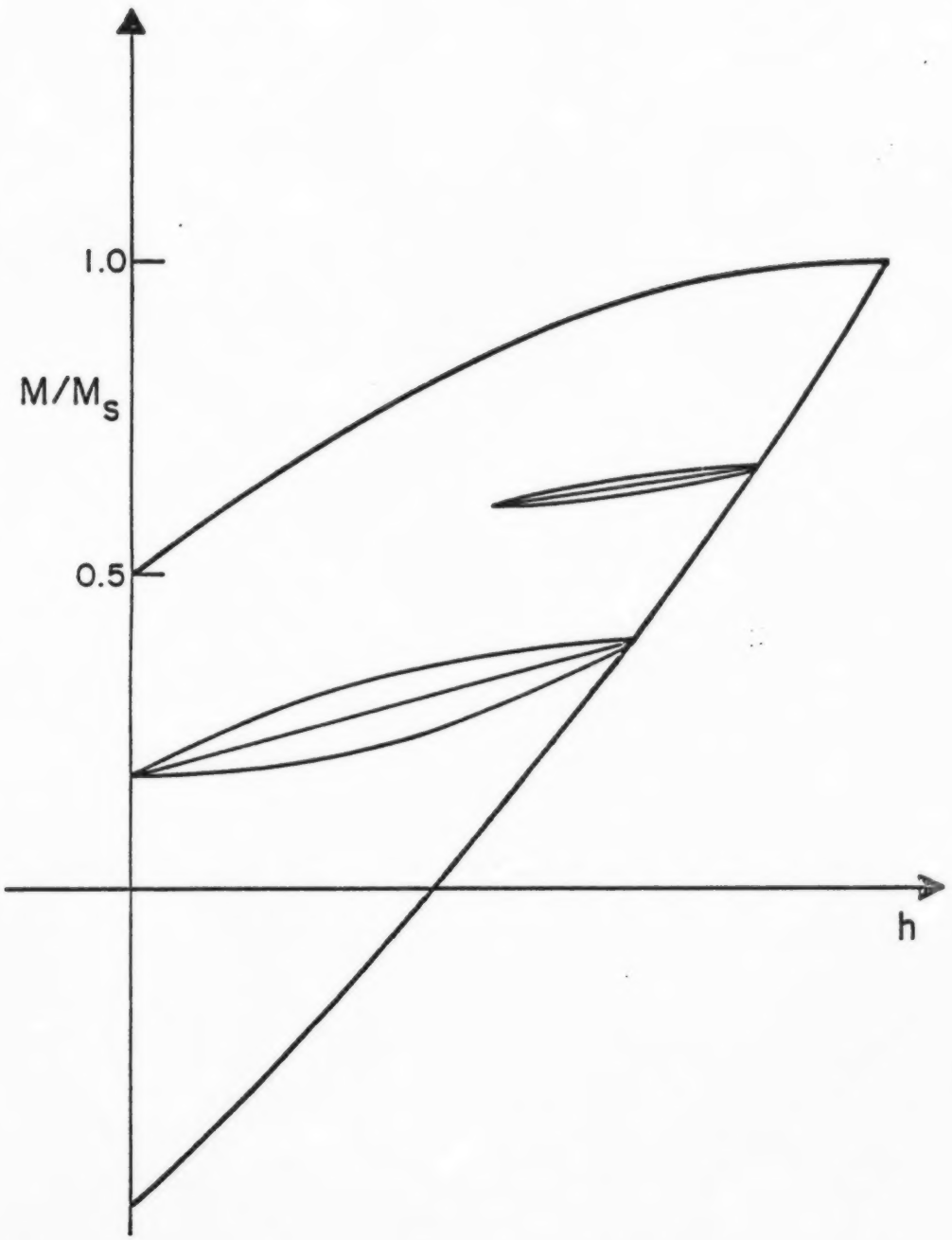

Abbaton, Szpiesar & Szpiesar. Fig 16

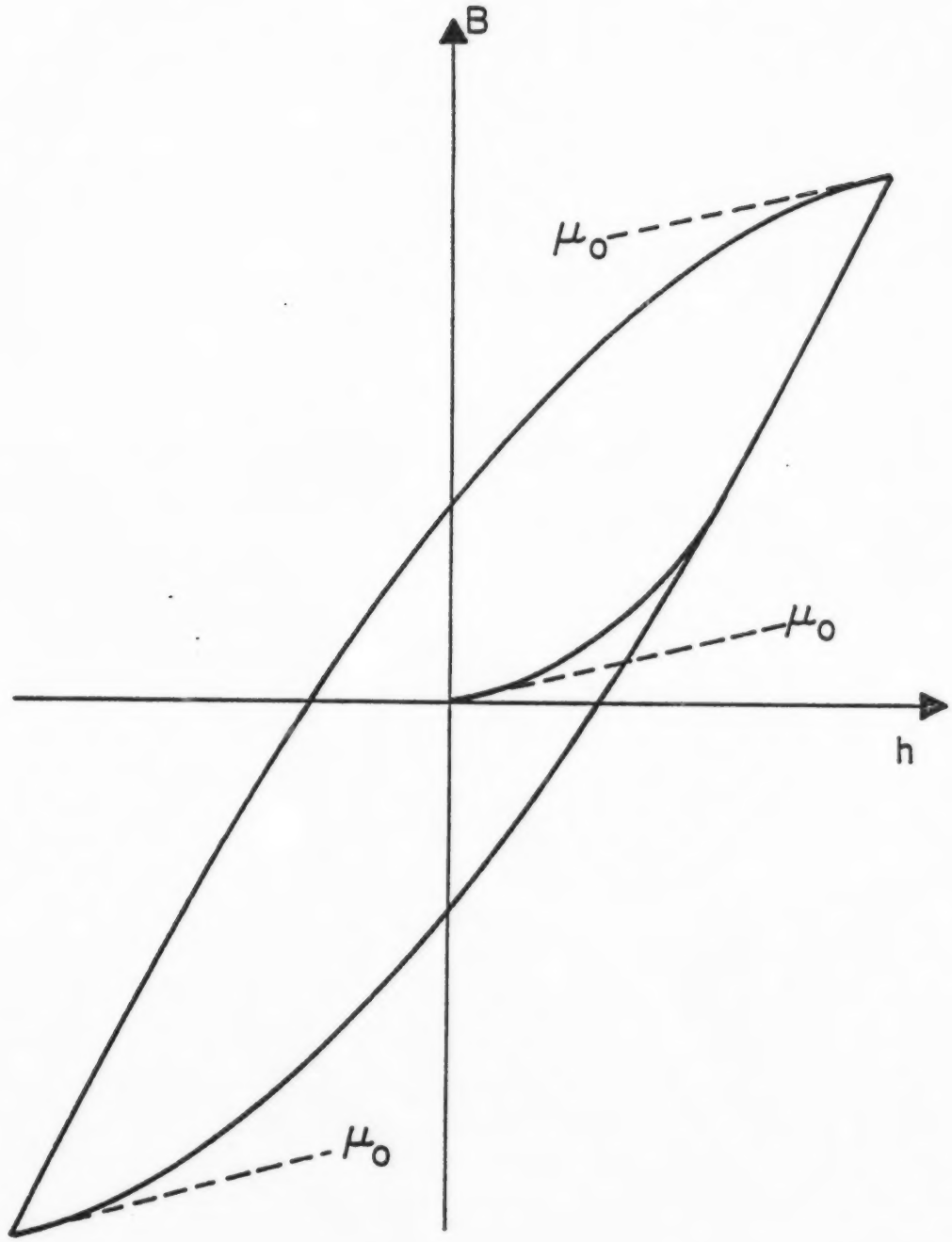

Fig 17

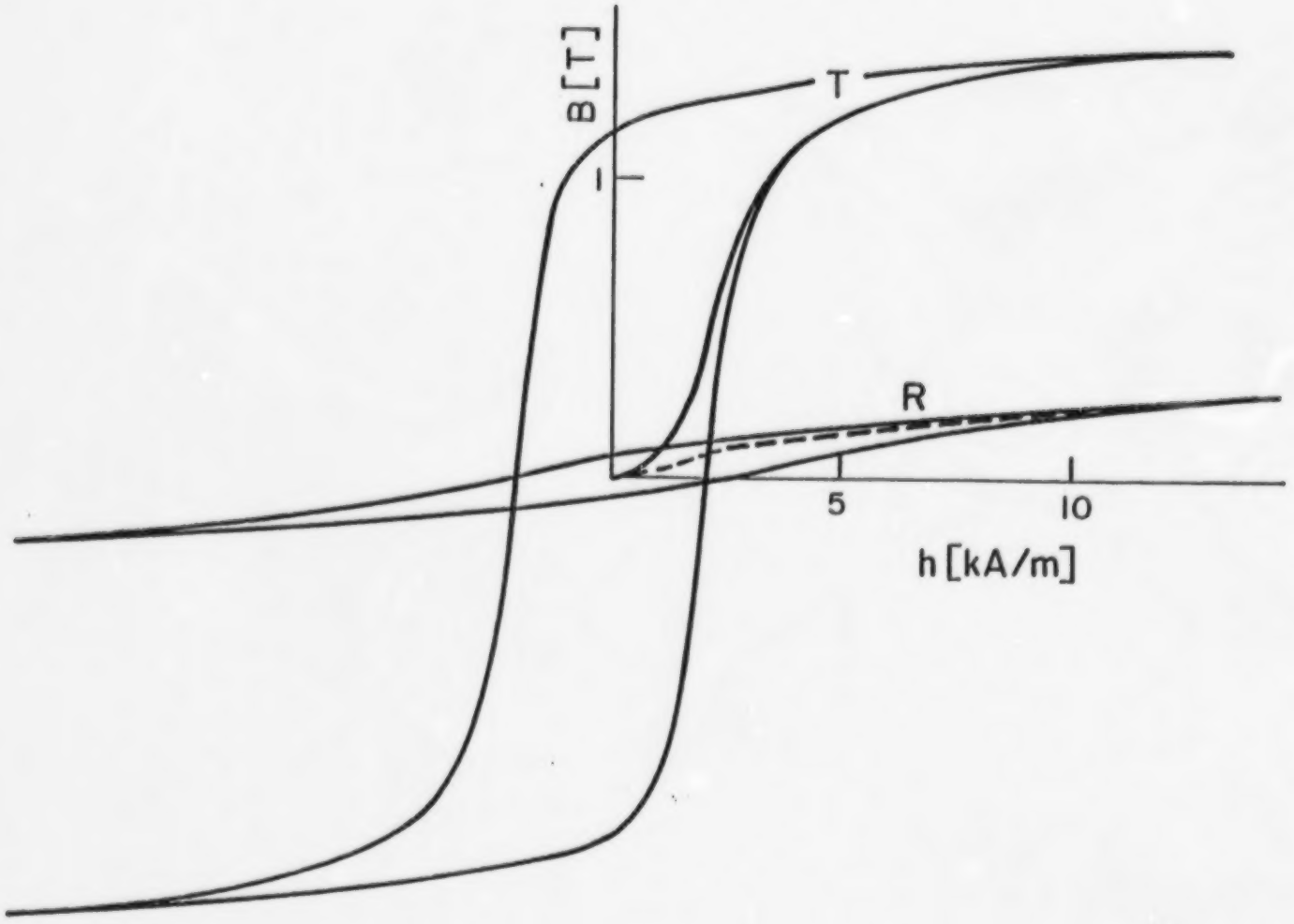

Atherton, Szpunar & Szpunar

Fig 18

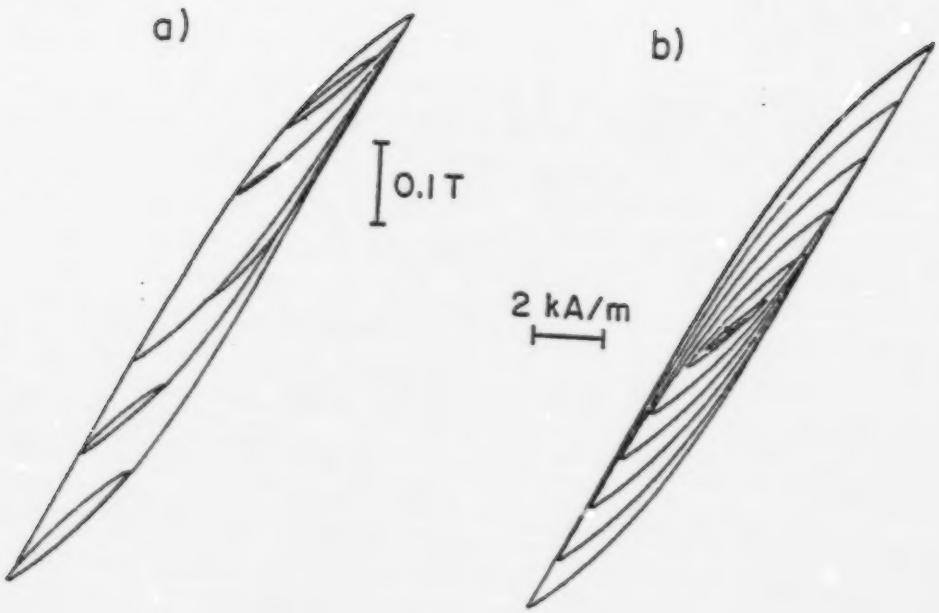

Abbess, Szpunar & Szpunar Fig 19

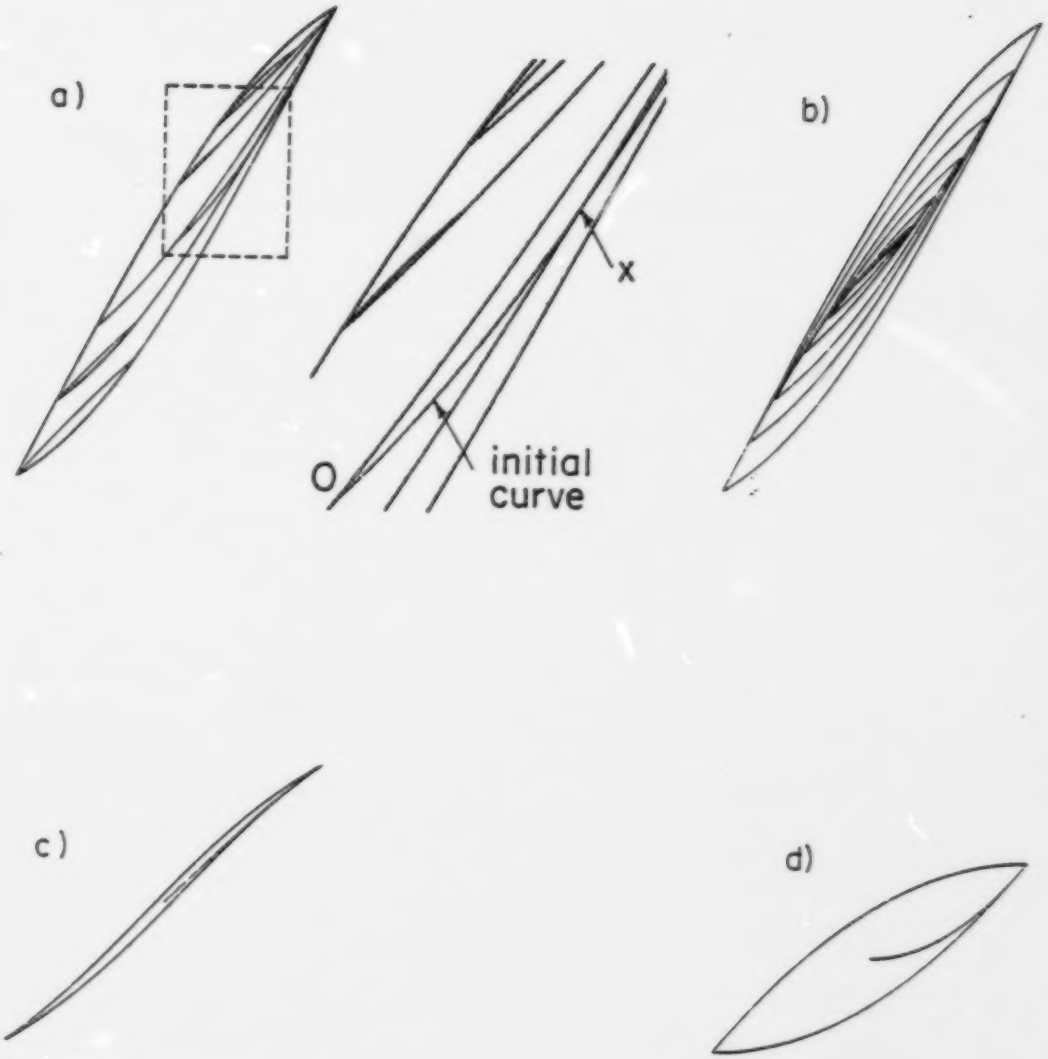

Fig 20